

Photochemical Water Oxidation at Dynamic Self-Assembled Interfaces



DISSERTATION ZUR ERLANGUNG DES
DOKTORGRADES DER NATURWISSENSCHAFTEN
(DR. RER. NAT.) DER FAKULTÄT CHEMIE UND PHARMAZIE
DER UNIVERSITÄT REGENSBURG

Vorgelegt von

Malte Hansen

Marburg an der Lahn

Regensburg 2015

The experimental work was carried out between December 2011 and June 2015 at the University of Regensburg, Institute of Organic Chemistry under the supervision of Prof. Dr. Burkhard König.

The PhD-thesis was submitted on: 13.11.2015

Date of colloquium: 16.12.2015

Board of Examiners:

Prof. Dr. Frank-Michael Matysik	(Chair)
Prof. Dr. Burkhard König:	(1 st Referee)
Prof. Dr. Arno Pfitzner	(2 nd Referee)
PD. Dr. Rainer Müller	(Examiner)

I, Malte Hansen, solemnly declare to have completed this work without any aid or help of any kind not mentioned in this thesis.

„Ich bin immer noch verwirrt, aber auf einem höheren Niveau.“

Enrico Fermi

to Anna & my family

Table of Contents

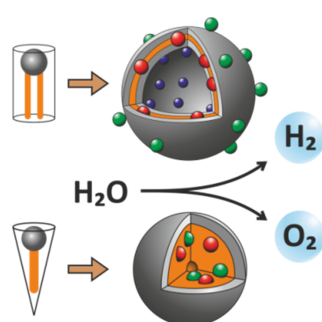
1	Artificial Photosynthesis at Dynamic Self-Assembled Interfaces in Water	1
1.1	Frontispiece	2
1.2	Introduction	3
1.3	Water Oxidation	5
1.3.1	Pioneering Work	5
1.3.2	Micellar Solutions for Water Oxidation.	7
1.3.3	Vesicles in Water Oxidation Systems	9
1.4	Photocatalytic Hydrogen Production	13
1.4.1	Vesicular Systems for Hydrogen Production	13
1.4.2	Micellar Systems for Hydrogen Production	23
1.5	Overall Water Splitting System at Vesicular Membranes.	27
1.6	Photocatalytic CO ₂ Reduction	28
1.7	Conclusion	29
1.8	References	30
2	Photocatalytic Water Oxidation at Soft Interfaces	37
2.1	Introduction	38
2.2	Results and Discussion	39
2.3	Conclusion	45
2.4	Experimental Part	46
2.4.1	General Methods and Material	46
2.4.2	Synthesis of Photosensitizer 2a	47
2.4.3	Synthesis of Catalyst 6b	49
2.4.4	Synthesis of Catalyst 3 and 7	52

2.4.5	Synthesis of Photosensitizers 2b , 2c and Catalyst 5	54
2.4.6	Vesicle Preparation and Characterization	54
2.4.7	Irradiation and Gas Chromatography	56
2.4.8	Influence of Solution Turbidity on Oxygen Evolution	58
2.4.9	Regeneration of the Catalytic Activity	59
2.4.10	Polarity at the Membrane Interface.	59
2.4.11	Determination of the Quantum Efficiency.	60
2.5	References	61
3	Quantum Dots as Photosensitizers in Photocatalytic Water Oxidation	65
3.1	Introduction	66
3.2	Results and Discussion.	70
3.2.1	Characterization of Quantum Dot Solutions	70
3.2.2	Incorporation of Quantum Dots into Vesicular Membranes.	71
3.2.3	Quantum Dots in Homogeneous Solution.	74
3.2.4	Fluorescence Quenching of Quantum Dots 3	77
3.2.5	Water Oxidation with Quantum Dots 3 and Methyl Viologen	81
3.3	Conclusion.	82
3.4	Experimental Part.	83
3.4.1	General Methods and Material	83
3.4.2	Synthesis of Photosensitizers and Catalysts	83
3.4.3	Quantum Dot Synthesis	83
3.4.4	Water Oxidation Experiments.	85
3.5	References	88
4	Photocatalytic Recycling of Ce^{IV} for Water Oxidation	91
4.1	Introduction	92
4.2	Results and Discussion.	94
4.2.1	Chemical Ce ^{IV} Generation	94
4.2.2	Generation of Ce ^{IV} with TPP.	94

4.2.3	Colorimetric Detection of Ce^{IV}	96
4.2.4	Water Oxidation as a Detection Method for Ce^{IV} Generation	99
4.2.5	Regeneration of CAN	100
4.2.6	Acr^+ -Mes for the Photochemical CAN Regeneration	102
4.3	Conclusion	104
4.4	Experimental Part	105
4.4.1	General Methods and Material	105
4.4.2	Synthesis of Catalyst 1	105
4.4.3	Stability of TPP	106
4.4.4	Detection of Ce^{IV} Generation by Methyl Viologen.	106
4.4.5	Calibration of the Ce^{IV} Detection Using AAP	107
4.4.6	Water Oxidation Experiments	108
4.5	References	110
5	Summary	113
6	Zusammenfassung	115
7	Abbreviations	117
8	Curriculum Vitae	120
9	Danksagung	122

1 Artificial Photosynthesis at Dynamic Self-Assembled Interfaces in Water

1.1	Frontispiece	2
1.2	Introduction	3
1.3	Water Oxidation	5
1.4	Photocatalytic Hydrogen Production	13
1.5	Overall Water Splitting System at Vesicular Membranes	27
1.6	Photocatalytic CO ₂ Reduction	28
1.7	Conclusion	29
1.8	References	30



Artificial photosynthesis is one of the big scientific challenges of today. Self-assembled dynamic interfaces, such as vesicles or micelles, have been used as microreactors to mimic biological photosynthesis. These aggregates can help to overcome typical problems of homogeneous photocatalytic water splitting. Microheterogeneous environments organize catalyst-photosensitizer assemblies at the interface in close proximity and thus enhance intermolecular interactions. Thereby vesicles and micelles may promote photoinitiated charge separation and suppress back electron transfer. The dynamic self-assembled interfaces solubilize non-polar compounds and protect sensitive catalytic units and intermediates against degradation. In addition, vesicles provide compartmentation that was used to separate different redox environments needed for an overall water splitting system. This Minireview provides an overview of the applications of micellar

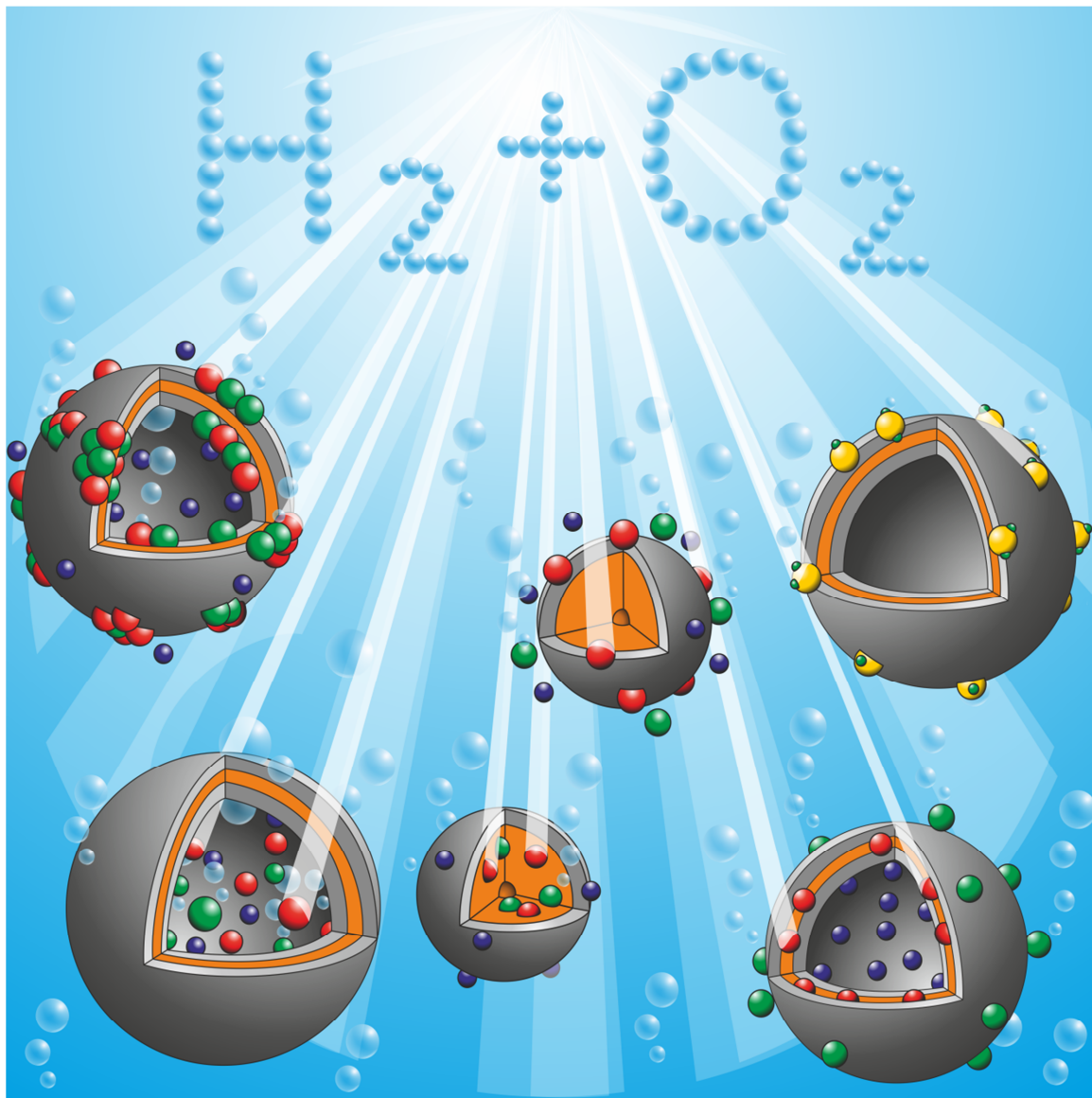
and vesicular microheterogeneous systems for solar energy conversion by photosensitized water oxidation and hydrogen generation.

This chapter was published in:

M. Hansen, S. Troppmann and B. König, "Artificial Photosynthesis at Dynamic Self-Assembled Interfaces in Water", *Chem. Eur. J.* **2015**, 10.1002/chem.201503712 - reproduced with permission from John Wiley & Sons

M. Hansen (oxidative part) and S. Troppmann (reductive part) wrote the manuscript and B. König supervised the project and is the corresponding author.

1.1 Frontispiece



1.2 Introduction

The efficient conversion of sunlight into usable chemical energy by water splitting, as in biological photosynthesis, is highly desirable, but remains a challenging task.^[1-3] The water splitting process can be divided into two independent half-reactions: first, the oxidation of water to dioxygen and second, the reduction of protons to dihydrogen. Sacrificial agents have to be used in these separated half cells (Figure 1.1).

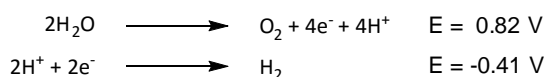


Figure 1.1 - Water oxidation and proton reduction reactions, with their half-cell potentials vs. NHE at pH 7.^[4]

The oxidation of water, which involves a four-electron transfer step, is considered particularly difficult compared with the two electron reduction of protons. Most of the reported efficient artificial photosynthetic systems perform either the oxidative or the reductive half reaction, but not both. The combination of oxidation and reduction in one catalytic system is difficult: different redox environments are needed, charge recombination must be avoided, and the different solubilities and the separation of the products, O₂ and H₂, must be addressed, as particularly the evolved oxygen interferes with the photoreactions. Dynamic self-assembled interfaces may help to overcome these problems.

In biological photosynthesis, chromophores and catalytic units are bound to a thylakoid membrane (Figure 1.2). The membrane plays a crucial role in establishing a proton gradient, which is utilized for the generation of reduction equivalents. It provides compartmentation and spatial organization of the active compounds.

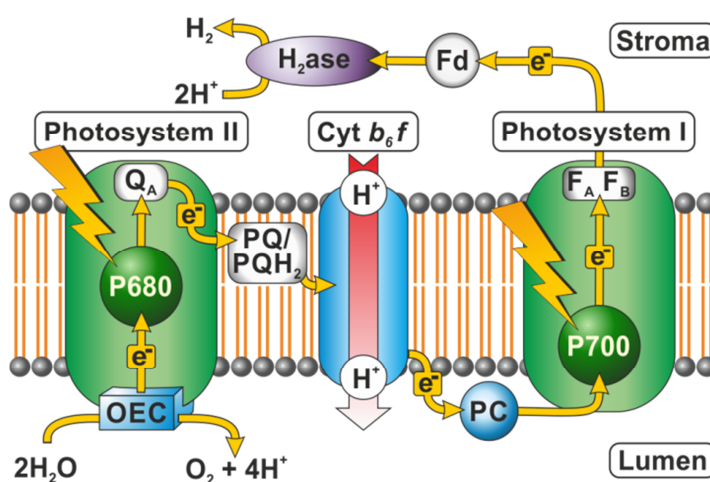


Figure 1.2 - Schematic representation of the biological photosynthetic process at the thylakoid membrane.

In particular, dynamic interfaces such as micelles and vesicles have been investigated to mimic photosynthesis. Micelles and vesicles are aggregates of amphiphilic molecules in water. Whereas conically shaped amphiphiles form micelles in water, cylindrical amphiphiles aggregate to form vesicles (Figure 1.3).^[5]

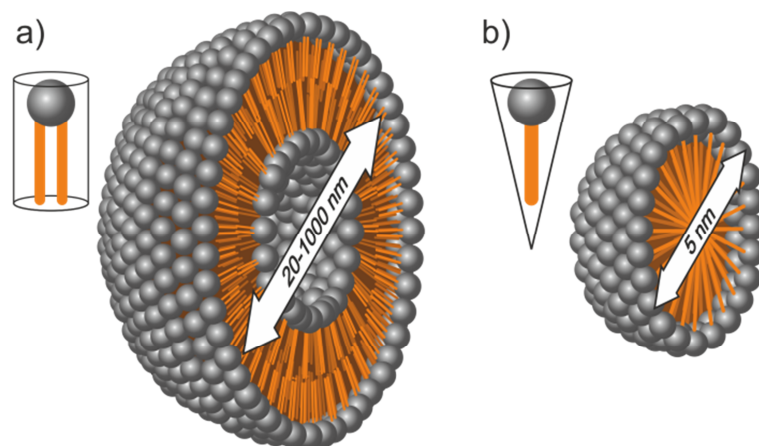


Figure 1.3.- Simplified scheme of a) a vesicle formed from cylindrically shaped amphiphiles and b) a micelle from conical surfactants.

A typical micelle forms an aggregate where the hydrophilic head groups are in contact with the surrounding media, while the hydrophobic tails form a nonpolar region in the middle of the aggregate. Different shapes are possible, depending on amphiphile geometry and solution conditions. Vesicles are self-assembled spherical bilayers of amphiphiles in water surrounding an aqueous cavity. The amphiphile's polar headgroups face the inner and outer aqueous solutions, while the hydrophobic chains form a nonpolar region in between the two interfaces.

Micelles have been utilized to dissolve hydrophobic compounds in aqueous environments and to protect photosensitizers and catalysts against degradation. Charged micellar surfaces can change reaction rates of detrimental pathways by coulombic forces. Vesicles provide compartmentation and allow charge separation over the membrane. Back electron transfer could be inhibited and vesicles have been successfully used to organize molecular assemblies at and in the membrane. They found use in the stabilization and synthesis of colloidal systems and kept semiconductor nanoparticles in solution by solving solubility issues.

Micelles and vesicles are therefore ideal models to study catalytic systems for light-driven water splitting into oxygen and hydrogen at interfaces or in dynamic assemblies. In this minireview, we focus on photocatalytic water oxidation and hydrogen production in dynamic self-assembled micelles and vesicles. Electrochemical hydrogen production in micelles^[6, 7]

and the utilization of reverse micelles as microenvironments for artificial photosynthesis are not within the scope of this Minireview.^[8,9] Moreover, photoinduced electron transfer across membranes,^[10-17] a key step in photosynthesis, is discussed only very briefly when directly connected to oxygen or hydrogen evolution. Instead, we give an overview of the application of micellar and vesicular microheterogeneous systems for solar energy conversion by photo-sensitized water oxidation and hydrogen generation.

1.3 Water Oxidation

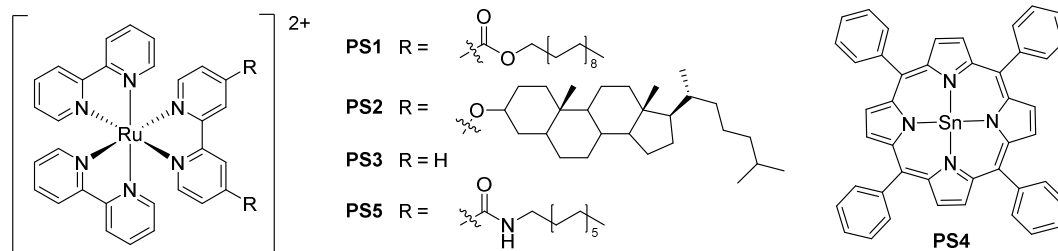
1.3.1 Pioneering Work

The groups of Whitten and Toyoshima reported two systems of self-assembled interfaces for water splitting that gained a lot of interest. However, these results were proved to be unreproducible or probably wrong. Nevertheless, these reports represent an interesting starting point in the field of dynamic self-assemblies for artificial photosynthesis.

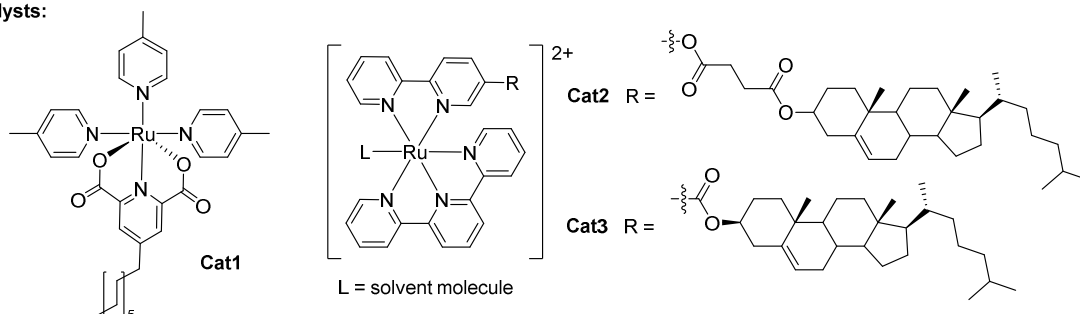
In 1976 Whitten and co-workers described the photochemical cleavage of water using a monolayer of surfactant analogues of $[\text{Ru}(\text{bpy})_3]^{2+}$ bearing dioctadecyl (**PS1**, Figure 1.4) or dihydrocholesteryl esters (**PS2**).^[18] When monolayers of **PS1** deposited on glass slides were immersed in water, the luminescence was quenched almost entirely. Irradiation of these glass slides with visible light resulted in a steady production of gases, which were identified as hydrogen and oxygen by mass spectrometry. After continuous irradiation for two weeks, they estimated the turnover number (TON) to be over 1000. Whitten and co-workers proposed a change in energy barriers for electron transfers in the assembly compared to homogeneous solution as the reason for the water cleavage.

Unfortunately, the reproduction of these results by Whitten and other groups failed.^[19-24] Gaines and co-workers found that these carboxy esters are very susceptible to hydrolysis and that preparations of **PS1** and **PS2** were partly hydrolyzed during synthesis, which was detected by HPLC and confirmed by other groups. The monolayers are affected by subtle factors, as indicated by the wide variance in luminescence and packing properties of different preparations of monolayers. The origin of the first **PS1** preparation's activity in water splitting remained unclear.

Photosensitizers:



Catalysts:



Charge transfer reagents:

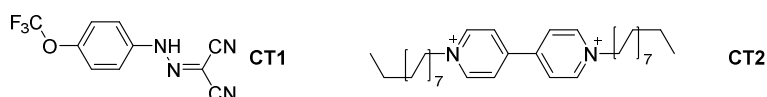


Figure 1.4 - Structures of the photosensitizers, catalysts and charge transfer agents used for water oxidation systems.

Toyoshima *et al.* claimed the successful oxidation of water by vesicles containing chlorophyll *a* and *b* under visible-light irradiation.^[25] They prepared lecithin vesicles from egg yolk functionalized with a preparation of chlorophyll *a* and *b* and pigments, such as carotene and xanthophyll derived from spinach leaves. Potassium ferricyanide in the interior of the vesicles served as the sacrificial electron acceptor and carbonyl cyanide *p*-(trifluoromethoxy)-phenylhydrazine (**CT1**, Figure 1.4) was added to enable charge transfer over the membrane. Oxygen evolution was measured with a Clark electrode under irradiation with visible light from a 500 W xenon lamp. They concluded that a chlorophyll radical cation, formed after an electron transfer from the excited state of chlorophyll to ferricyanide, served as the water oxidation catalyst.

However, one year later, Stillwell and Tien failed in the reproduction of the experiments.^[26, 27] Their main criticism was the absence of a temperature control in Toyoshima's experiments. Thus they concluded that the "oxygen" evolution was, in reality, a heating effect at the Clark electrode. Stillwell and Tien instead fused broken thylakoids with liposomes and

could prove oxygen evolution activity.^[28] The fusion of the thylakoids with phosphatidylcholine vesicles protected the oxygen evolving complex against aging.

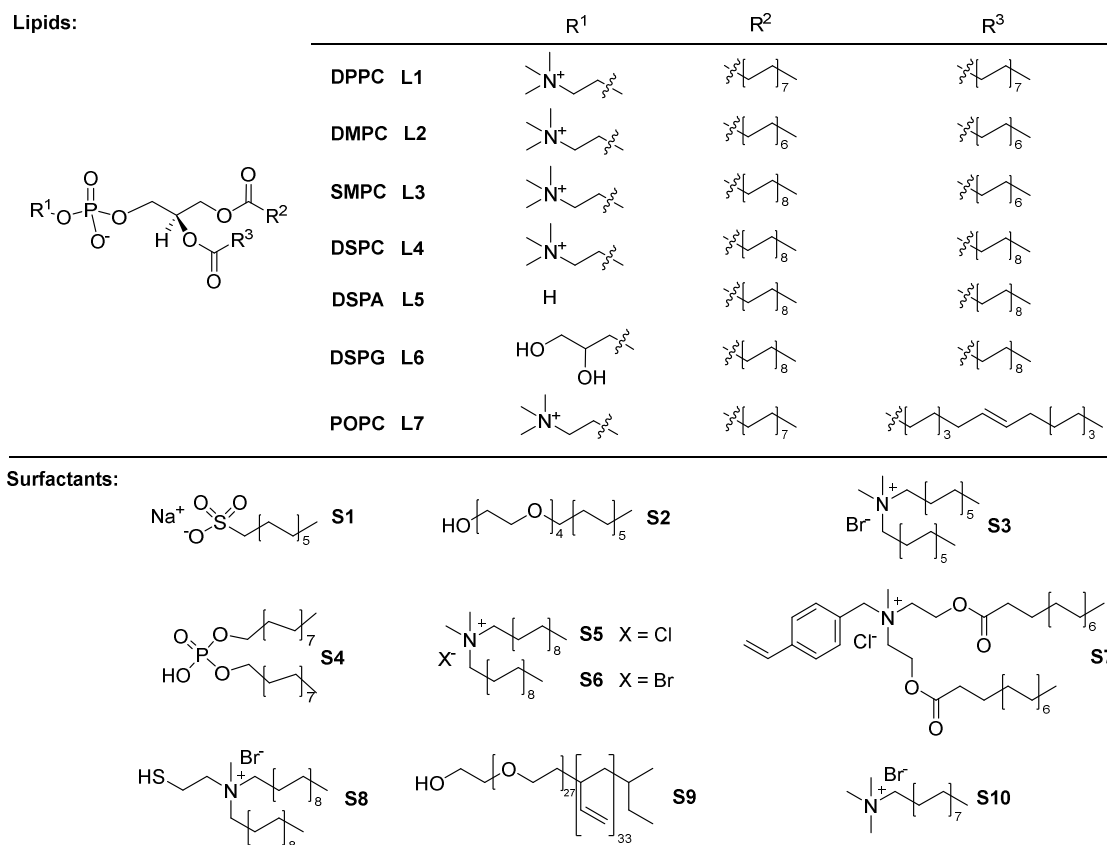


Figure 1.5 - Structures of lipids and surfactants in self-assembled vesicles and micelles for artificial photosynthesis

1.3.2 Micellar Solutions for Water Oxidation

In 1986, Tsvetkov *et al.* published different approaches to the photooxidation of water in microheterogeneous systems.^[29] They used $[\text{Ru}(\text{bpy})_3]^{2+}$ (**PS3**) as the photosensitizer and colloidal cobalt hydroxides as water oxidation catalysts in micellar solutions, microemulsions, and lipid vesicle suspensions.

A mixture of CoCl_2 , **PS3**, and an electron acceptor, $[\text{Co}(\text{NH}_3)_5\text{Cl}]^{2+}$ or sodium persulfate, was irradiated with white light in the presence and absence of sodium dodecylsulfate (SDS, **S1**, Figure 1.5) micelles. As a measure of the efficiency of these systems, they defined the selectivity β , which represents the ratio of evolved oxygen to its theoretical stoichiometric quantity after complete consumption of the acceptor. The selectivity β was not influenced by SDS micelles when $[\text{Co}(\text{NH}_3)_5\text{Cl}]^{2+}$ was used as the acceptor. Only the quenching rate con-

stant was increased (Table 1.1). This was explained by the attraction of both **PS3** and $[\text{Co}(\text{NH}_3)_5\text{Cl}]^{2+}$ to the negatively charged surface of the micelles. In contrast to these results, β was increased 10-fold when SDS micelles were added to persulfate containing samples. An extended longevity was also observed in these micellar systems.

The oxidation of organic compounds and the photosensitizer's ligands were claimed to be the most important side reactions causing the low selectivity for oxygen production. This was indicated by a small amount of CO_2 in every sample after irradiation. The destruction of the photosensitizer was much weaker when SDS was added to samples containing persulfate. The authors attributed this to a change in the rate constants of the main destruction pathway, which is most probably the reaction of the persulfate radical anion $\text{SO}_4^{\bullet-}$ with the ligands of **PS3**. The coulombic repulsion of the $\text{SO}_4^{\bullet-}$ radical and the negatively charged micelle suppresses the degradation of **PS3** leading to a higher selectivity for oxygen evolution. The coulombic forces play a major role, which is evident from the decrease in the quenching rate of **PS3** by $\text{S}_2\text{O}_8^{2-}$ in SDS (**S1**) micellar solutions (Table 1.1).

Table 1.1 - Selectivities for H_2O oxidation (β) and rate constants (k_q) of $[\text{Ru}(\text{bpy})_3]^{2+*}$ quenching by an acceptor in homogenous and micellar solutions.

Acceptor	Homogenous solution		Micellar solution	
	β (%)	k_q ($10^8 \text{ M}^{-1} \text{ s}^{-1}$)	β (%)	k_q ($10^8 \text{ M}^{-1} \text{ s}^{-1}$)
$[\text{Co}(\text{NH}_3)_5\text{Cl}]^{2+}$	0.4	16	0.3	57
$\text{S}_2\text{O}_8^{2-}$	1.7	6.2	22	0.73

In 2003 the group of Hori used micelles to both disperse hydrophobic tin-tetraphenylporphyrins (**PS4**) in water and protect the porphyrin against detrimental side reactions, which often occurred with hydrophilic porphyrins.^[30] Their catalytic system consisted of the acceptor $[\text{Co}(\text{NH}_3)_5\text{Cl}]\text{Cl}_2$, the photosensitizer **PS4**, and the water oxidation catalyst RuO_2 . From their experience with hydrogen evolution (see Section 3.2), they expected ionic micelles to shut down oxygen evolution, which they explained by the coulombic repulsion and attraction, respectively, of the micellar surface and either PS4^+ or OH^- . Non-ionic micelles from **S2** (Brij 30), a poly(ethylene glycol) (alkyl)ether instead proved to efficiently enhance the system's activity from a TON of 0.1 for the homogeneous to 17 for the microheterogeneous environment. Unfortunately, no statement was made regarding what ended the catalysis after 48 h.

1.3.3 Vesicles in Water Oxidation Systems

Parmon and co-workers used microemulsions as model systems for the internal cavities of vesicles to investigate a vesicular system for the spatial separation of the reductive and oxidative half-reaction of water splitting.^[29] They introduced $[\text{Ru}(\text{bpy})_3]^{2+}$ (**PS3**) and the electron acceptor $[\text{Co}(\text{NH}_3)_5\text{CO}_3]^+$ into the aqueous part of a microemulsion. After irradiation, the strong oxidant $[\text{Ru}(\text{bpy})_3]^{3+}$ was formed and the Co^{II} ions from the decomposed acceptor served as the precursor for the catalyst. The selectivity for oxygen evolution dropped to $\beta = 5\%$ in these microemulsions compared with 9.5 % in homogeneous aqueous solutions. The loss in selectivity was explained by the oxidation of organic compounds forming the microemulsion. These results showed that the selective oxidation of water in the presence of organic compounds is possible, but challenging.

The proof of concept that vesicles can be used for compartmentation of water splitting solutions was given by the introduction of $[\text{Co}(\text{NH}_3)_5\text{CO}_3]^+$ and $[\text{Ru}(\text{bpy})_3]^{2+}$ (**PS3**) in the inner cavities of lecithin vesicles in the presence of Na_2EDTA in the surrounding media (Figure 1.6, EDTA = ethylenediaminetetraacetate). Na_2EDTA provides the reductive conditions needed for hydrogen evolution, but efficiently shuts down any oxygen evolution in homogeneous systems.

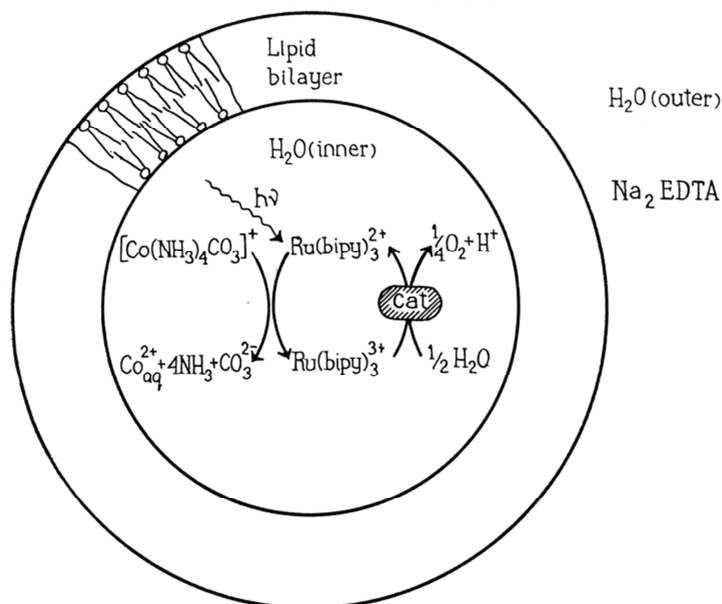


Figure 1.6 - O_2 evolution in the internal cavity of a lipid vesicle. Cat represents the water oxidation catalyst based on Co compounds (reprinted from reference [29] with permission from Taylor & Francis Group LLC - Books).

However, water oxidation continued in the vesicular system after the addition of Na₂EDTA. Unfortunately, the selectivity for oxygen production in the vesicular system was $\beta = 2\%$, thus even lower than in microemulsions or homogeneous systems. An increase in the total yield of oxygen by a factor of 40 could be achieved by the addition of NaIO₄ as an additional electron acceptor instead of Na₂EDTA in the outer aqueous solution. Cetyl viologen (**CT2**, Figure 1.4) ensured the necessary electron transfer over the membrane. However, the authors could not state with certainty that the oxygen generation was caused by an electron transfer over the lipid bilayer membrane instead of a penetration of NaIO₄ into the vesicle.

The selectivity β was enhanced to 11 % by using a system composed of **PS3**, S₂O₈²⁻, CoCl₂ and lecithin vesicles.^[31] In this system, the CoCl₂ forms colloidal Co^{III} hydroxides, which entirely adsorb to the membrane of the vesicles and catalyze water oxidation. The adsorption was confirmed by gel chromatography after the reaction, done to separate solutes from vesicles. These separated vesicles regained 69 % of their initial activity after addition of new **PS3** and S₂O₈²⁻, whereas the fraction of the surrounding media from the gel chromatography stayed nearly inactive. The selectivity β was increased up to 72 % in a dark reaction with [Ru(bpy)₃]³⁺. Thus, the reactions of persulfate and the sulfate radical anion SO₄^{•-} seem to be the most detrimental reactions in this photocatalytic system, as already observed in the micellar environment.

The group of Shilov utilized MnO₂ as a water oxidation catalyst in a system with [Ru(bpy)₃]³⁺ derived from the fact that manganese complexes play a major role in oxygen evolution in photosystem II of green plants. The system stayed active even when the [Ru(bpy)₃]³⁺ was generated photochemically by a reaction of [Ru(bpy)₃]^{2+*} with Mn^{IV} pyrophosphate, reaching a quantum yield of 0.3 %.^[32] Later, they could show that the oxygen evolution rate of this system was not only conserved, but even increased by nearly two orders of magnitude when placed into a lipid bilayer. The quantum yield was increased to 17 % as well.^[33] They sonicated a mixture of 1,2-dipalmitoyl-*sn*-glycero-3-phosphocholine (DPPC, **L1**) and MnSO₄·H₂O to form vesicles with manganese hydroxo complexes at the interface of the membrane (Figure 1.7).

The oxidation state of the manganese hydroxo complexes was determined to be +III both spectroscopically and by reaction with oxalic acid. A multinuclear manganese hydroxo complex with at least one manganese atom in the oxidation state +V was proposed as the active site for water oxidation, because vesicles with Mn^{IV} were inactive towards water splitting, due to an insufficient oxidation potential of 0.5 V vs. NHE.^[34]

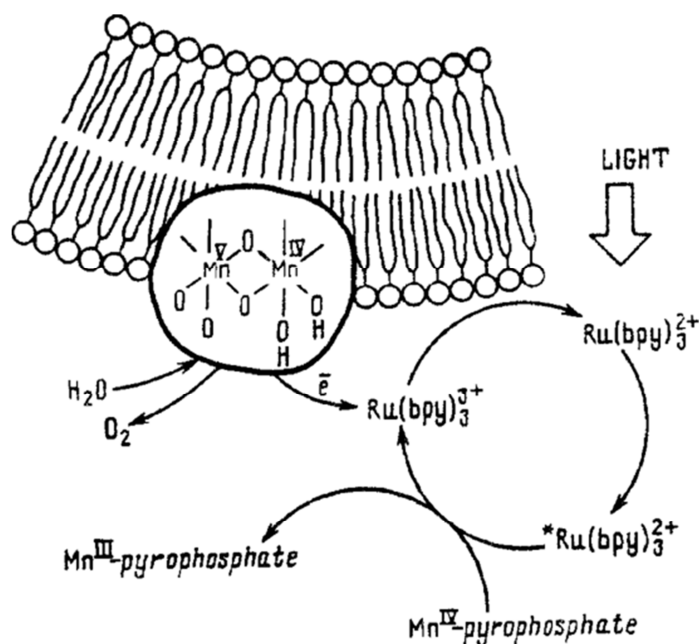


Figure 1.7 - Photocatalytic formation of oxygen at manganese complexes immobilized on the bilayer membrane of vesicles (reprinted from reference [34] with permission from Springer).

Membrane-bound manganese complexes could have been a first step on the evolution of the complex structure of photosystem II. A possible answer to the question why manganese was incorporated by nature instead of other metals, such as Cr, Fe, Co, Ni or Cu, was later given by Shilov, [34] who created water-oxidizing systems by adsorbing different metal ions at bilayer interfaces during the vesicle preparation and performed water oxidation with [Ru(bpy)₃]³⁺ or [Fe(bpy)₃]³⁺ as sacrificial electron acceptors at various pH values. Interestingly, only the manganese-functionalized liposomes were stable, whereas the other metals caused agglutination of the unilamellar vesicles. All metal hydroxo complexes except chromium produced oxygen when the stronger oxidant [Ru(bpy)₃]³⁺ was used, but the manganese complexes showed the highest activity at neutral pH and below. In addition, only Mn, Ni, and Co stayed active toward water oxidation with the weaker oxidant [Fe(bpy)₃]³⁺. Shilov also tested one of the most efficient water oxidation catalysts, RuO₂, immobilized at the interface of vesicles, but observed only CO₂ formation from the oxidation of the lipids. This work gave the first hints towards the nature of photosystem II in photosynthesis and claimed to be the closest model of the active site at that time.

Recently, König and co-workers took up the concept of using vesicles as supports for photochemical water oxidation systems and created, for the first time, a system in which both

photosensitizer **PS5** and catalyst **Cat1** were embedded as amphiphiles in a phospholipid bilayer membrane (Figure 1.8).^[35]

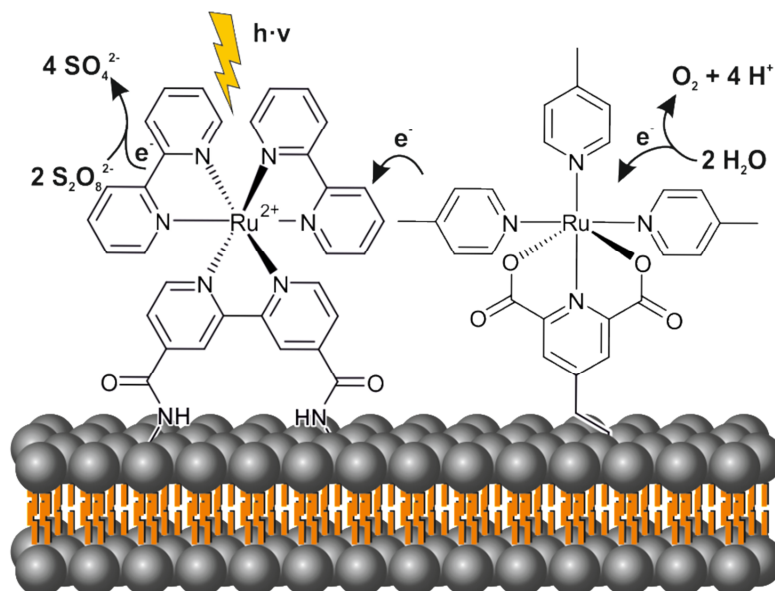


Figure 1.8 - Simplified representation of the proposed reaction mechanism for photochemical water oxidation by **PS5** and **Cat1** embedded in a phospholipid bilayer membrane, as reported by König and co-workers (adapted from reference [35] - with permission from the Royal Society of Chemistry).

A water oxidation system consisting of a $[\text{Ru}(\text{bpy})_3]^{2+}$ derivative and a ruthenium complex catalyst, previously established for homogeneous reactions by Sun and co-workers,^[36] was modified by introduction of alkyl chains. These artificial amphiphiles were co-embedded into DMPC (**L2**, Figure 1.5) membranes to bring them in close proximity. The vesicular water oxidation systems proved to be superior in catalytic turnover to a similar homogeneous system when the overall concentration of catalyst was very low. The membrane-bound system reached a TON of 394 at a 500 nM catalyst concentration, whereas the homogeneous one was inactive under similar conditions. The membrane fluidity influenced the catalytic performance due to a difference in the self-organization of the complexes. Gel-phase membranes from **L2** and SMPC (**L3**, Figure 1.5), where phase separation is favored, showed the highest TONs. The limiting factor of the vesicular system and in the related homogeneous systems is the stability of the photosensitizer **PS5**. This was verified by a reactivation of the system after the addition of new photosensitizer.

In 2015, Ohba and co-workers reported the regulation of a chemical water oxidation system bound to phospholipid vesicles (Figure 1.9).^[37] They regulated the system by the introduction of the ruthenium water oxidation catalysts **Cat2** and **Cat3** with different linker

lengths (Figure 1.4.). In addition, they adjusted the catalytic performance in Ce^{4+} -driven water oxidation by the nature of the lipids they used.

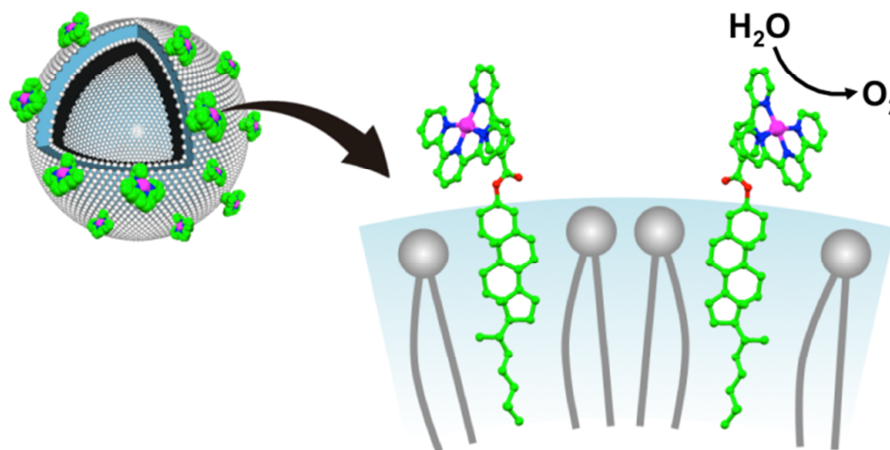


Figure 1.9 - Schematic representation of the composite of a liposome and the lipophilic Ru complex **Cat3** (reprinted from reference [37] with permission from the Royal Society of Chemistry).

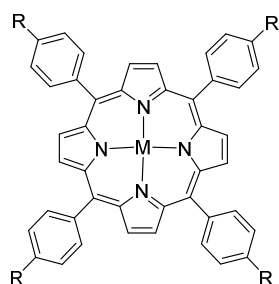
They could show that the ruthenium center of **Cat3** with the shorter linker is embedded in the head-group region of the membrane and thus has a reduced accessibility for the Ce^{4+} oxidant. Indeed the catalytic performance of **Cat3** is lower than that of **Cat2**. The nature of the lipid also played an important role. Vesicles comprised of negatively charged lipids with a net negatively charged surface, such as DSPA **L5** and DSPG **L6** (Figure 1.5), performed better in chemical water oxidation than vesicles made of the zwitterionic lipid DSPC (**L4**), which had had a net positive charge due to the catalyst. A UV/Vis spectroscopic analysis confirmed that functionalized vesicles prepared from **L5**, with small negatively charged head groups, showed the fastest reaction with Ce^{4+} . This was attributed to a better accessibility of the catalyst by Ce^{4+} .

1.4 Photocatalytic Hydrogen Production

1.4.1 Vesicular Systems for Hydrogen Production

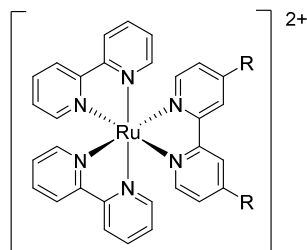
In 1983, Tsvetkov *et al.* successfully combined electron transfer across vesicle membranes with photocatalytic hydrogen production.^[38] The catalytic system consisted of lecithin vesicles with zinc tetraphenylporphyrin (**PS6**, Figure 1.10) as the photosensitizer located in the lipid bilayer, EDTA as the electron donor in the inner water pool, and methyl viologen (MV^{2+}) as the electron acceptor and relay in the surrounding media.

Photosensitizers:

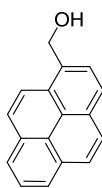
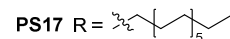
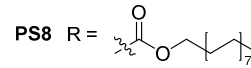
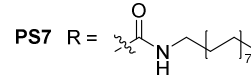
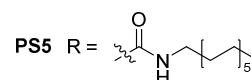


PS4 M = Sn, R = H

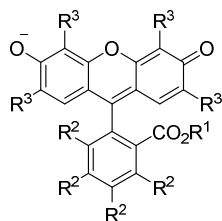
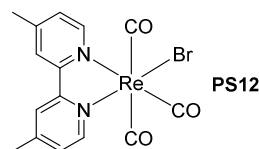
PS6 M = Zn, R = H

PS11 M = Zn, R = SO₃⁻

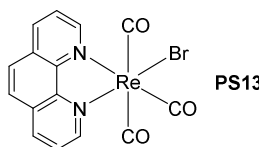
PS3 R = H



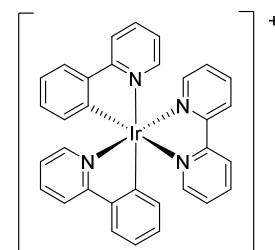
PS9

PS10 R¹ = , R² = H, R³ = BrPS15 R¹ = H, R² = H, R³ = BrPS16 R¹ = H, R² = Cl, R³ = I

PS12

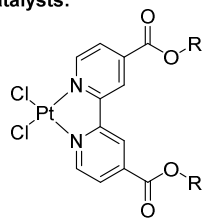


PS13

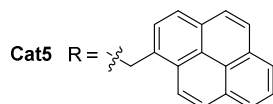


PS14

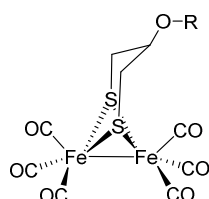
Catalysts:



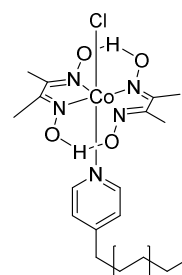
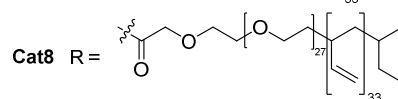
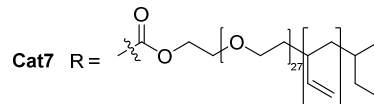
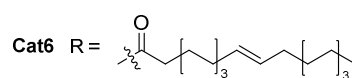
Cat4 R =



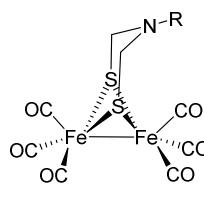
Cat5 R =



Cat9 R = H

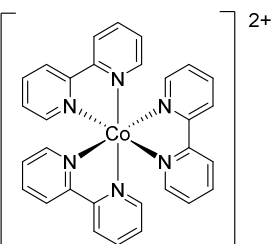


Cat10

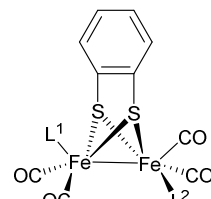
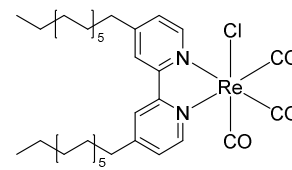


Cat11 R =

Cat12 R =



Cat13

Cat14 L¹ = L² = COCat15 L¹ = P(OMe)₃, L² = COCat16 L¹ = L² = P(OMe)₃

Cat17

Figure 1.10 - Structures of photosensitizers and catalysts used in self-assembled systems for the reductive half-reaction of water.

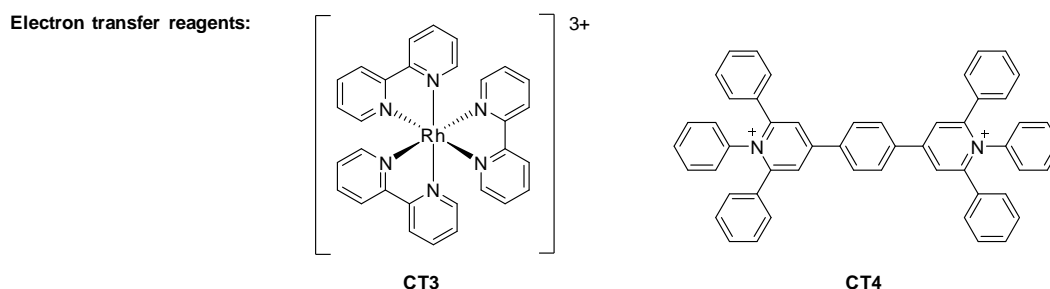


Figure 1.11 - Structures of the electron transfer agents used in proton reduction.

Photoinduced electron transfer across the vesicle membrane resulted in an accumulation of the methyl viologen cation radical ($MV^{\bullet+}$) on the outside of the vesicles (Figure 1.12). After external addition of a hydrogen-evolving catalyst, which was a heterogeneous polymer-supported colloidal rhodium catalyst, hydrogen was produced with a quantum yield of about $3.4 \times 10^{-3} \%$. When using a hydrogenase from *Thiocapsa roseopersicina* cells instead, a specific enzyme for $MV^{\bullet+}$, a steady-state concentration of $MV^{\bullet+}$ on the outside of the vesicles and an increased hydrogen evolution with a higher quantum yield of about $1.0 \times 10^{-2} \%$ were observed. Nevertheless, the rate of photocatalytic hydrogen generation using the more active hydrogenase catalyst was 10 times lower than in a dark reaction in the presence of chemically prepared $MV^{\bullet+}$.

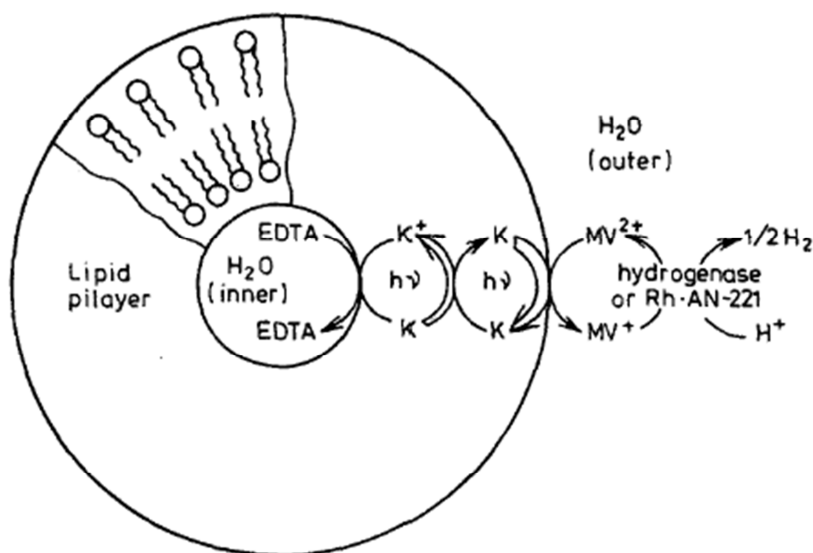


Figure 1.12 - Photoinduced transmembrane electron transfer in lecithin vesicles and hydrogen evolution in the surrounding aqueous solution. K stands for photosensitizer **PS6** (reprinted from reference [38] with permission from Springer).

Light-driven hydrogen generation from ruthenium-coated didodecyldimethylammonium bromide (**S3**) vesicles was described by Park.^[39] The amphiphilic ruthenium complex **PS7**, bearing two hydrophobic alkyl chains, was embedded in the vesicular membrane as the light-harvesting complex, whereas colloidal ruthenium covered the outer surface of the bilayered vesicular membrane as the reduction catalyst. The precursor RuCl_5^{2-} , which was added after vesicle preparation and binds to the positively charged vesicle surface, was reduced by addition of sodium borohydride to coat the surface with colloidal ruthenium. The attachment of the ruthenium catalyst on the wall of the vesicle was proven by control experiments in the absence of vesicle support. These experiments showed a precipitation of particles upon centrifugation, whereas in the presence of vesicles, no precipitation was observed. When the two-electron donors ferrous chloride ($\text{FeCl}_2 \times 4 \text{ H}_2\text{O}$) and a phenothiazine derivative were used simultaneously, the functionalized vesicles showed hydrogen generation upon blue-light irradiation with a quantum yield of 3.3×10^{-4} . The mixture of both electron donors was mandatory for hydrogen generation. Whereas the phenothiazine derivative was proposed to reductively quench the excited state of the amphiphilic photosensitizer **PS7**, ferrous chloride regenerated the oxidized phenothiazine derivative in the hydrogen-evolving system.

Between 1984 and 1988, Fendler and co-workers reported a series of studies on photocatalytic hydrogen production using in situ-generated Rh-coated CdS semiconductor particles dispersed and stabilized in vesicular membranes. They were prepared from anionic dihexadecylphosphate **S4** (DHP), cationic dioctadecyldimethylammonium chloride **S5** (DODAC) or bromide **S6** (DODAB), and the polymerizable cationic surfactant **S7**.^[40-43] These vesicles controlled the size of the in situ-synthesized catalytic particles and kept them stable in aqueous solution for months. CdS semiconductor particles were prepared from Cd^{2+} cations by an introduction of H_2S . The cadmium cations adsorbed spontaneously to negatively charged **S4** membranes or, after a charge inversion by complexation with EDTA, to positively charged surfaces of **S5**, **S6**, or **S7**. The reduction of adsorbed or EDTA-complexed Rh^{3+} to give catalytically active Rh^0 particles on the CdS semiconductor particles was performed either by UV irradiation in the absence of an electron donor or by visible-light irradiation in its presence. From spectroscopic studies and the fact that no precipitation was observed, even after months, the authors proposed that the Rh-coated CdS particles are membrane bound and partially buried in the bilayered **S4**, **S5**, or **S6** membrane. Polymerization of the styrene headgroups in unpolymerized surfactant vesicles prepared from **S7** resulted in the formation of surface clefts in the vesicle membrane, which were proposed to be the sites of the catalyst particles (Figure 1.13).

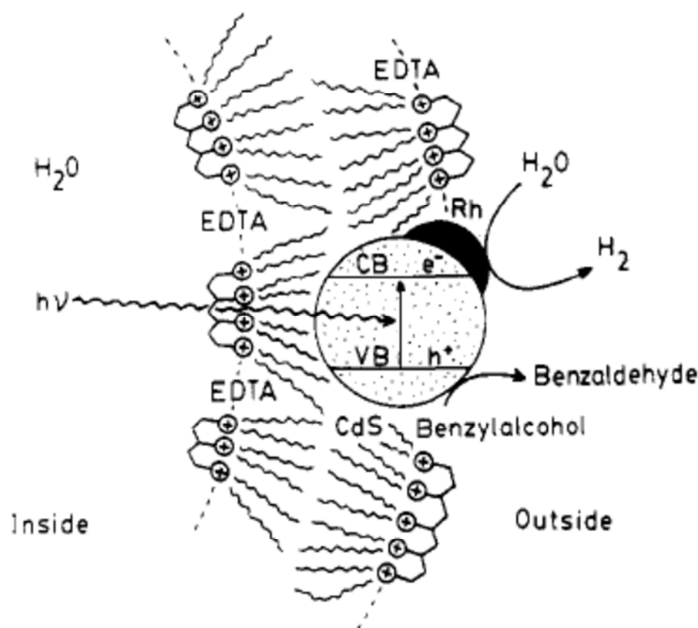


Figure 1.13 - Schematic representation of hydrogen generation in polymerized **S7** vesicles with colloidal Rh-coated CdS particles located in surface clefts (reprinted from reference [43] with permission from the American Chemical Society).

Light-driven hydrogen production was performed from anionic, cationic, unpolymerized, and polymerized surfactant vesicles in the presence of thiophenol (PhSH), EDTA, or benzyl alcohol as sacrificial electron donors. Hydrogen was produced with nearly complete consumption of PhSH in **S4** or **S5** vesicles and a quantum yield of 10 % was determined for hydrogen generation using benzyl alcohol in polymerized **S7** vesicles. Interestingly, EDTA was not suitable as the electron donor in unpolymerized surfactant **S7** vesicles, but efficiently promoted hydrogen generation in polymerized surfactant **S7** vesicles. This result supported the proposed clefts in polymerized membranes to be the sites of the catalytic Rh-CdS particles providing higher accessibility to the polar electron donor EDTA.

However, the use of electron donors in high concentrations and the accumulation of oxidized electron donors in the membrane bilayer, for example, hydrophobic PhSSPh from oxidation of PhSH, destabilized the vesicles. To inhibit precipitation and to enable more efficient hydrogen generation, the thiol-functionalized DODAC derivative **S8** was used, which served both as a surfactant and as a recyclable electron donor.^[44] Rh-coated CdS particles bound to mixed vesicles of DODAC (**S5**) and the surface-active electron donor **S8** showed photosensitized hydrogen evolution. It was promoted by the oxidation of membrane-embedded electron donor **S8**, which led to disulfide formation and dimerization of **S8**. The resulting vesicle-

embedded disulfide of **S8** could be regenerated by sodium borohydride and reused in further experiments with a constant rate of hydrogen evolution (Figure 1.14).

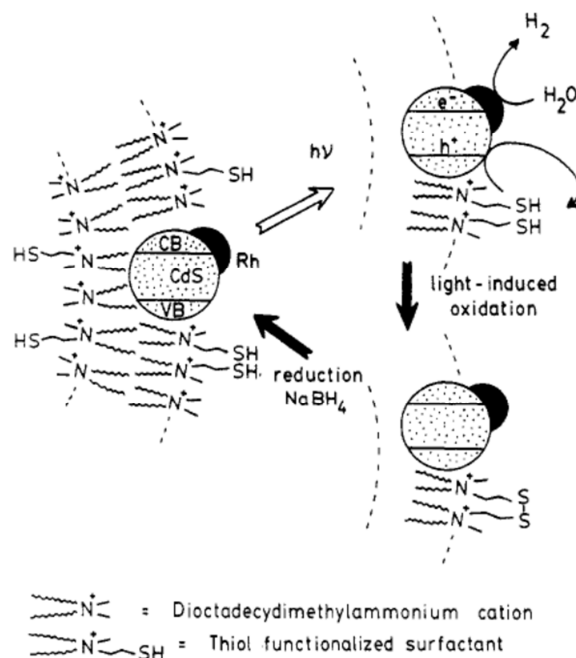


Figure 1.14 - Proposed hydrogen evolution from CdS semiconductor particles embedded in vesicles containing the thiol-functionalized surfactant **S8** as a recyclable electron donor (reprinted from reference [44] with permission from the American Chemical Society).

In a follow-up study, Fendler and co-workers replaced the Rh-coated CdS catalyst in DHP (**S4**) vesicles by ZnS-coated CdS or mixed crystals of $Zn_xCd_{1-x}S$ and observed hydrogen evolution in the absence of noble metal reducing catalysts.^[45] With benzyl alcohol as the sacrificial electron donor, ZnS-coated CdS gave more efficient photoinduced hydrogen evolution than $Zn_xCd_{1-x}S$ or pure CdS particles. The best results were obtained with a 1:1 ratio of Cd and Zn in coated semiconductor particles and substantial hydrogen generation was determined even after 48 h of illumination.

Maier and Shafirovich took advantage of the fact that vesicle membranes can be used for compartmentation when they studied hydrogen evolution in oxidizing media.^[46] A catalytic system consisting of the electron donor EDTA, the light-harvesting complex $[Ru(bpy)_3]^{2+}$ (**PS3**), the electron relay $[Rh(bpy)_3]^{3+}$ (**CT3**) and Pt particles as catalyst for hydrogen evolution was encapsulated into DPPC (**L1**) vesicles, whereas the oxidant $[Fe(CN)_6]^{3-}$ was present in the bulk solution outside the vesicles. Upon light irradiation, an accumulation of reduced Rh species on the inside of the Pt-deficient vesicles was observed. In the presence of catalytic Pt

particles, hydrogen was produced with a quantum yield of 2 % and a TON of 14, based on **PS3**, was calculated under optimized conditions. The surrounding oxidizing media containing $[\text{Fe}(\text{CN})_6]^{3-}$ affected neither the accumulation of reduced Rh species nor the hydrogen evolution. Therefore, the compartmentation of reducing and oxidizing media with vesicular bilayered membranes protected hydrogen evolution from oxidizing media.

The ability to use bilayered vesicles with aqueous cores for compartmentation was later verified by Efimova *et al.*^[47] In their catalytic system, the lipophilic, reversible electron relay **CT4** (Figure 1.11), which can be reduced chemically and photochemically by two electrons, served as a molecular wire. It promoted photoinduced electron transfer across **L1** vesicle membranes coupled with hydrogen generation from a dispersed vesicle-stabilized Pd catalyst. The catalytic system for light-driven hydrogen production was composed of EDTA as the electron donor, **PS3** as the photosensitizer, the electron mediator **CT4**, located in the hydrophobic interior of the lipid bilayer, and finely dispersed Pd particles as catalyst supported by **L1** vesicles. Photocatalytic hydrogen production continued after the addition of the oxidant $\text{K}_3[\text{Fe}(\text{CN})_6]$ to the outer water phase of a vesicular solution with EDTA, **PS3**, and the Pd catalyst located inside the vesicle cavities. Conversely, $\text{K}_3[\text{Fe}(\text{CN})_6]$ completely shut down hydrogen evolution when EDTA and **PS3** were located within the vesicle cavities and the Pd catalyst was supported only on the outer membrane surface. These results indicated that membrane compartmentation protected the catalytic system in the vesicle's inner cavities from the surrounding oxidizing media and that hydrogen evolution with EDTA and **PS3** on the inside and Pd catalyst on the outside of the vesicles was induced by electron transfer across the membrane mediated by **CT4** as electron carrier embedded in the hydrophobic bilayer.

Interestingly, photocatalytic hydrogen production has been accomplished by vesicles made only from the amphiphilic photosensitizer and surfactant **PS8**, which self-assembled into closed-spherical unilamellar vesicles in an aqueous solution without any additional surfactant.^[48, 49] With EDTA as the sacrificial electron donor, these **PS8** ruthenium photosensitizer vesicles showed superior light-induced photoreduction of methyl viologen (MV^{2+}) in comparison with vesicular systems with DODAB (**S6**) as additional surfactant or homogeneous non-vesicular systems with **PS3** as the light-harvesting complex. When the electron acceptor methyl viologen (MV^{2+}) was replaced by hydrogen-evolving catalysts, which were colloidal Rh particles attached to the vesicle surface, hydrogen was produced with vesicles prepared only from the photosensitizer **PS8**. The amount of evolved hydrogen increased from 23 in the absence of Rh catalyst particles to 1 mL in their presence after 3 h irradiation, with a quantum yield of $1.2 \times 10^{-2} \%$.

In 2011, Murata and co-workers reported hydrogen generation from vesicular systems with colloidal platinum or molecular platinum complexes as catalysts.^[50, 51] In both catalytic systems, hydrogen evolution was initiated by electron transfer from ascorbate encapsulated in the inner cavity of **L1** vesicles across the bilayered membrane to the electron mediator MV^{2+} dissolved in the surrounding aqueous solution. In the first system, 1-(hydroxymethyl)-pyrene **PS9** ($PyCH_2OH$) embedded in the vesicle bilayer efficiently sensitized the transmembrane electron transfer and the formation of reduced methyl viologen ($MV^{\bullet+}$) on the outside of the vesicles. The utilization of colloidal surfactant-protected platinum particles as catalysts in the vesicle surrounding aqueous solution resulted in the formation of hydrogen with a quantum yield of 0.16 %. However, the use of surfactant-protected Pt particles as catalyst was not satisfactory, since the platinum-protecting surfactant proved disadvantageous for the vesicle stability and limited the construction of more efficient catalytic vesicular systems.

To overcome this problem, hydrogen production was accomplished with molecular Pt complexes **Cat4** or **Cat5** embedded into **L1** vesicles. By combining the amphiphilic Pt complex **Cat4** and the hydrophobic photosensitizer **PS9**, both embedded in the vesicular membrane, transmembrane electron transfer from ascorbate to methyl viologen with the formation of the reduced methyl viologen ($MV^{\bullet+}$) in the outer solution was successfully linked to hydrogen production by complex **Cat4** (Figure 1.15). A TON of 30 was calculated for catalyst **Cat4**. Conversely, the embedded photocatalyst **Cat5**, in which light-harvesting pyrene moieties were covalently attached to the Pt catalyst, led neither to the formation of $MV^{\bullet+}$ nor to hydrogen evolution upon light irradiation. It was proposed that the photoexcited pyrene moieties are efficiently quenched by the covalently bound Pt complex, inhibiting electron transfer across the lipid bilayer and thus hydrogen production. However, photocatalyst **Cat5** was found to be an active hydrogen-evolving catalyst (TON = 51 based on **Cat5**) when triethanolamine (TEOA) and MV^{2+} were added to vesicular solutions with membrane-incorporated **Cat5** in the absence of ascorbate in the inner cavity.

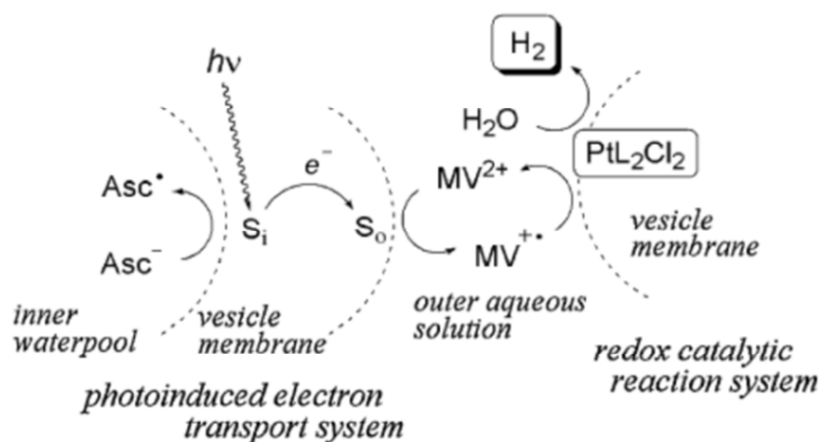


Figure 1.15 - Proposed mechanism for the photosensitized electron transfer across vesicle membranes coupled with hydrogen evolution from the membrane-embedded molecular platinum complex **Cat4** (abbreviated as PtL_2Cl_2). S stands for the pyrene photosensitizer **PS9** (reprinted from reference [51] with permission from the Chemical Society of Japan).

In a further approach using vesicle membranes as model systems mimicking photosynthesis, Menzel *et al.* described the synthesis and successful incorporation of the amphiphilic [2Fe2S] clusters **Cat6**, **Cat7** and **Cat8** (Figure 1.5) into vesicular structures.^[52] Synthetic iron-sulfur clusters serve as model complexes of the [2Fe2S] subunit in the hydrogen-evolving active site of [FeFe]-hydrogenases and are promising candidates in the development of efficient catalytic systems for hydrogen production. For incorporation into vesicles, the [2Fe2S] moiety **Cat9** was covalently attached to amphiphilic molecules of either oleic acid or the block copolymer 1,2-polybutadiene-poly(ethylene oxide) **S9** (PB-PEO) to give the [FeFe]-hydrogenase model complexes **Cat6** or **Cat7** and **Cat8**, respectively. The oleic acid-modified model complex **Cat6** was incorporated into POPC (**L7**, Figure 1.5) vesicles and Cryo-TEM images confirmed the formation of unilamellar and some multilamellar vesicles after extrusion. However, the extrusion process of the vesicle dispersions to obtain a homogeneous size distribution led to aggregation and loss of the amphiphilic [FeFe]-hydrogenase model complex **Cat6**. Therefore, only 3.15 mol% of **Cat6** could be embedded into **L7** vesicles. Polymer-modified iron-sulfur clusters **Cat7** and **Cat8** were embedded in a fraction of up to 28 mol% into vesicles formed from **S9** surfactants. In addition, it was possible to prepare stable assemblies consisting of 100 mol% amphiphilic iron-sulfur clusters **Cat7** and **Cat8** without the need of additional surfactants by a THF-injection method. In the latter case, besides vesicle formation, tube, network, or open structures were found, which were stable for at least one month, and a 100 % recovery of the hydrogenase model complexes **Cat7** or **Cat8** was possi-

ble. The reported functionalized vesicular structures with membrane-bound [FeFe]-hydrogenase model complexes may mimic natural photosynthesis. However, catalytic activity towards hydrogen production had not been investigated.

Recently, Troppmann and König reported the functionalization of vesicles for photocatalytic hydrogen production by the self-assembly of amphiphilic photosensitizers and a cobalt-based hydrogen-generating catalyst in phosphocholine lipid membranes (Figure 1.16).^[53] Ruthenium (**PS5**) or Eosin Y (**PS10**)-based photosensitizers and the cobaloxime reduction catalyst **Cat10** (Figure 1.10), bearing hydrophobic alkyl chains, were co-embedded in vesicles prepared from different phospholipids.

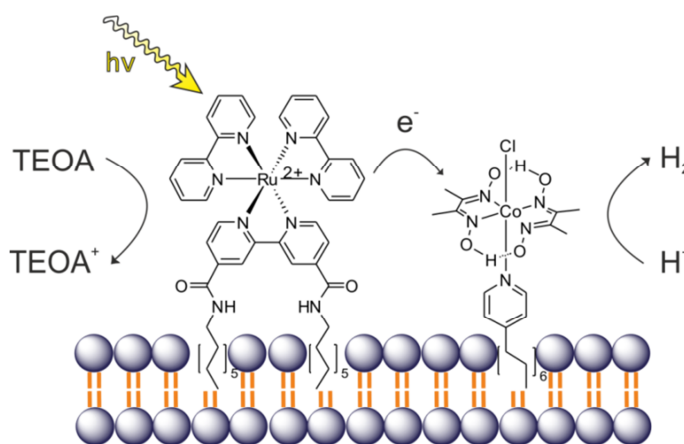


Figure 1.16 - Schematic representation of functionalized membranes for hydrogen production with co-embedded photosensitizer **PS5** and catalyst **Cat10** (adapted from reference [53] with permission from Wiley VCH).

In the presence of triethanolamine (TEOA) as the sacrificial electron donor, light-driven hydrogen generation was achieved yielding a TON of 165 for the cobalt catalyst **Cat10** in the presence of the ruthenium photosensitizer **PS5**. The activity of the two-dimensional catalytic arrangement was strongly influenced by the membrane fluidity. Superior hydrogen evolution was observed in fluid membranes, providing high mobility and dynamic self-reorganization of the co-embedded photosensitizer and catalyst, compared with rigid gel-phase membranes with restricted diffusion. Unfortunately, the catalytic activity decreased when using the amphiphilic metal-free Eosin Y photosensitizer **PS10**, most probably due to clustering and self-quenching of the embedded **PS10** in membrane patches. Therefore, besides the choice of suitable redox-active components, the physical properties of vesicles and the assembly structure in the membrane are important for creating highly efficient membrane-supported assemblies for artificial photosynthesis.

1.4.2 Micellar Systems for Hydrogen Production

In addition to closed-spherical bilayered vesicles, micelles are suitable dynamic self-assembling systems that can mimic photosynthetic cell membranes.

Inspired by biological systems with hydrogenase enzymes producing hydrogen with an outstanding efficiency, Okura and Amao used a purified hydrogenase from *Desulfovibrio vulgaris* as catalyst and investigated photocatalytic hydrogen production in micellar media.^[54-57] The effect of anionic, cationic, and non-ionic surfactants on a hydrogen evolution system consisting of triethanolamine (TEOA) as the sacrificial electron donor, a water-soluble zinc tetraphenylporphyrin tetrasulfonate **PS11** (ZnTPPS₄, Figure 1.10) as the photosensitizer, methyl viologen (MV²⁺) as the electron mediator, and the hydrogenase as the hydrogen-evolving catalyst was examined.

The addition of ionic and non-ionic surfactants in hydrogenase-free systems resulted in an increase in the rate of photoreduction of MV²⁺ by **PS11** and the lifetime of reduced methyl viologen (MV^{•+}) was prolonged. In addition, the rate constant for the back electron transfer from MV^{•+} to the oxidized **PS11** was significantly decreased in the presence of surfactants. These results verified that micelles are ideal dynamic assemblies for efficient charge separation and retardation of back electron transfer.

In photoinduced hydrogen production experiments with the above-mentioned system using hydrogenase as the catalyst, hydrogen evolution was remarkably increased in the presence of cationic and non-ionic surfactants. Under optimized conditions in cationic cetyltrimethylammonium bromide (CTAB, **S10**) micellar solutions, a 50-fold increase in the rate of hydrogen production was estimated in comparison with conventional conditions without the surfactant CTAB. Light-driven hydrogen production was also increased in various non-ionic surfactant micellar solutions. The addition of anionic SDS surfactants resulted in a denaturation of the hydrogenase and in little hydrogen production.^[58]

In natural photosynthesis, chlorophyll dyes play a crucial role in efficient light harvesting for solar energy conversion. Therefore, Tomonou and Amao used Mg chlorophyll *a* (MgChl *a*) as a photosensitizer with absorption bands in the visible and near-IR regions in light-driven hydrogen production.^[59-61] As MgChl *a* is water insoluble, cationic or non-ionic surfactants were added to overcome solubility problems in water by incorporation of the hydrophobic chromophore into the nonpolar micellar core. Visible and near-IR light-induced hydrogen evolution was observed when NADH or NADPH as the electron donor, MgChl *a* as the photosensitizer, methyl viologen as the electron mediator, and colloidal platinum par-

ticles as the catalyst were present in micellar solution. The hydrogen evolution depended on the surfactant used for solubilizing MgChl *a*. Cationic CTAB micelles were found to be more efficient than non-ionic micelles, which was explained by suppressed back electron transfer from reduced methyl viologen ($MV^{\bullet+}$) to oxidized MgChl *a* due to an electrostatic repulsion between the cationic $MV^{\bullet+}$ and the cationic photosensitizer MgChl *a* embedded in positively charged CTAB micelles. Among different cationic alkyltrimethylammonium bromide surfactants, which differ in the length of the alkyl chain, micelles formed from CTAB showed the highest activity in hydrogen evolution.^[62]

To overcome the problem of photodegradation of magnesium chlorophyll dyes in micellar solution, the negatively charged, hydrophilic carotenoid dye crocetin, which acted as a cut-off filter, was adsorbed to the positively charged surface of CTAB micelles with included chlorophyll dyes (Mg chlorophyll *a* and *b*).^[63] The immobilization of crocetin on the micellar surface resulted in a photoinduced energy transfer from adsorbed excited crocetin to micelle-embedded Mg chlorophyll *a* and *b* and suppressed the photodegradation of these chlorophyll dyes in the micellar interior. Therefore, when applied in photocatalytic hydrogen production by using NADH, methyl viologen, and colloidal platinum particles, the crocetin-chlorophyll micellar assembly gave rise to superior hydrogen evolution than in the absence of crocetin.

Hori and co-workers investigated photocatalytic hydrogen production by micellar systems with the incorporated hydrophobic tin tetraphenylporphyrin photosensitizer **PS4** (SnTPP), colloidal Pt particles as the catalyst, and 2-mercaptoethanol as the electron donor.^[64] In anionic and cationic micellar solutions, small amounts of hydrogen evolved and yielded 1 and 5 TONs, respectively after 6 h of irradiation. The coulombic attraction or repulsion of the charged surfaces in ionic micelles and either H^+ or the reduced photosensitizer $SnTPP^{\bullet-}$ was proposed to slow down efficient hydrogen production. However, by using non-ionic Brij 30 (**S2**) micelles, these unfavorable coulombic interactions were avoided and the amount of evolved hydrogen was enhanced to 9 and 30 turnovers after 6 and 12 h of irradiation, respectively.

Wang *et al.* used SDS micelles to solubilize the water-insoluble rhenium photosensitizers **PS12** and **PS13** as well as the diiron proton reduction catalysts **Cat11** and **Cat12** in aqueous solution (Figure 1.17).^[65] The incorporation of these lipophilic photosensitizers and catalysts into the hydrophobic interior of SDS micelles was verified by spectroscopic studies, showing significantly enhanced water solubility with increased absorbance and emission upon addition of a SDS micellar solution to these water-insoluble complexes. Light-induced hydrogen generation was observed for approximately 1 h with a maximal TON of 0.13 based on cata-

lyst **Cat11** in the presence of **PS12** as the photosensitizer and ascorbic acid as both the electron donor and the proton source, which was proposed to be incorporated in the micelles as well. Since the complexes **PS12** and **Cat11** had a higher solubility in SDS micelles than the complexes **PS13** and **Cat12**, it was proposed that the close proximity in a mixture of **PS12** and **Cat11**, both incorporated in the micellar hydrophobic core, promoted the hydrogen evolution. Besides the remarkably increased water solubility of the hydrophobic catalytic subunits, which allowed hydrogen production in water, the micellar assembly enhanced the stability of the Fe_2S_2 complexes **Cat11** and **Cat12** toward light irradiation, in comparison with CH_3CN solution.

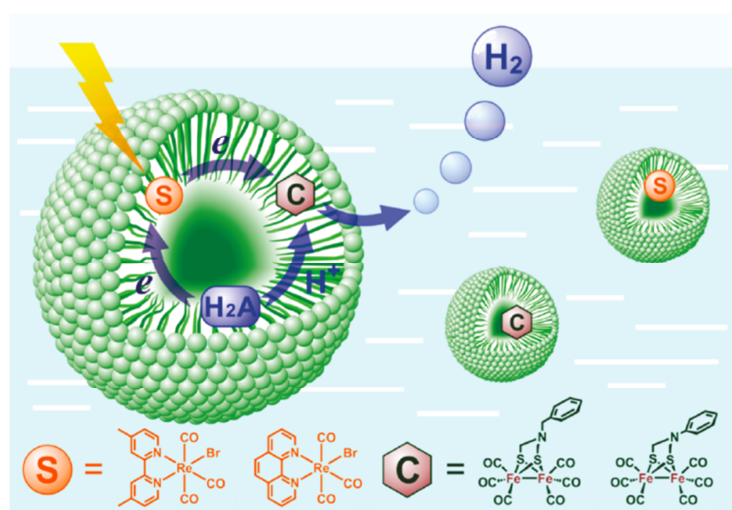


Figure 1.17 - Schematic representation of micellar hydrogen evolution reported by Wang *et al.* H_2A represents ascorbic acid. (reprinted from reference [65] with permission from the American Chemical Society).

Beside the use of micelles as support in water, the utilization of micellar environments to enhance hydrogen production in a mixture of water and organic solvent was also reported.^[66] The effect of cationic, anionic and non-ionic micelles on light-driven hydrogen evolution from a multicomponent system in a mixture of water and acetonitrile (8:2) was investigated. The catalytic system consisted of $[\text{Ir}(\text{ppy})_2(\text{bpy})]^+$ (**PS14**) as the photosensitizer, $[\text{Co}(\text{bpy})_3]^{2+}$ (**Cat13**) as the catalyst, and the sacrificial electron donor TEOA. The presence of cationic CTAB micelles efficiently enhanced hydrogen production from a $\text{TON} = 13$ for the iridium photosensitizer in homogeneous solution to $\text{TON} = 79$ in 100 mM micellar CTAB solution after 6 h of irradiation. Upon continuous irradiation for 20 h, the TON could even be enhanced to 135 in 30 mM aqueous micellar solution containing CTAB micelles. It was found that hydrogen evolution was promoted in the order of cationic micelles > non-ionic micelles > anionic micelles > homogeneous water/acetonitrile solution. Luminescence experiments

showed the incorporation of the catalytic subunits into the micellar structures with enhanced luminescence quenching of **PS14** in the presence of micelles. As the catalytic subunits are well soluble in a mixture of water and acetonitrile (8:2), the solubilization effect of the micellar media on the hydrogen production efficiency was excluded. Instead, an assembly effect of photosensitizer and catalyst in the interior or at the interface of the microheterogeneous environment, resulting in high concentration and close proximity, was proposed to enhance intermolecular interactions and hydrogen evolution. Although not investigated, the authors claimed that the balance of coulombic and hydrophobic interactions in cationic micelles locates the catalytic subunits close to the interface with high penetration of TEOA and protons, whereas in anionic micelles, the photosensitizer and catalyst are deeply buried within the hydrophobic region.

Recently, micelles were used for photocatalytic hydrogen production in aqueous solutions with a noble metal-free catalytic system consisting of the xanthene dye photosensitizers Eosin Y (**PS15**) or Rose Bengal (**PS16**) in combination with the iron-sulfur complexes **Cat14**, **Cat15**, or **Cat16**.^[67] These synthetic iron clusters, which served as model complexes of [FeFe]-hydrogenases, catalyzed proton reduction in basic aqueous micellar SDS solutions (pH 10.5). The most active system, consisting of Eosin Y and the iron-based catalyst **Cat14** in aqueous SDS solution, produced hydrogen with a quantum yield of 1.1 % (TON = 117 based on catalyst **Cat14**) in the presence of triethylamine as the sacrificial electron donor under continuous blue-light irradiation for 4.5 h. Hydrogen production in this system was mainly limited by the destruction of the organic photosensitizer. However, with high concentrations of Eosin Y, hydrogen evolved over a period of more than 30 h, indicating a significant stability of catalyst **Cat14** in SDS micelles. In addition, an enhanced stability of the reduced form of the catalyst **Cat14**, a $\text{Fe}^0\text{Fe}^{\text{I}}$ species, which is involved in the photocatalytic H_2 production, was observed. The beneficial influence of the micellar media was further verified with a homogeneous experiment in ethanol/water (1:1) in the absence of SDS. The TONs were four times lower than in aqueous micellar SDS solutions. Less efficient hydrogen evolution was observed when either the photosensitizer was exchanged for Rose Bengal (**PS16**) or the catalyst for **Cat15** or **Cat16**, due to a smaller driving force for the electron transfer.

1.5 Overall Water Splitting System at Vesicular Membranes

A system for water splitting without sacrificial reagents using vesicles was reported by Park and co-workers in 1993.^[68] Vesicles composed of the detergent dioctadecyldimethylammonium bromide (S5) were used as the support for colloidal HgS particles. HgS has a band gap broad enough to both reduce protons and oxidize water. Rhodium particles on the colloidal HgS functioned as the reduction catalyst. Interestingly, they did not use a catalyst for the direct oxidation of water to dioxygen, but proposed a mechanism whereby hydroxide ions are oxidized to hydroxyl radicals, which consequently form hydrogen peroxide at the HgS surface. This hydrogen peroxide is converted into oxygen by sodium borate to form sodium metaborate. Metaborate and water are in equilibrium with borate to close the catalytic cycle (Figure 1.18).

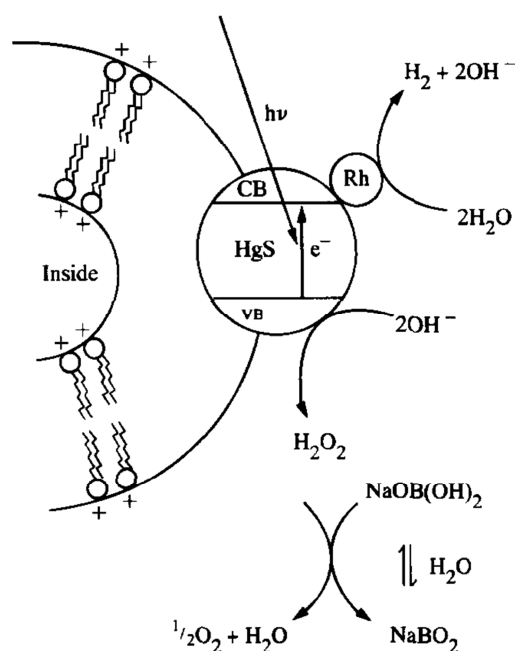


Figure 1.18 - Proposed mechanism for the generation of hydrogen and oxygen from water with vesicle-stabilized HgS colloids with Rh particles and NaBO₂ (reprinted from reference [69] with permission from Elsevier).

A year later, they could support the proposed mechanism by performing the water splitting in isotopically-labelled water H₂¹⁸O.^[69] Masses of 36 and 34 were detected with mass spectrometry, derived from ¹⁸O=¹⁸O and ¹⁸O=¹⁶O, respectively. The adsorption of HgS at the vesicle membranes was verified by transmission electron microscopy. The reason that the amount of oxygen in a first run was less than the expected stoichiometric ratio remains un-

clear, but, in a second run, the system produced hydrogen and oxygen in the expected 2:1 ratio. Park *et al.* also showed that HgS can be replaced by colloidal CdS particles, which exhibit comparable behavior.^[70]

1.6 Photocatalytic CO₂ Reduction

In addition to photocatalytic water splitting into oxygen and hydrogen, the conversion of sunlight into chemical energy by light-driven CO₂ reduction is of great interest in the field of artificial photosynthesis. Photocatalytic reduction of CO₂ has the potential to produce carbon-based fuels and chemicals from CO₂ as a sustainable feedstock.

Murata and co-workers described light-driven CO₂ reduction to CO in aqueous buffer solution using functionalized unilamellar DPPC (**L1**) vesicles with co-embedded amphiphilic ruthenium photosensitizer (**PS17**) and rhenium catalyst **Cat17** (Figure 1.10).^[71] For incorporation into vesicular membranes, both subunits were modified with hydrophobic alkyl chains. Size exclusion chromatography revealed the incorporation of about 85 % of the catalytic subunits after vesicle preparation. In the presence of ascorbate as the electron donor, a TON for photocatalytic CO₂ reduction of 190 based on the catalyst **Cat17** was obtained along with the formation of a small amount of H₂ as a byproduct. Photocatalytic CO₂ reduction ceased after 15 h of irradiation, which was attributed to the degradation of photosensitizer **PS17** under the experimental conditions. On the basis of a linear relationship between the initial rate of CO formation and the light intensity, the authors concluded that only one photon is required for a single two-electron reduction of CO₂ to CO. They proposed a second non-light-induced electron transfer step from ascorbate to the Re-CO₂ adduct involved in the formation of CO from CO₂.

1.7 Conclusion

In summary, self-assembled vesicles and micelles have found interesting applications as microreactors in the field of artificial photosynthesis. These dynamic aggregates were established as model systems for natural photosynthesis, as they could provide some advantages in developing catalytic systems for solar energy conversion. Vesicles and micelles are able to solubilize hydrophobic photosensitizers and catalysts in water without the need of organic solvents and protect incorporated catalytic units and intermediates against degradation. The microheterogeneous systems concentrate and assemble catalytic complexes in close contact in the interior or at the interface resulting in enhanced intermolecular interactions and high catalytic activity, even at very low concentrations. Efficient light-induced charge separation with suppressed back electron transfer has been reported. Enhanced reaction rates and more efficient photocatalytic oxygen and hydrogen production were observed in self-assembled vesicular or micellar systems than in homogeneous systems. The compartmentation provided by vesicular membranes allows separation of the reaction products and combination of different redox environments by spatial separation. In addition, energy transduction through efficient electron transfer across membranes was successfully connected to water oxidation and reduction. Therefore, artificial functionalized membranes may contribute to the development of more efficient photosensitized overall water splitting in the absence of sacrificial electron acceptors and donors when combining the two membrane-separated half reactions with transmembrane electron transfer resulting in simultaneous oxygen and hydrogen evolution at each side of the membrane.

1.8 References

- [1] R. Eisenberg, D. G. Nocera, "Preface: Overview of the Forum on Solar and Renewable Energy", *Inorg. Chem.* **2005**, 44, 6799-6801.
- [2] N. S. Lewis, D. G. Nocera, "Powering the planet: Chemical challenges in solar energy utilization", *PNAS* **2006**, 103, 15729-15735.
- [3] T. R. Cook, D. K. Dogutan, S. Y. Reece, Y. Surendranath, T. S. Teets, D. G. Nocera, "Solar Energy Supply and Storage for the Legacy and Nonlegacy Worlds", *Chem. Rev.* **2010**, 110, 6474-6502.
- [4] P. Du, R. Eisenberg, "Catalysts made of earth-abundant elements (Co, Ni, Fe) for water splitting: Recent progress and future challenges", *Energy Environ. Sci.* **2012**, 5, 6012-6021.
- [5] Z. Raoul, in Book "Introduction to Surfactants and Surfactant Self-Assemblies", CRC Press, **2005**, pp. 1-35.
- [6] F. Quentel, G. Passard, F. Gloaguen, "A Binuclear Iron-Thiolate Catalyst for Electrochemical Hydrogen Production in Aqueous Micellar Solution", *Chem. Eur. J.* **2012**, 18, 13473-13479.
- [7] F. Quentel, G. Passard, F. Gloaguen, "Electrochemical hydrogen production in aqueous micellar solution by a diiron benzenedithiolate complex relevant to [FeFe] hydrogenases", *Energy Environ. Sci.* **2012**, 5, 7757-7761.
- [8] R. Hilhorst, C. Laane, C. Veeger, "Photosensitized production of hydrogen by hydrogenase in reversed micelles", *PNAS* **1982**, 79, 3927-3930.
- [9] M. Meyer, C. Wallberg, K. Kurihara, J. H. Fendler, "Photosensitized charge separation and hydrogen production in reversed micelle entrapped platinized colloidal cadmium sulphide", *J. Chem. Soc., Chem. Commun.* **1984**, 90-91.
- [10] J. N. Robinson, D. J. Cole-Hamilton, "Electron transfer across vesicle bilayers", *Chem. Soc. Rev.* **1991**, 20, 49-94.
- [11] S. V. Lymar, V. N. Parmon, K. I. Zamarev, "Photoinduced Electron Transfer III ", Vol. 159, Springer, **1991**.
- [12] J. J. Grimaldi, S. Boileau, J.-M. Lehn, "Light-driven, carrier-mediated electron transfer across artificial membranes", *Nature* **1977**, 265, 229-230.
- [13] R. F. Khairutdinov, J. K. Hurst, "Cyclic transmembrane charge transport by pyrylium ions in a vesicle-based photocatalytic system", *Nature* **1999**, 402, 509-511.

- [14] G. Steinberg-Yfrach, P. A. Liddell, S.-C. Hung, A. L. Moore, D. Gust, T. A. Moore, "Conversion of light energy to proton potential in liposomes by artificial photosynthetic reaction centres", *Nature* **1997**, 385, 239-241.
- [15] S. Bhosale, A. L. Sisson, P. Talukdar, A. Fürstenberg, N. Banerji, E. Vauthey, G. Bollot, J. Mareda, C. Röger, F. Würthner, N. Sakai, S. Matile, "Photoproduction of Proton Gradients with π -Stacked Fluorophore Scaffolds in Lipid Bilayers", *Science* **2006**, 313, 84-86.
- [16] A. Perez-Velasco, V. Gorteau, S. Matile, "Rigid Oligoperylenediimide Rods: Anion- π Slides with Photosynthetic Activity", *Angew. Chem. Int. Ed.* **2008**, 47, 921-923.
- [17] R. Aboshi, S.-y. Takizawa, S. Murata, "Visible-light-driven Electron Transport across Vesicle Membrane Sensitized by Cationic Iridium Complexes", *Chem. Lett.* **2015**, 44, 563-565.
- [18] G. Sprintschnik, H. W. Sprintschnik, P. P. Kirsch, D. G. Whitten, "Photochemical reactions in organized monolayer assemblies. III. Photochemical cleavage of water: a system for solar energy conversion using monolayer-bound transition metal complexes", *J. Am. Chem. Soc.* **1976**, 98, 2337-2338.
- [19] L. Yellowlees, R. Dickinson, C. Halliday, J. Bonham, L. Lyons, "Attempts to observe the photocleavage of water in the presence of a ruthenium complex", *Aust. J. Chem.* **1978**, 31, 431-433.
- [20] G. L. Gaines, P. E. Behnken, S. J. Valenty, "Monolayer films of surfactant ester derivatives of tris(2,2'-bipyridine)ruthenium(II)²⁺", *J. Am. Chem. Soc.* **1978**, 100, 6549-6559.
- [21] K.-P. Seefeld, D. Möbius, H. Kuhn, "Electron Transfer in Monolayer Assemblies with Incorporated Ruthenium (II) Complexes", *Helv. Chim. Acta* **1977**, 60, 2608-2632.
- [22] S. J. Valenty, G. L. Gaines, "Preparation and properties of monolayer films of surfactant ester derivatives of tris(2,2'-bipyridine)ruthenium(II)²⁺", *J. Am. Chem. Soc.* **1977**, 99, 1285-1287.
- [23] A. Harriman, "Photochemistry of a surfactant derivative of tris(2,2[prime or minute]-bipyridyl)ruthenium(II)", *J. Chem. Soc., Chem. Commun.* **1977**, 777-778.
- [24] G. Sprintschnik, H. W. Sprintschnik, P. P. Kirsch, D. G. Whitten, "Photochemical reactions in organized monolayer assemblies. 6. Preparation and photochemical reactivity of surfactant ruthenium(II) complexes in monolayer assemblies and at water-solid interfaces", *J. Am. Chem. Soc.* **1977**, 99, 4947-4954.
- [25] Y. Toyoshima, M. Morino, H. Motoki, M. Sukigara, "Photo-oxidation of water in phospholipid bilayer membranes containing chlorophyll a", *Nature* **1977**, 265, 187-189.
- [26] W. Stillwell, H. T. Tien, "Oxygen production from chlorophyll-liposomes", *Nature* **1978**, 273, 406-406.

- [27] W. Stillwell, H. T. Tien, "Oxygen evolution from broken thylakoids fused with liposomes", *Biochem. Biophys. Res. Commun.* **1978**, 81, 212-216.
- [28] H. T. Tien, "Membrane photobiophysics and photochemistry", *Prog. Surf. Sci.* **1989**, 30, 1-199.
- [29] I. M. Tsvetkov, O. V. Gerasimov, S. V. Lymar, V. N. Parmon, in Book "Photocatalytic Redox Reactions Sensibilized by Tris-Bipyridineruthenium(II) Complex in Microheterogeneous Systems" (Eds.: Y. Yermakov, V. Likholobov), VNU Science Press BV, Utrecht, **1986**, pp. 751-763.
- [30] S. Wang, T. Hori, "Oxygen evolution sensitized by tin porphyrin in microheterogeneous system and membrane systems", *J. Porphyrins Phthalocyanines* **2003**, 07, 37-41.
- [31] O. V. Gerasimov, S. V. Lymar, T. M. Tsvetkov, V. N. Parmon, "Cobalt water oxidation catalyst immobilized on membranes of lipid vesicles", *React. Kinet. Catal. Lett.* **1988**, 36, 145-149.
- [32] V. Y. Shafirovich, N. K. Khannanov, A. E. Shilov, "Inorganic models of photosystem II of plant photosynthesis. Catalytic and photocatalytic oxidation of water with participation of manganese compounds", *J. Inorg. Biochem.* **1981**, 15, 113-129.
- [33] N. P. Luneva, E. I. Knerelman, V. Y. Shafirovich, A. E. Shilov, "A manganese cluster bound to a bilayer membrane: a chemical model for the oxygen-forming centre of photosynthesis", *J. Chem. Soc., Chem. Commun.* **1987**, 1504-1505.
- [34] A. E. Shilov, "Organized molecular systems in catalysis", *B. Acad. Sci. USSR Ch.* **1990**, 39, 2185-2199.
- [35] M. Hansen, F. Li, L. Sun, B. Konig, "Photocatalytic water oxidation at soft interfaces", *Chem. Sci.* **2014**, 5, 2683-2687.
- [36] L. Duan, Y. Xu, M. Gorlov, L. Tong, S. Andersson, L. Sun, "Chemical and Photochemical Water Oxidation Catalyzed by Mononuclear Ruthenium Complexes with a Negatively Charged Tridentate Ligand", *Chem. Eur. J.* **2010**, 16, 4659-4668.
- [37] T. Koshiyama, N. Kanda, K. Iwata, M. Honjo, S. Asada, T. Hatae, Y. Tsuji, M. Yoshida, M. Okamura, R. Kuga, S. Masaoka, M. Ohba, "Regulation of a cerium(IV)-driven O₂ evolution reaction using composites of liposome and lipophilic ruthenium complexes", *Dalton Trans.* **2015**, 44, 15126-15129.
- [38] I. M. Tsvetkov, E. R. Buyanova, S. V. Lymar, V. N. Parmon, "Photocatalytic evolution of dihydrogen from aqueous solutions of lipid vesicles", *React. Kinet. Catal. Lett.* **1983**, 22, 159-163.
- [39] Y. T. Park, "Hydrogen Generation from Vesicles with Ru Catalyst on the Wall", *Bull. Korean Chem. Soc.* **1983**, 4, 149-150.

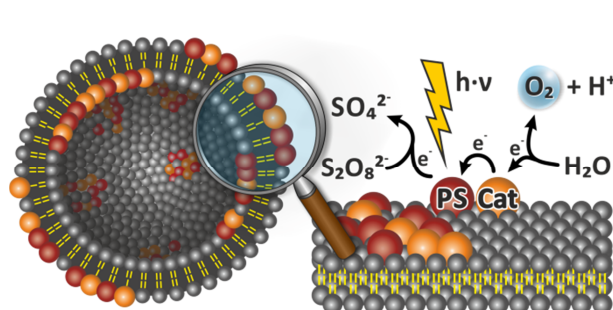
- [40] Y. M. Tricot, J. H. Fendler, "Visible light induced hydrogen production from in situ generated colloidal rhodium-coated cadmium sulfide in surfactant vesicles", *J. Am. Chem. Soc.* **1984**, 106, 2475-2476.
- [41] Y. M. Tricot, J. H. Fendler, "Colloidal catalyst-coated semiconductors in surfactant vesicles: in situ generation of rhodium-coated cadmium sulfide particles in dihexadecyl phosphate vesicles and their utilization for photosensitized charge separation and hydrogen generation", *J. Am. Chem. Soc.* **1984**, 106, 7359-7366.
- [42] R. Rafaeloff, Y. M. Tricot, F. Nome, J. H. Fendler, "Colloid-catalyst-coated semiconductors in surfactant vesicles. In situ generation of rhodium-coated cadmium sulfide particles in dimethyldioctadecylammonium halide surfactant vesicles and their utilization in photosensitized charge separation and hydrogen generation", *J. Phys. Chem.* **1985**, 89, 533-537.
- [43] Y. M. Tricot, A. Emeren, J. H. Fendler, "In situ generation of catalyst-coated cadmium sulfide particles in polymerized and unpolymerized surfactant vesicles and their utilization for efficient visible-light-induced hydrogen production", *J. Phys. Chem.* **1985**, 89, 4721-4726.
- [44] R. Rafaeloff, Y. M. Tricot, F. Nome, P. Tundo, J. H. Fendler, "Incorporation of a recyclable surface-active electron donor in synthetic vesicles: application to photosensitized hydrogen formation by vesicle-stabilized rhodium-coated colloidal cadmium sulfide particles", *J. Phys. Chem.* **1985**, 89, 1236-1238.
- [45] H. C. Youn, S. Baral, J. H. Fendler, "Dihexadecyl phosphate, vesicle-stabilized and in situ generated mixed cadmium sulfide and zinc sulfide semiconductor particles: preparation and utilization for photosensitized charge separation and hydrogen generation", *J. Phys. Chem.* **1988**, 92, 6320-6327.
- [46] V. E. Maier, V. Y. Shafirovich, "Light-induced hydrogen evolution in oxidising media promoted by catalytic sites encapsulated by phospholipid membranes", *J. Chem. Soc., Chem. Commun.* **1985**, 1063-1065.
- [47] E. V. Efimova, S. V. Lyman, V. N. Parmon, "1,4-Bis(1,2,6-triphenyl-4-pyridyl)benzene as a novel hydrophobic electron relay for dihydrogen evolution in photocatalytic systems based on lipid vesicles", *J. Photochem. Photobiol. A* **1994**, 83, 153-159.
- [48] Y. T. Park, S.-G. Noh, "The Synthesis of Bis-(2,2'-bipyridine) [4,4'-di-(hexadecyloxy carbonyl)-2,2'-bipyridine] ruthenium(II) and Its Application for Photolysis of Water", *Bull. Korean Chem. Soc.* **1994**, 15, 922-924.
- [49] Y. T. Park, S. G. Noh, "Photo-production of hydrogen from an aqueous solution of photosensitizer vesicles", *Int. J. Hydrogen Energy* **1995**, 20, 789-792.
- [50] K. Watanabe, K. Moriya, T. Kouyama, A. Onoda, T. Minatani, S.-y. Takizawa, S. Murata, "Photoinduced transmembrane electron transport in DPPC vesicles: Mechanism and application to a hydrogen generation system", *J. Photochem. Photobiol. A* **2011**, 221, 113-122.

- [51] K. Watanabe, S.-y. Takizawa, S. Murata, "Hydrogen Generation Using a Photoinduced Electron-transport System with a Molecular Catalyst in Vesicles", *Chem. Lett.* **2011**, 40, 345-347.
- [52] K. Menzel, U.-P. Apfel, N. Wolter, R. Rüger, T. Alpermann, F. Steiniger, D. Gabel, S. Förster, W. Weigand, A. Fahr, "[FeFe]-Hydrogenase models assembled into vesicular structures", *J. Lipos. Res.* **2014**, 24, 59-68.
- [53] S. Troppmann, B. König, "Functionalized Membranes for Photocatalytic Hydrogen Production", *Chem. Eur. J.* **2014**, 20, 14570-14574.
- [54] Y. Amao, I. Okura, "Effect of cationic surfactant on photoinduced hydrogen evolution with hydrogenase", *J. Mol. Catal. A: Chem.* **1995**, 103, L69-L71.
- [55] Y. Amao, I. Okura, "Effective photoinduced hydrogen evolution with hydrogenase in surfactant micelles", *J. Mol. Catal. A: Chem.* **1996**, 105, 125-130.
- [56] Y. Amao, Y. Tomonou, Y. Ishikawa, I. Okura, "Photoinduced hydrogen production with water-soluble zinc porphyrin and hydrogenase in nonionic surfactant micellar system", *Int. J. Hydrogen Energy* **2002**, 27, 621-625.
- [57] Y. Amao, Y. Tomonou, I. Okura, "Highly efficient photochemical hydrogen production system using zinc porphyrin and hydrogenase in CTAB micellar system", *Sol. Energy Mater. Sol. Cells* **2003**, 79, 103-111.
- [58] I. Okura, T. Kita, S. Aono, N. Kaji, A. Yamada, "Photoinduced hydrogen evolution in micellar system", *Inorg. Chim. Acta* **1986**, 122, 169-173.
- [59] Y. Tomonou, Y. Amao, "Visible light induced hydrogen production with Mg chlorophyll-a from spirulina and colloidal platinum", *Biometals* **2002**, 15, 391-395.
- [60] Y. Tomonou, Y. Amao, "Visible and near-IR light induced biohydrogen production using the system containing Mg chlorophyll-a from Spirulina and colloidal platinum", *Biometals* **2003**, 16, 419-424.
- [61] Y. Tomonou, Y. Amao, "Effect of micellar species on photoinduced hydrogen production with Mg chlorophyll-a from spirulina and colloidal platinum", *Int. J. Hydrogen Energy* **2004**, 29, 159-162.
- [62] N. Sugiyama, M. Toyoda, Y. Amao, "Photoinduced hydrogen production with chlorophyll-platinum nano-conjugated micellar system", *Colloids Surf., A* **2006**, 284-285, 384-387.
- [63] Y. Amao, Y. Maki, Y. Fuchino, "Photoinduced Hydrogen Production with Artificial Photosynthesis System Based on Carotenoid-Chlorophyll Conjugated Micelles", *J. Phys. Chem. C* **2009**, 113, 16811-16815.

- [64] S. Wang, I. Tabata, K. Hisada, T. Hori, "Hydrogen evolution sensitized by tin-porphyrin in microheterogeneous systems", *Dyes Pigm.* **2002**, 55, 27-33.
- [65] H.-Y. Wang, W.-G. Wang, G. Si, F. Wang, C.-H. Tung, L.-Z. Wu, "Photocatalytic Hydrogen Evolution from Rhenium(I) Complexes to [FeFe] Hydrogenase Mimics in Aqueous SDS Micellar Systems: A Biomimetic Pathway", *Langmuir* **2010**, 26, 9766-9771.
- [66] L. He, C. Luo, Y. Hou, C. Li, Q. Zhou, Y. Sun, W. Wang, B. Zhang, X. Wang, "The effects of micellar media on the photocatalytic H₂ production from water", *Int. J. Hydrogen Energy* **2011**, 36, 10593-10599.
- [67] C. Orain, F. Quentel, F. Gloaguen, "Photocatalytic Hydrogen Production Using Models of the Iron-Iron Hydrogenase Active Site Dispersed in Micellar Solution", *ChemSusChem* **2014**, 7, 638-643.
- [68] S.-G. L. Yong-Un Kim, Yong-Tae Park, "Light-Induced Hydrogen and Oxygen Generation from Water with Vesicle-Stabilized Colloidal Mercury Sulfide and Sodium Metaborate", *Bull. Korean Chem. Soc.* **1993**, 14, 168-169.
- [69] Y.-T. Park, Y.-U. Kim, S.-G. Lee, "Hydrogen and oxygen production from water", *Int. J. Hydrogen Energy* **1994**, 19, 291-293.
- [70] Y. T. Park, S. G. Lee, Y. U. Kim, "Light-induced hydrogen and oxygen generation from water", *Int. J. Hydrogen Energy* **1995**, 20, 711-715.
- [71] N. Ikuta, S.-Y. Takizawa, S. Murata, "Photochemical reduction of CO₂ with ascorbate in aqueous solution using vesicles acting as photocatalysts", *Photochem. Photobiol. Sci.* **2014**, 13, 691-702.

2 Photocatalytic Water Oxidation at Soft Interfaces

2.1	Introduction	38
2.2	Results and Discussion	39
2.3	Conclusion	45
2.4	Experimental Part	46
2.5	References	61



Molecular water oxidation catalysts have been, for the first time, co-embedded with a photosensitizer into phospholipid membranes. The functionalized small unilamellar vesicles produce molecular oxygen by photocatalysis when irradiated with visible light in aqueous buffer. The two dimensional assembly of the catalysts at the lipid-water interface mimics photoactive membranes in biology and allows photocatalytic water oxidation at very low catalyst concentrations of 500 nM, which cannot be reached in homogeneous systems. Highest TONs are obtained below the membrane's main transition temperature indicating

that phase separation, clustering and a limited dynamic enhance the photocatalytic activity of the assembly. The concept of membrane co-embedding can be applied to various combinations, ratios and concentrations of photosensitizers and water oxidizing catalysts, providing a new approach for artificial photosynthesis.

This chapter was published in:

M. Hansen, F. Li, L. Sun and B. König, "Photocatalytic water oxidation at soft interfaces", *Chem. Sci.* **2014**, 5, 2683-2687 - Published by The Royal Society of Chemistry

M. Hansen performed the experimental work and wrote the manuscript. F. Li, S. Sun and B. König supervised the project and are the corresponding authors.

2.1 Introduction

Efficient photochemical water splitting is still a scientific challenge.^[1, 2] The overall process consists of an oxidative and a reductive half reaction with the water oxidation step involving a four electron transfer and highly reactive oxygen intermediates being considered as particularly difficult.^[3] Heterogeneous and homogeneous photocatalysts have been developed. A typical homogeneous catalyst for photooxidation of water consists of two subunits: A light absorbing photoredox active dye or sensitizer and the water oxidizing catalyst. The two subunits can be covalently connected (Figure 2.1, 1, top), which ensures an efficient electron transfer, but requires the synthesis of complex ligands and linkers.^[4-8] If dye and oxidation catalyst are prepared as separate entities (Figure 2.1, 4 and 5, bottom) different combinations can be easily realized, but the electron transfer between the subunits in homogeneous solution is diffusion controlled and depends on the concentration.^[9]

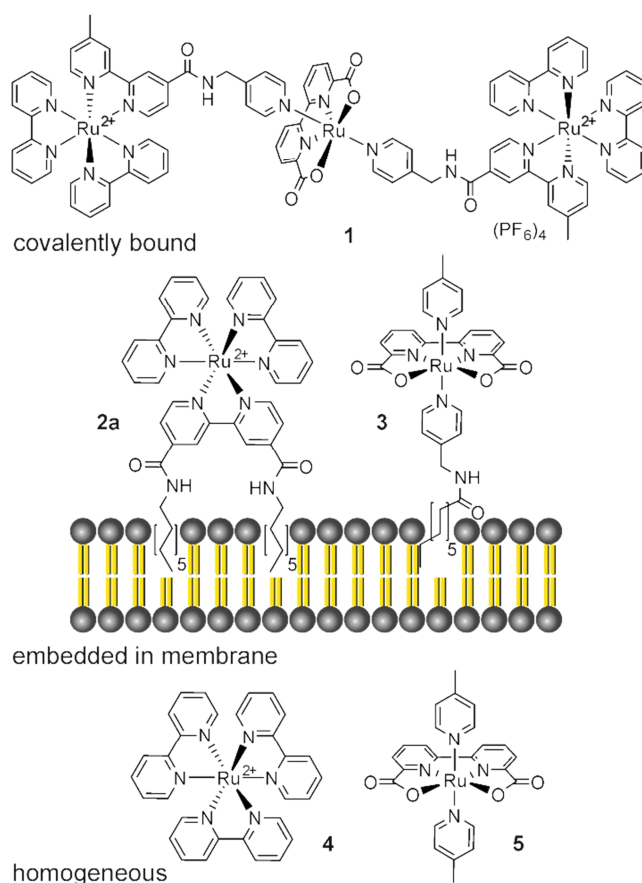


Figure 2.1 - Interaction of photosensitizer - water oxidation catalysts, which are covalently connected (top),^[8] membrane co-embedded (middle) or in homogeneous solution (bottom).^[10]

In biological photosynthesis, chromophores and catalytic units are bound to membranes. Compared to homogeneous solution this two dimensional assembly increases the local concentration of the redox partners and shortens the average distance for electron transfer between them.^[11-16] Clustering of membrane embedded compounds and phase separation may increase this effect further. Compared to covalently connected sensitizer - catalyst pairs,^[17] the assembly in fluid membranes remains dynamic allowing continuous self-assembly and reorganization of the catalytic subunits, which may be advantageous for the catalytic performance. Following this biological model we have prepared phospholipid membranes with co-embedded amphiphilic photosensitizers and water oxidation catalysts.

Such functionalized vesicles place the catalytic subunits in close proximity even at very low overall concentrations while still allowing the easy variation of sensitizer - catalyst combinations, ratios and concentrations.

2.2 Results and Discussion

For anchoring into a self-assembled membrane the photosensitizer and the water oxidation catalyst should be amphiphilic and bear a hydrophobic alkyl chain. Derivative **2a** of the widely used photosensitizer ruthenium tris-bipyridine (**4**) is suitable for membrane embedding and was prepared according to reported procedures.^[18-22] Three amphiphilic water oxidation catalysts **3**, **6b** and **7** (Figure 2.2) were derived from literature known catalysts^[23-25] that have shown good performance in chemical and photochemical water oxidation in homogeneous solution. Details of their synthesis and characterization are given in the experimental part (Section 2.4.2).

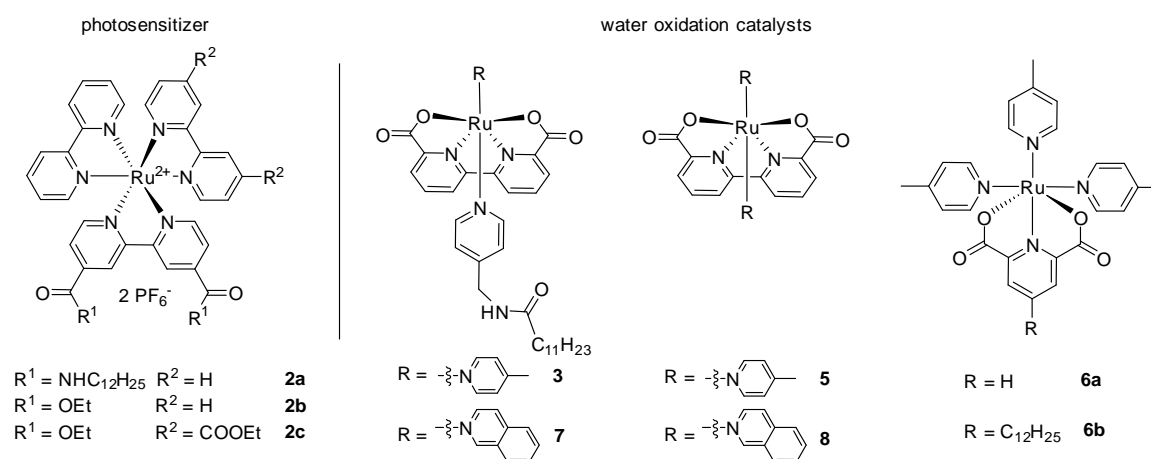


Figure 2.2 - Chemical structures of amphiphilic photosensitizers **2** and water oxidation catalysts **3**, **5-8**.

Vesicles were prepared by sonication of phospholipid films with added photosensitizer **2a** (12.5 mol%) and water oxidation catalysts **6b**, **3** or **7** (0.05 - 1.25 mol%) in phosphate buffer (50 mM, pH = 7.0) containing the sacrificial electron acceptor sodium persulfate. Dynamic light scattering confirmed a narrow size distribution of the vesicles in all cases and UV spectra of the solutions showed absorption maxima and extinction coefficients of the photosensitizer comparable to a homogeneous solution. The influence of vesicle size and solution turbidity on oxygen evolution was negligible (for data see experimental part 2.4.8).

Degassed solutions of the functionalized vesicles containing photosensitizer **2a** and water oxidation catalyst **6b** were irradiated with high power LEDs ($\lambda = 455$ nm; 200 mW/cm² light intensity) and the oxygen evolution was monitored by an optical probe and quantified by head space gas chromatography. The experimental details and data are given in the experimental part, Section 2.4.6. Figure 2.3 shows the proposed reaction mechanism.

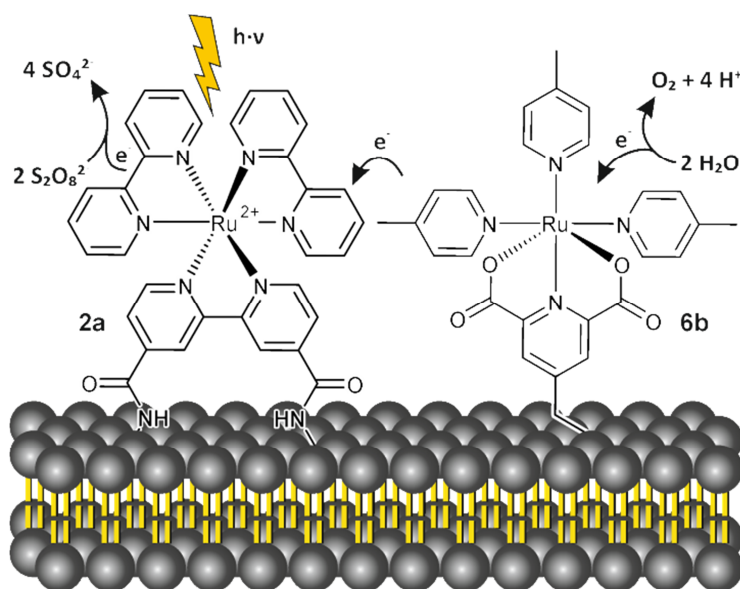


Figure 2.3 - Proposed reaction mechanism of photocatalytic oxygen evolution with phospholipid membrane co-embedded amphiphilic photosensitizer **2a** and water oxidation catalysts **6b** in aqueous phosphate buffer (50 mM, pH = 7.0) containing 2.5 mM of sodium persulfate.

To investigate the effect of the membrane embedding on the efficiency of the photocatalytic water oxidation, the oxygen evolution of a homogeneous aqueous solution containing photosensitizer **2b** (125 μ M) and water oxidation catalyst **6a** (12.5 μ M)^[23] was compared under otherwise identical conditions with a vesicular DMPC (1,2-dimyristoyl-*sn*-glycero-3-phosphocholine, **9**, Figure 2.6) solution containing photosensitizer **2a** (125 μ M) and water

oxidation catalyst **6b** (12.5 μM). The observed turnover numbers (TON) of 49 for the homogeneous and 55 for the vesicular solution are comparable (Table 2.1).

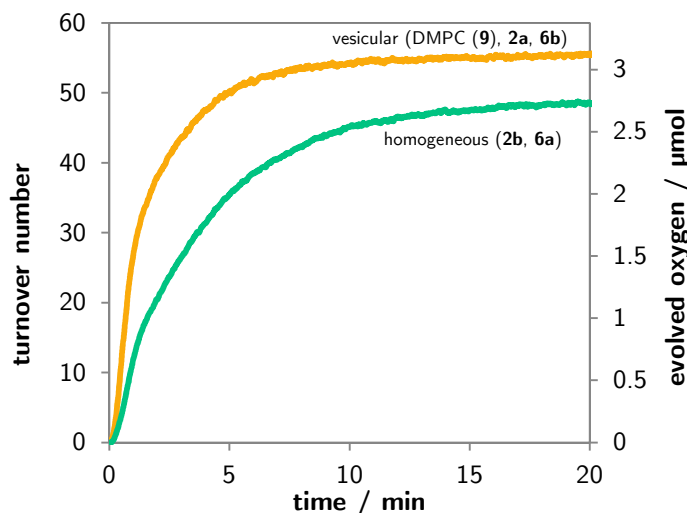


Figure 2.4 - Oxygen evolution vs irradiation time of a vesicular and a homogeneous sample. The reactions were performed using catalysts **6a** or **6b** (12.5 μM), photosensitizer **2a** or **2b** (125 μM) and 2.5×10^{-2} M of sodium persulfate in phosphate buffer (50 mM, pH = 7.0).

Next, in a series of experiments the amount of the water oxidizing catalyst **6** was reduced and the performances of the homogeneous and the vesicular system were compared. A concentration of 6.25 μM of complex **6a** in homogeneous solution or complex **6b** in vesicular solution corresponds to a catalyst to sensitizer ratio of 1:20 and gave TONs of oxygen evolution of 37 (Table 2.1, entry 4) and 75 (entry 3), respectively. At a ratio of 1:50 using a concentration of the catalysts **6** of 2.5 μM in the presence of 125 μM of the photosensitizer **2** the difference in TONs in homogeneous solution of 22 (entry 6) and the vesicular solution of 192 (entry 5) were even more pronounced (Table 2.1). At 500 nM concentration of catalyst **6** water photooxidation is negligible in homogeneous solution, while in the membrane a TON of 394 is observed (entry 7). Control experiments without catalyst **6b** (entry 9) and photosensitizer **2b** (entry 10), respectively, resulted in no detectable oxygen formation.

The results demonstrate one advantage of the co-embedding of photosensitizer and water oxidation catalyst in a vesicle membrane: the two dimensional arrangement at the lipid water interface places the subunits of the catalyst even at low overall concentrations in close proximity, which favors the electron transfer and their concerted action in the water oxidation. Photocatalytically active sensitizer catalyst combinations are possible in the vesicular system at ratios and concentrations, which cannot be realized in homogeneous solution.

Table 2.1 - Evolved molecular oxygen after 20 min light irradiation and TON of photosensitizers (PS) **2** (125 μM) and water oxidations catalysts (cat) **6** in homogeneous solution (shaded in grey) and DMPC (**9**) phospholipid vesicles at identical concentrations and a sodium persulfate concentration of 2.5 mM. Control experiments without catalyst or photosensitizer under otherwise identical conditions.

Entry	cat	PS	Ratio cat:PS	c_{cat} [μM]	c_{DMPC} [μM]	n_{O_2} [μmol]	TON
1	6b	2a	1:10	12.5	863	3.1	55
2	6a	2b	1:10	12.5	-	2.8	49
3	6b	2a	1:20	6.25	869	2.1	75
4	6a	2b	1:20	6.25	-	1.0	37
5	6b	2a	1:50	2.5	873	2.1	192
6	6a	2b	1:50	2.5	-	0.2	22
7	6b	2a	1:250	0.5	873	0.6	394
8	6a	2b	1:250	0.5	-	0	0
9	-	2a	-	-	875	0	0
10	6b	-	-	12.5	988	0	0

In previous studies, the non-amphiphilic derivatives **5** and **8** of ruthenium complexes **3** and **7** have shown a better water oxidation performance compared to complex **6** in homogeneous solution.^[10, 24] To prove the versatility of membrane co-embedding for the preparation of water photooxidation assemblies, catalysts **3** or **7** (2.5 μM) and photosensitizer **2a** (125 μM) were added to DMPC (**9**) vesicles. Vesicular and homogeneous samples were irradiated with a 500 W xenon lamp (cut off filter $\lambda > 400$ nm; 450 mW/cm² light intensity) and the amount of evolved oxygen was determined (Table 2.2). The catalyst to sensitizer ratio of 1:50 gave TONs of 157 for catalyst **3** (entry 2) and of 185 for catalyst **7** (entry 3), which are higher compared to the TON of 109 obtained in homogeneous solutions (entry 1) using the non-amphiphilic derivative of **3** bearing 2 axial 4-methylpyridine ligands (**5**)^[10] (Figure 2.2) and the photosensitizer **2a**, but otherwise identical conditions.

The performance of the water photooxidizing system is known to be limited by the stability of the photosensitizer,^[24] which applies also for the vesicular assemblies. By embedding of new photosensitizer into the membrane of used, irradiated vesicles they regain about 60 % of their initial TON (Table 2.2, entry 4) when irradiated again after removal of oxygen from the sample (see experimental part Section 2.4.9 for data).

Table 2.2 - Evolved molecular oxygen after 20 min light irradiation and TON of photosensitizers (PS) **2** (125 μM) and water oxidations catalysts (cat) **3** and **7** embedded in DMPC (**9**) phospholipid vesicles; for comparison the performance of a homogeneous solution of catalyst **5** and photosensitizer **2c** at identical concentrations is given (shaded grey). Sodium persulfate concentration: 2.5 mM

Entry	cat	PS	Ratio cat:PS	c_{cat} [μM]	c_{DMPC} [μM]	n_{O_2} [μmol]	TON
1	5	2c	1:50	2.5	-	2.2	109
2	3	2a	1:50	2.5	873	3.1	157
3	7	2a	1:50	2.5	873	3.7	185
4	7	2a	1:50	- ^a	873	2.3	113

^areuse of the membrane from entry 3.

The physical properties of phospholipid membranes change significantly with the nature of the lipid. To investigate the effect on the water photooxidation the activity of embedded photosensitizer **2a** (125 μM) and complex **6b** (12.5 μM) were investigated in three membranes prepared from DMPC (**9**), SMPC (1-stearoyl-2-myristoyl-*sn*-glycero-3-phosphocholine) (**10**) and DOPC (1,2-dioleoyl-*sn*-glycero-3-phosphocholine) (**11**). The three lipids have the same dipolar head group and differ only in the length and structure of the hydrocarbon chains (Figure 2.6). The polarity at the lipid water interface is therefore expected to be very similar, which was confirmed by the embedded amphiphilic solvatochromic dansyl dye **12** showing the same optical properties in all three membranes (see experimental part section 2.4.10).

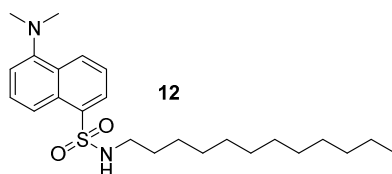
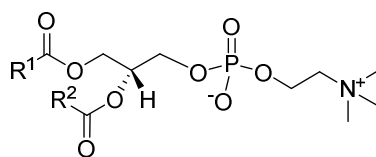


Figure 2.5 - Structure of the amphiphilic, solvatochromic dansyl dye (**12**).

However, in DMPC (**9**) and SMPC (**10**) (Table 2.3) the co-embedded complexes produced oxygen upon irradiation ($\lambda = 455 \text{ nm}$; 200 mW/cm^2 light intensity), while the activity in DOPC (**11**) (entry 1) was significantly lower. We explain the effect by the distinct differences in membrane fluidity. DMPC (**9**) and SMPC (**10**) have main phase transition temperatures from the gel to the liquid crystalline phase of 24°C and 30°C ,^[26] but DOPC (**11**) with a transition temperature of -21°C is already in the liquid crystalline phase at the temperature of the experiment. Photooxidation experiments of DMPC (**9**) and SMPC (**10**) vesicles with embedded photosensitizers and catalyst at temperatures above their transition temperatures (en-

tries 5 and 7) showed a reduced activity, while the activity remains unchanged at temperatures below the phase transition (entries 4 and 6).



	R ¹	R ²	PTT
DOPC (11)	Δ -9- <i>cis</i> -C ₁₇ H ₃₃		-21 °C
DMPC (9)	C ₁₃ H ₂₇		24 °C
SMPC (10)	C ₁₇ H ₃₅	C ₁₃ H ₂₇	30 °C

Figure 2.6 - Structures and phase transition temperatures (PTT) of the phospholipids DMPC (**9**), SMPC (**10**) and DOPC (**11**).

We conclude that phase separation and clustering of the embedded complexes, expected for the amphiphilic additives **2a** and **6b** below the transition temperature of a lipid membrane, enhances the photocatalytic activity of the assembly.^[27] This is supported by the difference in quantum efficiency $\varphi = (1-I/I_0)$ determined from the fluorescence quenching of **2a** with sodium persulfate under the reaction conditions.^[28] While DMPC (**9**) and SMPC (**10**) vesicles show a quantum efficiency of $\varphi = 35\%$ and 30% , respectively, a significantly lower value of $\varphi = 10\%$ was determined for DOPC (**11**) vesicles (see experimental part section 2.4.11 for data).

Table 2.3 - Dependence of evolved molecular oxygen after 20 min light irradiation and TON of co-embedded photosensitizer **2a** (125 μ M) and water oxidations catalyst **6b** (12.5 μ M) depending on the phospholipid and the reaction temperature at a sodium persulfate concentration of 2.5 mM.

Entry	Phospholipid	T [°C]	n _{O₂} [μ mol]	TON
1	DOPC (11)	25	0.2	3 \pm 1
2	DMPC (9)	25	3.1	55 \pm 2
3	SMPC (10)	25	3.6	64 \pm 4
4	DMPC (9)	14	3.2	66 \pm 4
5	DMPC (9)	34	2.4	52 \pm 3
6	SMPC (10)	20	3.6	65 \pm 2
7	SMPC (10)	40	1.7	29 \pm 6

2.3 Conclusion

In summary, we have, for the first time, self-assembled photosensitizer - catalyst water oxidation systems by co-embedding of two amphiphilic ruthenium complexes into the phospholipid bilayer membrane of small unilamellar vesicles. The observed oxygen production upon light irradiation is comparable to similar systems in homogeneous solutions, but superior at low concentrations of the water oxidation catalysts. Membrane embedded water photooxidation systems remain catalytically active at concentrations, where homogeneous mixtures of photosensitizer and water oxidation catalyst are inoperable.

Phase separation and patch formation cluster the complexes in the membrane, which might facilitate the intermolecular electron transfer processes. The fluidity of the membrane affects the self-organization of the embedded complexes and therefore their photocatalytic performance. Highest TONs are observed in gel phase membranes, where phase separation is favored. The method was applied to different combinations of sensitizers and oxidation catalysts and allows a rapid screening of sensitizer - catalyst combinations, ratios and concentration ranges. Functionalized vesicles may be transferred and spread onto a variety of surfaces, which may allow the processing, immobilization or printing of photocatalytically active membranes for further applications in functional devices for artificial photosynthesis.

2.4 Experimental Part

2.4.1 General Methods and Material

For NMR-spectroscopy, a Bruker Avance 400 (^1H : 400 MHz, ^{13}C : 101 MHz, $T = 300\text{ K}$) was utilized. All chemical shifts are reported in δ [ppm] (multiplicity, coupling constant J , number of protons, assignment of proton) relative to the solvent residual peak as the internal standard. The coupling constants are given in Hertz [Hz]. Abbreviations used for signal multiplicity: ^1H -NMR: s = singlet, d = doublet, dd = double doublet, t = triplet, q = quartet, sep = septet, m = multiplet, p = pseudo. ^{13}C -NMR: (+) = CH, CH_3 , (-) = CH_2 , q = quaternary carbon. The used solvent is reported for every spectrum.

Absorption spectra were recorded on a Varian Cary BIO 50 UV/VIS/NIR spectrometer. A 10 mm Hellma quartz cuvette was used.

IR-Spectra were measured on a Bio-Rad-FT-IR-Spectrometer Excalibur FTS 3000 equipped with a Golden Gate Diamond Single Reflection ATR System. Signal intensity is abbreviated with s = strong, m = medium and w = weak.

Fluorescence spectroscopy has been carried out on a Varian Cary Eclipse fluorimeter with 10 mm Hellma quartz cuvettes at $25\text{ }^\circ\text{C}$.

Dynamic light scattering was performed on a Malvern Zetasizer Nano at $25\text{ }^\circ\text{C}$ using either a disposable Polystyrene or Polymethyl methacrylate cuvette purchased from Kartell.

Mass-spectrometry: ThermoQuest Finnigan TSQ 7000, Finnigan MAT 95 and Finnigan MAT SSQ 710 A.

Melting points were determined on a Stanford Research Systems OptiMelt MPA 100 with a heating rate of $1\text{ }^\circ\text{C}/\text{min}$.

Elemental analysis was carried out on a Vario EL III.

Pre-coated TLC-sheets ALUGRAM Xtra SIL G/UV254 from Macherey-Nagel were used. The detection was done by UV light (254 nm or 366 nm).

Two different silica gels were used for column chromatography: Macherey-Nagel silica gel 60 M (230 - 440 mesh; column chromatography); Macherey-Nagel silica gel 60 (70 - 230 mesh; flash chromatography).

For size exclusion chromatography, Sephadex LH-20 from Sigma was used.

A Fibox 3 fibre optic oxygen sensor purchased from PreSens Precision Sensing GmbH was used for monitoring the amount of oxygen.

A Bandelin Sonorex RK 102 H was used for the sonication of vesicular samples.

Gas chromatography was performed on a Inficon Micro GC 3000 with a 3 Å mol sieve column, a thermal conductivity detector and Ar as carrier gas.

2.4.2 Synthesis of Photosensitizer 2a

Compounds **14**,^[20] **15**^[18] and **17**^[19] were prepared according to literature procedures. The synthesis of ligand **16**^[21] and complex **2a**^[22] follows procedures previously reported for similar compounds.

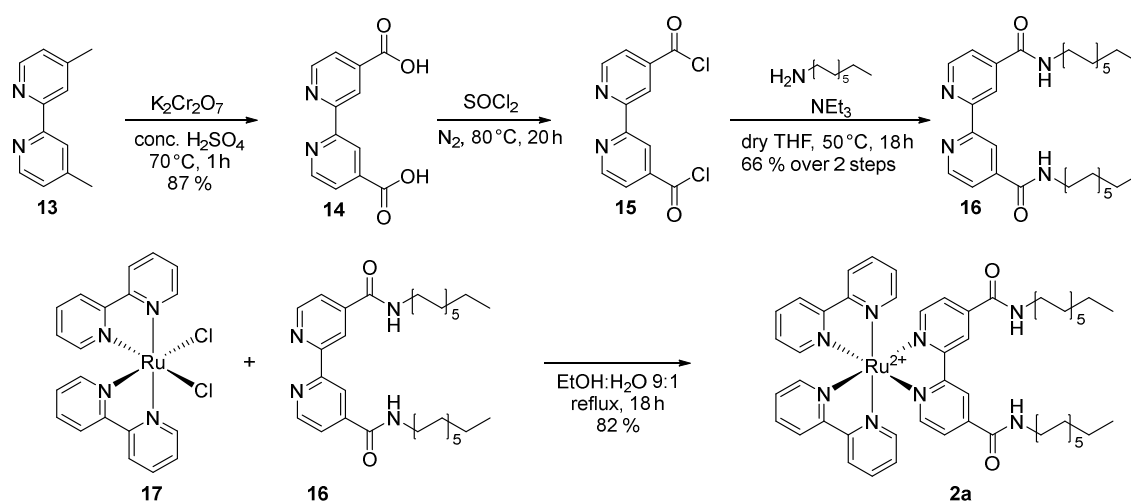


Figure S 2.1 - Synthesis of complex **2a**.

Didodecyl-[2,2'-bipyridine]-4,4'-dicarboxamide (**16**)^[21]

Compound **15** (562 mg, 2.0 mmol) was dissolved in 100 mL of dry THF in a Schlenk round bottomed flask under N₂. Dodecyl amine (890 mg, 4.4 mmol) and triethyl amine (520 µL, 2.0 mmol) were added and a white precipitate was observed. The reaction mixture was heated to 50 °C and stirred overnight. The precipitate was filtered off and washed with water (20 mL), acetone (20 mL) and DCM (20 mL). The white crystalline powder was dried in vacuum yielding 767 mg of **16** (66 %, 1.32 mmol).

m.p.: 232 °C

IR: $\tilde{\nu}$ [cm⁻¹]: 3307 (s), 2919 (s), 2849 (s), 1631 (s), 1591 (m), 1524 (s), 1465 (m), 1304 (m), 1099 (m), 1070 (w), 895 (m), 863 (s), 760 (s), 695 (s), 645 (s)

MS: ESI m/z = 579.3 (MH^+)

E.A.: calc. [%] for $C_{36}H_{58}N_4O_2$ M = 578.87: C 74.69, H 10.10, N 9.68; found: C 74.18, H 9.97, N 9.30

Ruthenium^{II}(didodecyl-(2,2'-bipyridine)-4,4'-dicarboxamide)bis(2,2'-bipyridine)-bis-(hexafluorophosphate) (2a)^[22]

Compound **17** (102 mg, 0.19 mmol) and **16** (114 mg, 0.19 mmol) were dissolved in a mixture of EtOH:H₂O (9:1) under N₂ atmosphere, heated to reflux and stirred overnight. The solvent was removed *in vacuo* and the resulting solid was purified by a size exclusion chromatography with Sephadex LH-20. The column was firstly eluted with MeCN to remove a purple band from the starting material and secondly with a mixture of MeCN:EtOH (9:1) to obtain the dichloride salt of **2a** as a red solid. The solid was dissolved in a minimum amount of water. 5 mL of a saturated NH₄PF₆ solution were added to precipitate **2a** as a dark red solid. After filtration and drying in high vacuum, 200 mg (82 %, 0.16 mmol) of **2a** could be isolated.

¹H-NMR (400 MHz, CD₃CN): δ [ppm]: 8.94 (d, J = 1.3 Hz, 2H), 8.51 (m, 4H), 8.07 (m, 4H), 7.87 (d, 2H, J = 5.9 Hz), 7.70 (m, 8H, H₃) 7.40 (m, 4H), 3.39 (pq, J = 7.0 Hz, 4H), 1.60 (m, 4H), 1.2-1.4 (m, 36H), 0.87 (t, J = 6.8 Hz, 6H)

¹³C-NMR (101 MHz, CD₃CN): δ [ppm]: 162.6 (q), 157.1 (q), 156.6 (q), 156.5 (q), 152.1 (+), 151.4 (+), 151.3 (+), 142.6 (q), 137.8 (+), 127.4 (+), 127.4 (+), 124.6 (+), 124.0 (+), 121.7 (+), 39.6 (-), 31.3 (-), 29.1 (-), 29.0 (-), 29.0 (-), 29.0 (-), 28.8 (-), 28.7 (-), 28.6 (-), 26.3 (-), 22.0 (-), 13.0 (+)

³¹P-NMR (162 MHz, CD₃CN): δ [ppm]: -143.26 (sep, J = 706.5 Hz, PF₆)

¹⁹F-NMR (162 MHz, CD₃CN): δ [ppm]: -72.89 (d, J = 707.8 Hz, PF₆)

IR: $\tilde{\nu}$ [cm⁻¹]: 3419 (w), 2924 (m), 2853 (m), 1666 (m), 1532 (m), 1465 (m), 1446 (m), 1313 (w), 1226 (w), 1162 (w), 1026 (w), 825 (s), 759 (s), 729 (m), 554 (s)

HR-MS: ESI⁺ calc. for $C_{56}H_{74}N_8O_2Ru$ (M^{2+}) m/z = 496.2489; found 496.2501

UV/Vis: (in MeCN) λ_{max} = 247 nm, λ_{max} = 288 nm, λ_{max} = 461 nm

2.4.3 Synthesis of Catalyst 6b

Compounds **18**^[29] and **22**^[19] were prepared according to literature procedures. The synthesis of Ligand **21** and its precursors **19** and **20** is described below. Complex **6b**^[23] was prepared following the procedure for catalyst **6a**.

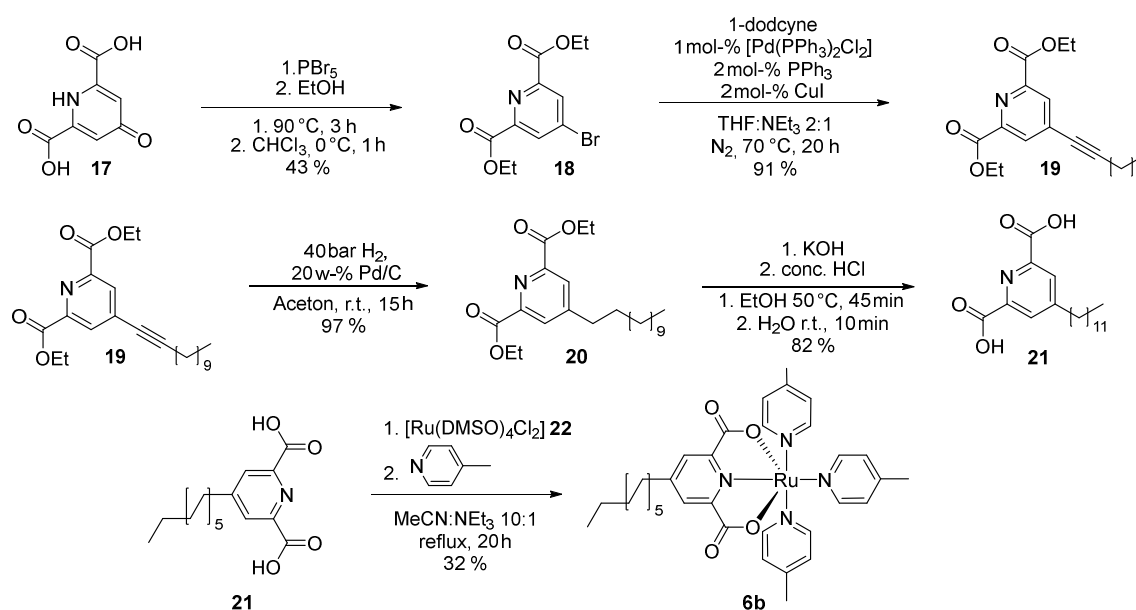


Figure S 2.2 - Synthesis of complex **6b**.

Diethyl 4-(dodecynyl)pyridine-2,6-dicarboxylate (**19**)

Compound **18** (228 mg, 0.75 mmol), 1-dodecyne (161 µL, 0.75 mmol), [Pd(PPh₃)₂Cl₂] (5.3 mg, 1 mol%), PPh₃ (4.0 mg, 2 mol%) and CuI (2.9 mg, 2 mol%) were dissolved in a degassed mixture of 16 mL THF and 8 mL triethyl amine under a nitrogen atmosphere. After stirring for 20 h at 70 °C, the solvents were evaporated under reduced pressure. The residue was dissolved in 15 mL of DCM and washed three times with water (10 mL). The combined aqueous phases were extracted once with 10 mL of DCM. The combined organic phase was dried over MgSO₄ and the solvent was evaporated. The residue was subjected to column chromatography (SiO₂, petroleum ether / ethyl acetate 3:1) to yield 264 mg (91 %, 0.68 mmol) of **19** as a white solid.

m.p: 72 °C

¹H-NMR (400 MHz, CDCl₃): δ [ppm]: 8.10 (s, 2H), 4.39 (q, J = 7.1 Hz, 4H), 2.37 (t, J = 7.1 Hz, 2H), 1.53 (m, 2H), 1.36 (m, 8H), 1.28-1.13 (m, 12H), 0.78 (t, J = 6.8 Hz, 3H)

¹³C-NMR (101 MHz, CDCl₃): δ [ppm]: 164.2 (q), 148.6 (q), 135.0 (q), 129.6 (+), 99.0 (q), 77.4 (q), 62.2 (-), 31.8 (-), 29.5 (-), 29.4 (-), 29.2 (-), 29.0 (-), 28.9 (-), 28.1 (-), 22.6 (-), 19.4 (-), 14.1 (+), 14.0 (+)

MS: EI m/z = 387.2 (M⁺)

IR: $\tilde{\nu}$ [cm⁻¹]: 2916 (s), 2849 (s), 2231 (m), 1714 (s), 1600 (m), 1469 (m), 1408 (m), 1373 (s), 1344 (s), 1246 (s), 1152 (m), 1131 (m), 1020 (m), 782 (s), 580 (m)

E.A.: calc. [%] for C₂₃H₃₃NO₄ M = 387.51 g/mol: C 71.35, H 8.59, N 3.62; found: C 71.33, H 8.52, N 3.17

Diethyl 4-dodecylpyridine-2,6-dicarboxylate (**20**)

Compound **19** (200 mg, 0.52 mmol) was dissolved in 5 mL of acetone and Pd/C (20 mg) was added. The solution was stirred overnight in an autoclave at a hydrogen pressure of 3 bar. The catalyst was filtered off over celite and the solvent was evaporated *in vacuo* to yield 192 mg (94 %, 0.49 mmol) of **20** as a colorless oil.

¹H-NMR (400 MHz, CDCl₃): δ [ppm]: 8.08 (s, 2H, H_{3,5}), 4.46 (q, J = 7.1 Hz, 4H), 2.73 (t, J = 7.1 Hz, 2H), 1.67 (m, 2H), 1.44 (t, J = 7.1 Hz, 6H), 1.37-1.15 (m, 18H), 0.85 (t, J = 6.8 Hz, 3H)

¹³C-NMR (101 MHz, CDCl₃): δ [ppm]: 165.0 (q), 154.8 (q), 148.6 (q), 128.0 (+), 62.2 (-), 35.3 (-), 31.9 (-), 30.2 (-), 29.6 (-), 29.6 (-), 29.6 (-), 29.5 (-), 29.3 (-), 29.1 (-), 22.7 (-), 14.2 (+), 14.1 (+)

IR: $\tilde{\nu}$ [cm⁻¹]: 2924 (s), 2854 (m), 1748 (m), 1717 (s), 1601 (m), 1465 (m), 1375 (m), 1339 (m), 1239 (s), 1204 (s), 1058 (m), 1025 (s), 782 (m)

HR-MS: ESI⁺ calc. for C₂₃H₃₇NO₄ (MH⁺) m/z = 392.2801; found 392.2795

4-Dodecylpyridine-2,6-dicarboxylate (**21**)

KOH (850 mg), dissolved in 15 mL of ethanol, was added to compound **20** (195 mg, 0.5 mmol). Immediately after the addition, a white solid started to crystallize. The solution was stirred at 50 °C for 45 min. The precipitate was filtered off and dried in high vacuum to give 200 mg (0.48 mmol, 97 %) of the dipotassium salt of **21**. The solid was dissolved in water (ca. 50 mL) and conc. hydrochloric acid was added drop wise, until the pH reached a value of 1. The solution was stirred at room temperature for 10 min and the white precipitate was filtered off. The residue was washed with 10 mL of water and dried in high vacuum to yield 138 mg (82 %, 0.4 mmol) of **21** as a white solid.

m.p.: 143 °C (decomp.)

¹H-NMR (400 MHz, DMSO-*d*₆): δ [ppm]: 8.08 (s, 2H), 2.77 (t, *J* = 7.6 Hz, 2H), 1.61 (m, 2H), 1.32-1.12 (m, 18H), 0.84 (t, *J* = 6.7 Hz, 3H)

¹³C-NMR (101 MHz, DMSO-*d*₆): δ [ppm]: 165.6 (q), 154.5 (q), 148.1 (q), 127.3 (+), 34.1 (-), 31.3 (-), 29.7 (-), 29.0 (-), 29.00 (-), 29.0 (-), 28.9 (-), 28.7 (-), 28.4 (-), 22.1 (-), 14.0 (+)

IR: $\tilde{\nu}$ [cm⁻¹]: 3473 (w), 2915 (s), 2849 (s), 1745 (s), 1681 (m), 1605 (m), 1471 (m), 1328 (m), 1172 (s), 1002 (m), 904 (m), 681 (s), 511 (m)

E.A.: calc. [%] for C₁₉H₂₉NO₄·H₂O *M* = 353.45 g/mol: C 64.56, H 8.84, N 3.96; found: C 63.58, H 8.89, N 3.72

Ruthenium^{II} (4-dodecylpyridine-2,6-dicarboxylate) tris (4-methylpyridine) (6b)^[23]

A mixture of MeCN (10 mL) and triethyl amine (1 mL) was degassed by the freeze-pump-thaw method. Compound **21** (130 mg, 0.37 mmol) and **22** (180 mg, 0.37 mmol) were added to the solvent under nitrogen. The solution was heated to reflux and stirred overnight. The color changed from light yellow to red. 4-Methylpyridine (Pic, 5 mL, 56.2 mmol) was added and the solution was stirred for additional 4.5 h under reflux. After cooling to room temperature, the solvent was removed *in vacuo* and the 4-methylpyridine was removed in high vacuum at 40 °C. The residue was dissolved in DCM (15 mL) and washed with water (3 × 10 mL). After removal of the solvent, the crude product was purified by column chromatography (SiO₂, EtOH:Et₂O 8:1). The second fraction was collected and dissolved in a mixture of 5 mL of MeCN, 0.5 mL of triethyl amine and 5 mL (56.2 mmol) of 4-methylpyridine, degassed by nitrogen and heated to reflux for 5 h. After removal of the solvent *in vacuo*, the crude product was purified by flash column chromatography (SiO₂, EtOH:Et₂O 10:1). The second fraction was collected and yielded 87 mg (32 %, 0.12 mmol) of **6b** as a dark red-brownish solid.

¹H-NMR (400 MHz, CDCl₃): δ [ppm]: 8.74 (d, *J* = 6.3 Hz, 2H), 8.12 (d, *J* = 6.5 Hz, 4H), 7.82 (s, 2H), 7.04 (d, *J* = 5.8 Hz, 2H), 6.85 (d, *J* = 6.1 Hz, 4H), 2.64 (t, *J* = 7.8 Hz, 2H), 2.34 (s, 3H), 2.19 (s, 6H), 1.64 (m, 2H) 1.32-1.16 (m, 18H), 0.88 (t, *J* = 6.9 Hz, 3H)

¹³C-NMR (101 MHz, CDCl₃): δ [ppm]: 174.8 (q), 154.4 (q), 153.1 (+), 152.7 (+), 147.8 (q), 147.4 (q), 146.6 (q), 127.3 (+), 125.4 (+), 125.1 (+), 35.9 (-), 31.9 (-), 30.1 (-), 29.7 (-), 29.6 (-), 29.5 (-), 29.4 (-), 29.4 (-), 29.3 (-), 22.7 (-), 21.1 (+), 20.8 (+), 14.1 (+)

HR-MS: ESI⁺ calc. for C₃₇H₄₉N₄O₄Ru (MH⁺) *m/z* = 715.2797; found 715.2806

IR: $\tilde{\nu}$ [cm⁻¹]: 2923 (m), 2851 (m), 1630 (s), 1496 (m), 1414 (m), 1315 (w), 1206 (m), 1033 (w), 920 (w), 819 (s), 735 (m), 506 (m)

2.4.4 Synthesis of Catalyst 3 and 7

Compounds **23**, **24** and **25** were prepared according the previously reported procedure.^[30] The synthesis of catalysts **3** and **7** is described below.

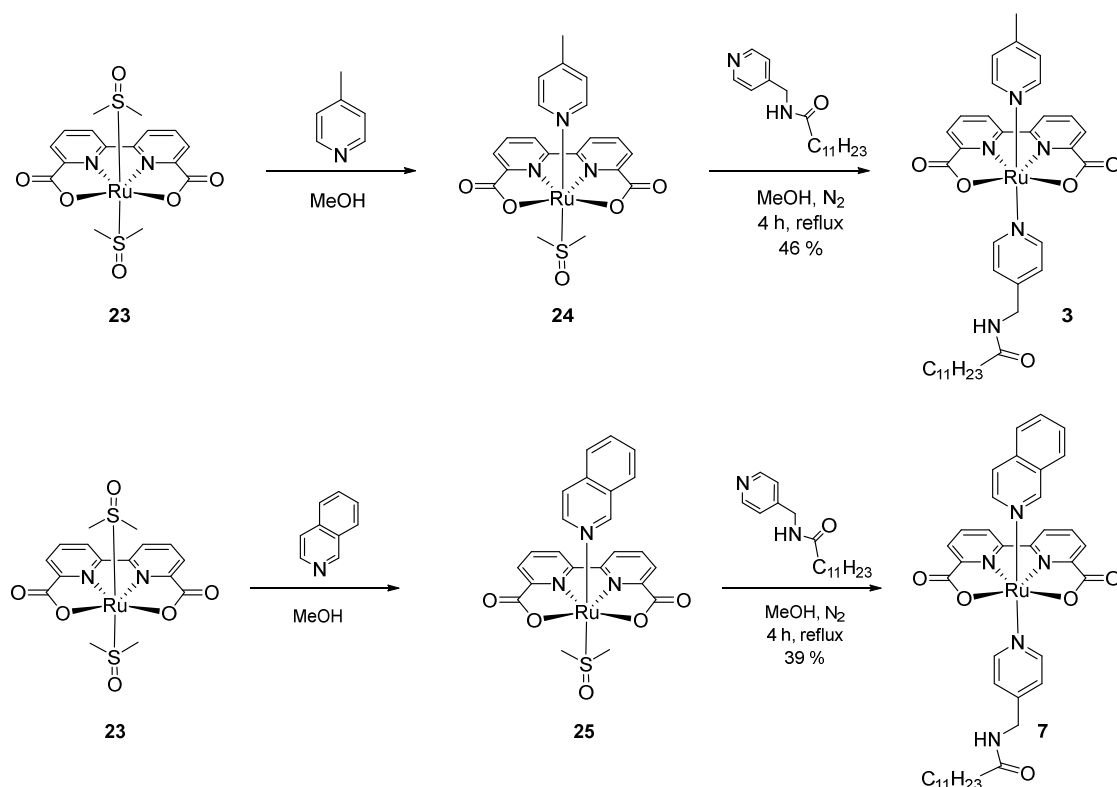


Figure S 2.3 - Synthesis of catalysts **3** and **7**.

Ruthenium^{II} ([2,2'-bipyridine]-6,6'-dicarboxylate) (*N*-(pyridin-4-ylmethyl)dodecanamide) (4-methylpyridine) (**3**)

A mixture of **24** (310 mg, 0.6 mmol) and *N*-(pyridin-4-ylmethyl) dodecanamide (140 mg, 0.6 mmol) in methanol (30 ml) was degassed by N₂ and refluxed for 4 h. The solvent was removed under reduced pressure and the dark red solid obtained was purified by column chromatography on silica gel (MeOH/CH₂Cl₂ 1:5) to give 200 mg of catalyst **3** (46 %, 0.28 mmol).

¹H-NMR (400 MHz, CD₃OD): δ[ppm]: 8.02 (s, 2H), 7.89 (t, *J* = 8 Hz, 2H), 7.75 (d, 2H, *J* = 8 Hz), 7.65 (d, 2H, *J* = 8 Hz), 7.09 (d, 2H, *J* = 8 Hz), 7.04 (d, 2H, *J* = 4 Hz), 4.26 (s, 2H), 2.26 (s, 3H), 2.19 (t, 2H, *J* = 8 Hz), 1.56 (m, 2H), 1.28 (m, 16H), 0.90 (t, *J* = 8 Hz, 3H)

¹³C-NMR (101 MHz, CDCl₃): δ[ppm]: 176.44, 157.25, 152.96, 152.37, 152.35, 151.35, 150.81, 133.09, 127.15, 126.85, 126.40, 124.57, 42.46, 36.83, 33.06, 30.70, 30.56, 30.46, 30.34, 30.31, 26.82, 23.73, 20.67, 14.45

HR-MS: ESI⁺ calc. for C₃₆H₄₃N₅O₅Ru (MH⁺) m/z = 728.2386; found 728.2398

UV/Vis: (in methanol) λ_{max} / nm (ε / M⁻¹cm⁻¹): 250 (20900), 300 (31900), 370 (12200), 480 (4833), 530 (4200)

Ruthenium^{II}([2,2'-bipyridine]-6,6'-dicarboxylate)(*N*-(pyridin-4-ylmethyl)dodecanamide) (isoquinoline) (7)

A mixture of **25** (330 mg, 0.6 mmol) and *N*-(pyridin-4-ylmethyl)dodecanamide (140 mg, 0.6 mmol) in methanol (30 ml) was degassed with N₂ and refluxed for 4 h. The solvent was removed under reduced pressure and the dark red solid obtained was purified by column chromatography on silica gel (MeOH/CH₂Cl₂ 1:5) to yield 180 mg of catalyst **7** (39 %, 0.23 mmol).

¹H-NMR (400 MHz, CDCl₃): δ[ppm]: 8.64 (t, J = 8 Hz, 3H), 8.04 (m, 2H), 7.93 (m, 2H), 7.93-7.76 (m, 4H), 7.73 (m, 1H), 7.64-7.56 (m, 3H), 7.12 (d, J = 4 Hz, 2H), 4.28 (s, 2H), 2.19 (t, 2H, J = 8 Hz), 1.56 (m, 2H), 1.28 (m, 16H), 0.90 (t, J = 8 Hz, 3H)

¹³C-NMR (101 MHz, CDCl₃): δ[ppm]: 175.08, 156.12, 151.60, 150.08, 142.47, 134.77, 132.03, 128.52, 126.17, 125.24, 123.25, 121.74, 41.09, 35.44, 31.66, 29.30, 29.16, 29.07, 28.92, 25.42, 22.34, 13.06

HR-MS: ESI⁺ calc. for C₃₉H₄₃N₅O₅Ru (MH⁺) m/z = 764.2386; found 764.2396

UV/Vis: (in methanol) λ_{max} / nm (ε / M⁻¹cm⁻¹): 250 (23100), 300 (36600), 395 (14900), 530 (4700)

2.4.5 Synthesis of Photosensitizers 2b, 2c and Catalyst 5

Photosensitizers **2b**,^[31] **2c**^[32] and catalyst **5**^[10] were prepared according to literature procedures.

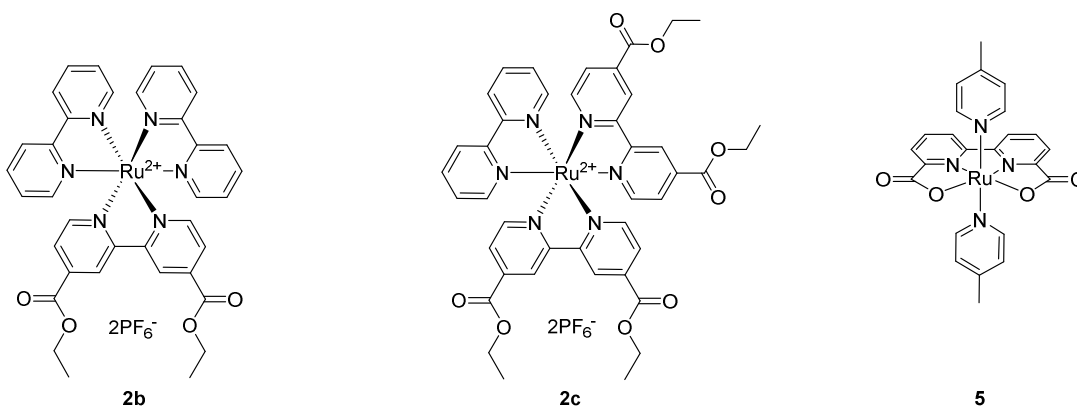


Figure S 2.4 - Structures of photosensitizers **2b**, **2c** and water oxidation catalyst **5**.

2.4.6 Vesicle Preparation and Characterization

Preparation of Vesicles with Catalyst **6b**:

Appropriate volumes of stock solutions of amphiphiles in chloroform or acetonitrile were mixed in a 10 mL crimp top vial to obtain a total amphiphile concentration of 1 mM and the solvent was removed at 85 °C and under reduced pressure. 4.5 mL of aqueous phosphate buffer (50 mM, pH = 7.0) containing 2.5 mM sodium persulfate were added and the vial was closed with a septum-cap. Sonication in an ultrasonic bath at 20 °C above the main phase transition temperature for 20 min yielded a vesicular solution with a narrow size distribution.

Table S 2.1 - Composition of a typical vesicular sample containing catalyst **6b**.

V_{6b}^a [μ L]	V_{2a}^b [μ L]	V_{lipid}^c [μ L]	c_{6b} [μ M]	c_{2a} [μ M]	c_{lipid} [μ M]	$c_{S_2O_8^{2-}}$ [μ M]	V_{buffer} [mL]
56.3	281	388	12.5	125	863	2.5	4.5
^a c (stock solution) = 1 mM			^b c (stock solution) = 2 mM			^c c (stock solution) = 10 mM	

Preparation of Vesicles with Catalyst **3** or **7**:

Appropriate volumes of stock solutions of amphiphiles in chloroform or acetonitrile were mixed in a 25 mL round bottom flask to obtain a total amphiphile concentration of 1 mM and the solvent was removed at the rotatory evaporator and in high vacuum. 8.5 mL of aqueous phosphate buffer (50 mM, pH = 7.0) containing 2.5 mM sodium persulfate were added and the vial was closed. Sonication in an ultrasonic bath at 20 °C above the main phase transition temperature for 20 min yielded a vesicular solution with a narrow size distribution.

Table S 2.2 - Composition of a typical vesicular sample containing catalyst **3** or **7**.

$V_{\text{cat}}^{\text{a}}$ [μL]	$V_{2\text{a}}^{\text{b}}$ [μL]	$V_{\text{lipid}}^{\text{c}}$ [μL]	c_{cat} [μM]	$c_{2\text{a}}$ [μM]	c_{lipid} [μM]	$c_{\text{S}_2\text{O}_8^{2-}}$ [μM]	V_{buffer} [mL]
21	531	742	2.5	125	863	2.5	8.5
^a c (stock solution) = 1 mM			^b c (stock solution) = 2 mM			^c c (stock solution) = 10 mM	

Size Distribution:

The size distribution of the vesicular dispersion was determined by dynamic light scattering.

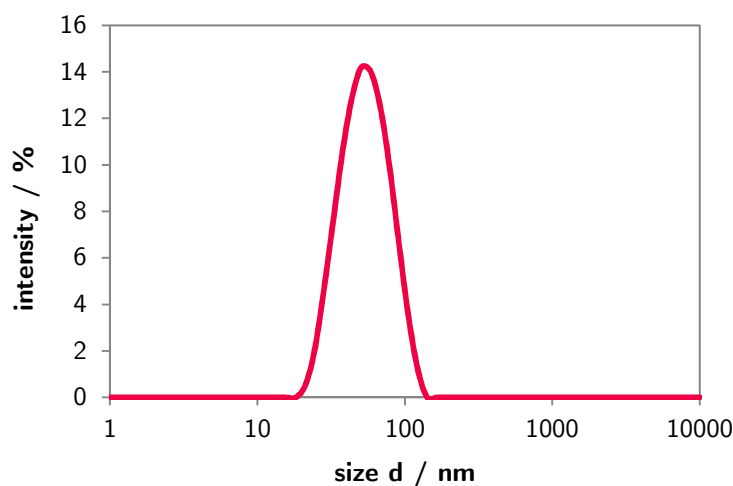


Figure S 2.5 - Typical size distribution of DMPC (**9**) vesicles containing 12.5 mol% **2a** and 1.25 mol% **6b** with a poly dispersity index of 0.25 and an average diameter of 57 nm.

UV Spectra:

UV Spectra of all samples were measured in a 10 mm cuvette at a 62.5 μM concentration of the photosensitizer. All samples showed UV spectra comparable to the homogeneous solution.

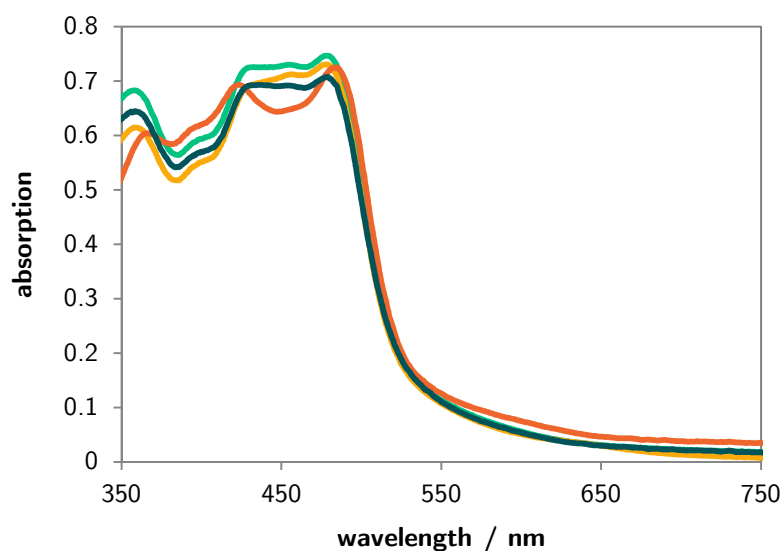


Figure S 2.6 - UV-Vis spectra of DMPC (**9**) vesicles (dark green trace), SMPC (**10**) vesicles (yellow trace), DOPC (**11**) vesicles (light green trace) containing 12.5 mol% **2a** and of equimolar homogeneous solution of **6b** (orange trace). All samples had a photosensitizer concentration of 62.5 μM and were measured in phosphate buffer (pH 7.0, 50 mM).

2.4.7 Irradiation and Gas Chromatography

Samples Containing Catalyst **6b**:

After the sonication all samples were degassed by bubbling argon through the solution for 5 min. The degassed samples were then stirred with a magnetic stirrer and irradiated with high power OSRAM Oslon SSL 80 royal-blue LEDs for 20 min. For temperature control a aluminium cooling block connected to a thermostat was used (Figure S 2.7). After irradiation the amount of evolved oxygen in the gas phase was determined by directly connecting the sample vial to a Inficon micro GC 3000 equipped with a 5 Å mol sieve column, a thermal conductivity detector and Ar as carrier gas. For monitoring the oxygen concentration during the reaction a vial equipped with an oxygen sensor spot and a Fibox 3 oxygen sensor purchased from PreSens Precision Sensing was used.

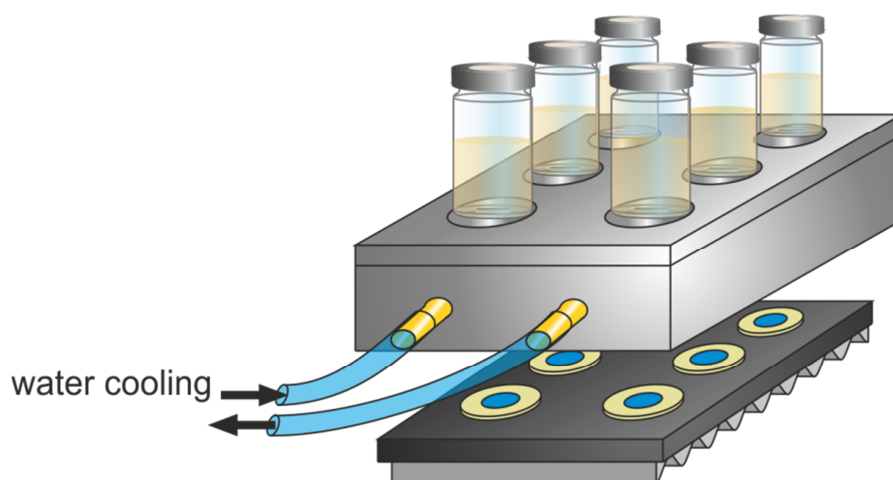


Figure S 2.7 - Schematic setup of the irradiation device for samples containing catalysts **6**.

Samples Containing Catalyst 3 or 7:

For the irradiation 8 mL of the vesicular solution were filled in a 25 mL vial. The vial was closed with a septum and the solution was degassed with argon for 10 min. This solution was stirred magnetically and irradiated for 20 min with a 500 W Xenon lamp (cut off filter, $\lambda > 400$ nm; 450 mW light intensity) under water cooling at 25 °C (Figure S 2.8). After irradiation a 500 μ L sample of the gaseous phase above the reaction solution was injected into a Techcomp GC 7890T gas chromatograph, with a 5 Å mol sieve column, a thermal conductivity detector and Ar as carrier gas.

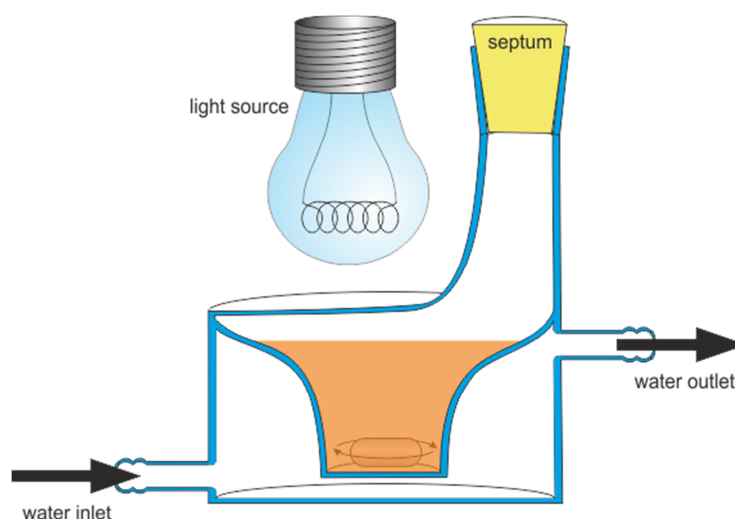


Figure S 2.8 - Schematic setup of the irradiation device for samples containing catalyst **3** and **7**.

2.4.8 Influence of Solution Turbidity on Oxygen Evolution

To determine the influence of the turbidity of a vesicular solution on oxygen evolution three vesicular samples were prepared by different techniques. A vesicular stock solution was prepared by creating a lipid film composed of appropriate amounts of DMPC (**9**) (863 μM), catalyst **6b** (12.5 μM) and photosensitizer **2b** (125 μM). This film was hydrated with phosphate buffer (pH = 7.0, 50 mM) creating a polydisperse vesicular solution. Two aliquots of this solution were homogenized by extrusion through a polycarbonate membrane (pore size 100 nm), using a LiposoFast extruder purchased from Avestin, and ultrasound, respectively. The third aliquot was used directly. The size distribution is shown in Figure S 2.9. The oxygen evolution in the liquid phase was monitored with the Fibox 3 system (Figure S 2.10). The difference in oxygen evolution for all three samples is within the standard error of the experiments. This shows that the size and polydispersity has no important influence on the catalytic performance.

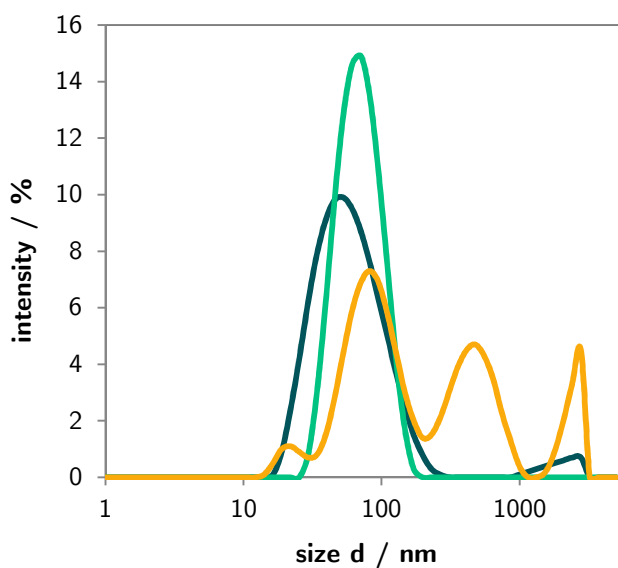


Figure S 2.9 - Size distribution of the extruded (light green trace), sonicated (dark green trace) and polydisperse (yellow trace) vesicular samples.

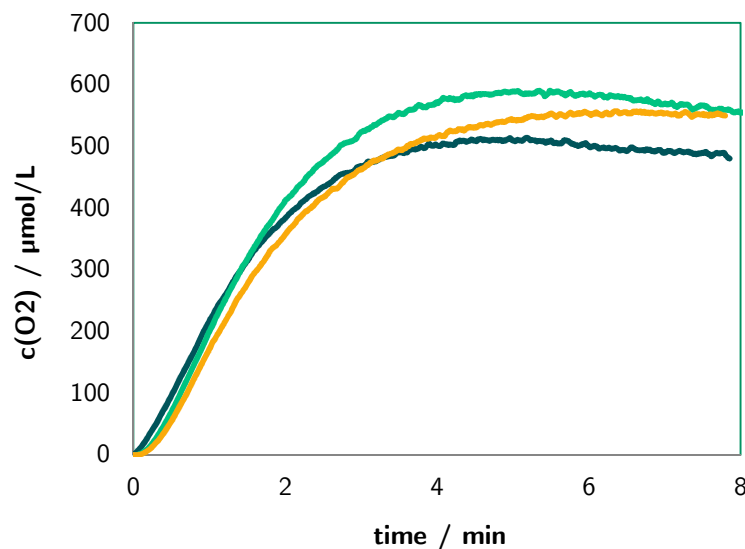


Figure S 2.10 - Oxygen evolution of the extruded (dark green trace), sonicated (yellow trace) and the polydisperse (light green trace) vesicular sample.

2.4.9 Regeneration of the Catalytic Activity

It is known in literature that the activity of a water photooxidizing system is often limited by the stability of the photosensitizer.^[24] We could regain about 60 % of the initial TON by embedding new photosensitizer to the membrane and adding new sacrificial electron acceptor (Table 2). A vesicular solution containing DMPC (**9**), **2a** and **7** was prepared and irradiated as described above. A lipid film of photosensitizer **2a** was prepared by adding 470 μL of a 2 mM stock solution to a round bottom flask and evaporating the solvent. 7.5 mL of the vesicular solution after irradiation were added to the lipid film and the mixture was stirred for 2 h at 60 °C. Sodium persulfate was added to this solution and the sample was degassed by Ar. After 20 min of illumination the amount of evolved oxygen was determined by gas chromatography.

2.4.10 Polarity at the Membrane Interface

The dansyl dye **12** was synthesized according to a literature known procedure.^[33] The polarity at the interface was determined by embedding **6** into DMPC (**9**), SMPC (**10**) or DOPC (**11**) bilayer membranes (5 mol%) and exciting the dye at a wavelength of 335 nm.^[34] The emission maximum wavelength was measured and no significant difference was obtained (Figure S 2.11).

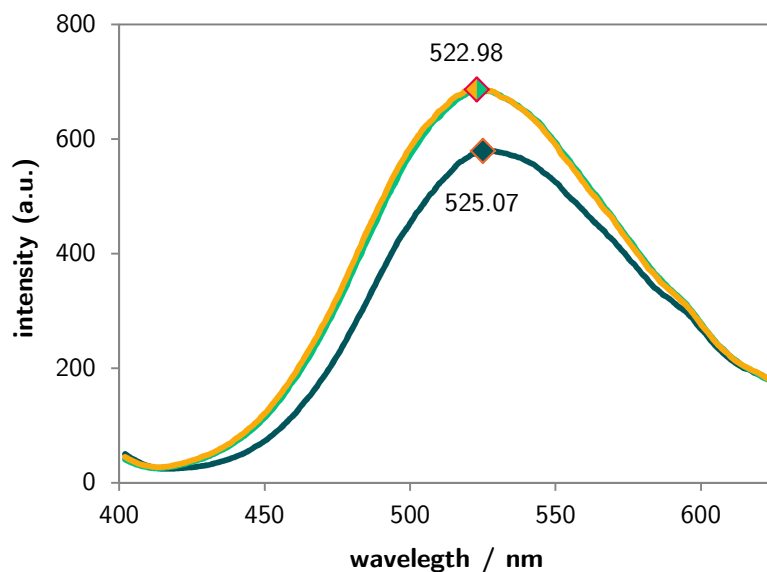


Figure S 2.11 - Emission spectra of dansyl dye **12** embedded in DOPC (**11**) (dark green trace), DMPC (**9**) (light green trace) and SMPC (**10**) (yellow trace) vesicles.

2.4.11 Determination of the Quantum Efficiency

The quantum efficiency ϕ for the oxidant generation between $\text{Ru}(\text{bpy})_3$ and sodium persulfate can be determined by measuring the the emission intensity of the $\text{Ru}(\text{bpy})_3^{2+}$ in the absence and presence of persulfate under the same condiaitons used in the reaction.^[28] This was done by preparing vesicular samples as described in section 2.4.6 without sodium persulfate. After degassing with Ar the emission intensity of **2a** at 665 nm was measured. Then sodium persulfate was added and the emission intensity was determined again (Table S 2.3). With this data the qauntum efficiency $\phi = 1 - I/I_0$ was calculated.

Table S 2.3 - Determined emission intensities at 665 nm of vesicular samples containing 125 μM **2a**, 12.5 μM **6b** and 863 μM phospholipid and calculated quantum efficiencies ϕ .

Entry	phospholipid	I_0 (without $\text{S}_2\text{O}_8^{2-}$)	I (with $\text{S}_2\text{O}_8^{2-}$)	ϕ ($1 - I/I_0$) [%]
1	DMPC (9)	699	454	35
2	SMPC (10)	633	445	30
3	DOPC (11)	758	685	10

2.5 References

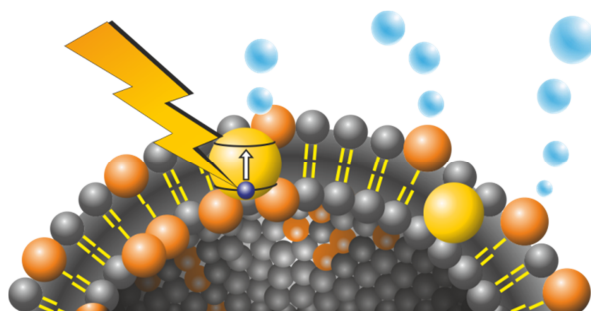
- [1] T. R. Cook, D. K. Dogutan, S. Y. Reece, Y. Surendranath, T. S. Teets, D. G. Nocera, "Solar Energy Supply and Storage for the Legacy and Nonlegacy Worlds", *Chem. Rev.* **2010**, 110, 6474-6502.
- [2] N. S. Lewis, D. G. Nocera, "Powering the planet: Chemical challenges in solar energy utilization", *PNAS* **2006**, 103, 15729-15735.
- [3] M. Hambourger, G. F. Moore, D. M. Kramer, D. Gust, A. L. Moore, T. A. Moore, "Biology and technology for photochemical fuel production", *Chem. Soc. Rev.* **2008**, 38, 25-35.
- [4] P. D. Frischmann, K. Mahata, F. Würthner, "Powering the future of molecular artificial photosynthesis with light-harvesting metallosupramolecular dye assemblies", *Chem. Soc. Rev.* **2013**, 42, 1847-1870.
- [5] M. R. Norris, J. J. Concepcion, D. P. Harrison, R. A. Binstead, D. L. Ashford, Z. Fang, J. L. Templeton, T. J. Meyer, "Redox Mediator Effect on Water Oxidation in a Ruthenium-Based Chromophore-Catalyst Assembly", *J. Am. Chem. Soc.* **2013**, 135, 2080-2083.
- [6] N. Kaveevivitchai, R. Chitta, R. Zong, M. El Ojaimi, R. P. Thummel, "A Molecular Light-Driven Water Oxidation Catalyst", *J. Am. Chem. Soc.* **2012**, 134, 10721-10724.
- [7] L. Kohler, N. Kaveevivitchai, R. Zong, R. P. Thummel, "Component Analysis of Dyads Designed for Light-Driven Water Oxidation", *Inorg. Chem.* **2013**, 53, 912-921.
- [8] F. Li, Y. Jiang, B. Zhang, F. Huang, Y. Gao, L. Sun, "Towards A Solar Fuel Device: Light-Driven Water Oxidation Catalyzed by a Supramolecular Assembly", *Angew. Chem. Int. Ed.* **2012**, 51, 2417-2420.
- [9] D. J. Wasylenko, R. D. Palmer, C. P. Berlinguette, "Homogeneous water oxidation catalysts containing a single metal site", *Chem. Commun.* **2013**, 49, 218-227.
- [10] L. Duan, Y. Xu, P. Zhang, M. Wang, L. Sun, "Visible Light-Driven Water Oxidation by a Molecular Ruthenium Catalyst in Homogeneous System", *Inorg. Chem.* **2009**, 49, 209-215.
- [11] S. Bhosale, A. L. Sisson, P. Talukdar, A. Fürstenberg, N. Banerji, E. Vauthey, G. Bollot, J. Mareda, C. Röger, F. Würthner, N. Sakai, S. Matile, "Photoproduction of Proton Gradients with π -Stacked Fluorophore Scaffolds in Lipid Bilayers", *Science* **2006**, 313, 84-86.
- [12] J. J. Grimaldi, S. Boileau, J.-M. Lehn, "Light-driven, carrier-mediated electron transfer across artificial membranes", *Nature* **1977**, 265, 229-230.
- [13] R. F. Khairutdinov, J. K. Hurst, "Cyclic transmembrane charge transport by pyrylium ions in a vesicle-based photocatalytic system", *Nature* **1999**, 402, 509-511.

- [14] A. Perez-Velasco, V. Gorteau, S. Matile, "Rigid Oligoperylenediimide Rods: Anion- π Slides with Photosynthetic Activity", *Angew. Chem. Int. Ed.* **2008**, 47, 921-923.
- [15] G. Steinberg-Yfrach, P. A. Liddell, S.-C. Hung, A. L. Moore, D. Gust, T. A. Moore, "Conversion of light energy to proton potential in liposomes by artificial photosynthetic reaction centres", *Nature* **1997**, 385, 239-241.
- [16] L. Zhu, R. F. Khairutdinov, J. L. Cape, J. K. Hurst, "Photoregulated Transmembrane Charge Separation by Linked Spiropyran-Anthraquinone Molecules", *J. Am. Chem. Soc.* **2005**, 128, 825-835.
- [17] H. Dau, C. Limberg, T. Reier, M. Risch, S. Roggan, P. Strasser, "The Mechanism of Water Oxidation: From Electrolysis via Homogeneous to Biological Catalysis", *ChemCatChem* **2010**, 2, 724-761.
- [18] W. S. Aldridge, B. J. Hornstein, S. Serron, D. M. Dattelbaum, J. R. Schoonover, T. J. Meyer, "Synthesis and Characterization of Oligoproline-Based Molecular Assemblies for Light Harvesting", *J. Org. Chem* **2006**, 71, 5186-5190.
- [19] V. Aranyos, A. Hagfeldt, H. Grennberg, E. Figgemeier, "Electropolymerisable bipyridine ruthenium(II) complexes: synthesis, spectroscopic and electrochemical characterisation of 4-((2-thienyl) ethenyl)- and 4,4'-di((2-thienyl) ethenyl)-2,2'-bipyridine ruthenium complexes", *Polyhedron* **2004**, 23, 589-598.
- [20] S. Földner, R. Mild, H. I. Siegmund, J. A. Schroeder, M. Gruber, B. König, "Green-light photocatalytic reduction using dye-sensitized TiO₂ and transition metal nanoparticles", *Green Chem.* **2010**, 12, 400-406.
- [21] D. Pucci, G. Barberio, A. Bellusci, A. Crispini, M. Ghedini, E. I. Szerb, "Supramolecular Columnar Mesomorphism Induced by Silver(I) Coordination of 2,2'-bipyridine-4,4'-diamides", *Mol. Cryst. Liq. Cryst.* **2005**, 441, 251-260.
- [22] M. S. Vickers, K. S. Martindale, P. D. Beer, "Imidazolium functionalised acyclic ruthenium(II) bipyridyl receptors for anion recognition and luminescent sensing", *J. Mater. Chem.* **2005**, 15, 2784-2790.
- [23] L. Duan, Y. Xu, M. Gorlov, L. Tong, S. Andersson, L. Sun, "Chemical and Photochemical Water Oxidation Catalyzed by Mononuclear Ruthenium Complexes with a Negatively Charged Tridentate Ligand", *Chem. Eur. J.* **2010**, 16, 4659-4668.
- [24] L. Wang, L. Duan, L. Tong, L. Sun, "Visible light-driven water oxidation catalyzed by mononuclear ruthenium complexes", *J. Catal.* **2013**, 306, 129-132.
- [25] L. Duan, C. M. Araujo, M. S. G. Ahlquist, L. Sun, "Highly efficient and robust molecular ruthenium catalysts for water oxidation", *PNAS* **2012**, 109, 15584-15588.

- [26] J. R. Silvius, *"Lipid-Protein Interactions"*, John Wiley & Sons, Inc, New York, **1982**.
- [27] The varying fluorescence signals obtained from different lipid vesicular solutions without persulfate indicate a diverse chemical environment, which could be also influenced by other parameters like rigidity of the membrane, solvation of the artificial amphiphiles as well as a possibly different positioning within the bilayer (see supplementary information for data).
- [28] A. Lewandowska-Andralojc, D. E. Polyansky, *"Mechanism of the Quenching of the Tris(bipyridine)ruthenium(II) Emission by Persulfate: Implications for Photoinduced Oxidation Reactions"*, *J. Phys. Chem. A* **2013**, 117, 10311-10319.
- [29] H. Takalo, J. Kankare, H. Lund, L. Makmur, R. Norrestam, *"Synthesis of Dimethyl and Diethyl 4-(Phenylethynyl)-2,6-pyridinedicarboxylate"*, *Acta Chem. Scand.* **1987**, 41b, 219-221.
- [30] Y. Jiang, F. Li, B. Zhang, X. Li, X. Wang, F. Huang, L. Sun, *"Promoting the Activity of Catalysts for the Oxidation of Water with Bridged Dinuclear Ruthenium Complexes"*, *Angew. Chem. Int. Ed.* **2013**, 52, 3398-3401.
- [31] H. Xia, Y. Zhu, D. Lu, M. Li, C. Zhang, B. Yang, Y. Ma, *"Ruthenium(II) Complexes with the Mixed Ligands 2,2'-Bipyridine and 4,4'-Dialkyl Ester-2,2'-bipyridine as Pure Red Dopants for a Single-Layer Electrophosphorescent Device"*, *J. Phys. Chem. B* **2006**, 110, 18718-18723.
- [32] V. Shklover, M. K. Nazeeruddin, S. M. Zakeeruddin, C. Barbé, A. Kay, T. Haibach, W. Steurer, R. Hermann, H. U. Nissen, M. Grätzel, *"Structure of Nanocrystalline TiO₂ Powders and Precursor to Their Highly Efficient Photosensitizer"*, *Chem. Mater.* **1997**, 9, 430-439.
- [33] Y. Kitano, Y. Nogata, K. Matsumura, E. Yoshimura, K. Chiba, M. Tada, I. Sakaguchi, *"Design and synthesis of anti-barnacle active fluorescence-labeled probe compounds and direct observation of the target region in barnacle cypris larvae for dimethyl-isocyanoalkyl compounds"*, *Tetrahedron* **2005**, 61, 9969-9973.
- [34] B. Gruber, E. Kataev, J. Aschenbrenner, S. Stadlbauer, B. König, *"Vesicles and Micelles from Amphiphilic Zinc(II)-Cyclen Complexes as Highly Potent Promoters of Hydrolytic DNA Cleavage"*, *J. Am. Chem. Soc.* **2011**, 133, 20704-20707.

3 Quantum Dots as Photosensitizers in Photocatalytic Water Oxidation

3.1	Introduction	66
3.2	Results and Discussion	70
3.3	Conclusion	82
3.4	Experimental Part	83
3.5	References	88



Quantum dots as a replacement for the commonly used single molecule photosensitizers in photocatalytic water oxidation could solve major challenges such as the limited longevity of those systems. Different-sized CdSe quantum dots with several ligand environments were synthesized and characterized. They were used in vesicular and homogeneous systems and different combinations and ratios of quantum dots and water oxidation catalysts were investigated towards oxygen generation. A charge transfer between quantum dots and water oxidation catalysts was observed by fluorescence quenching experiments. However, a working photocatalytic water oxidation system could not be achieved by any combination of quantum dots and molecular catalysts.

3.1 Introduction

Efficient photocatalytic water oxidation systems are needed to solve the world's energy consumption issues and a tremendous progress has been achieved in the last decades.

Since the discovery of the “blue dimer” $[\text{cis,cis-}[\text{Ru}(\text{bpy})_2(\text{H}_2\text{O})]_2(\mu\text{-O})]^{4+}$ by Meyer *et al.*,^[1,2] which was one of the first examples of a homogeneous water oxidation catalyst, different highly efficient catalysts based on Ru, Ir, and non-noble metals have been developed.^[3] The activities in chemical water oxidation utilizing Ce^{4+} as the sacrificial electron acceptor for example increased from several turnovers to more than 100.000 TONs in the most efficient water oxidation systems, which were reported by Sun *et al.*^[4]

However, a multi-component system consisting of a water oxidation catalyst and a photosensitizer is needed to utilize solar energy for photochemical water oxidation. The performance of these photocatalytic systems is mainly limited by the degradation of the commonly used single molecule photosensitizers, such as tris-bipyridine ruthenium $[\text{Ru}(\text{bpy})_3]^{2+}$ and its derivatives. Water oxidation catalysts, that are known to last thousands of catalytic cycles in chemical water oxidation, barely reach several hundred turnovers under photochemical conditions in a combination with a single molecule photosensitizer.^[5]

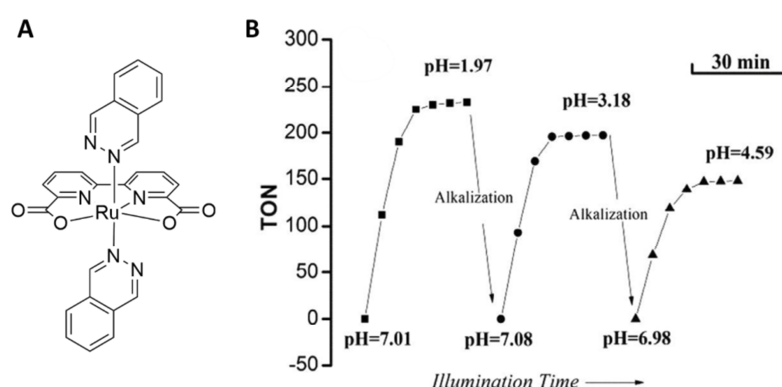


Figure 3.1 - A: Structure of the water oxidation catalyst used for reactivation of the photocatalytic water oxidation system. **B:** Repetitive reactivation of the photochemical water oxidation system by addition of new photosensitizer, electron acceptor and adjustment of the pH value (Reprinted from [5], with permission from Elsevier).

The inactivation of a typical multi-component system due to a degraded photosensitizer was proven by an addition of new photosensitizer to a used photocatalytic water oxidation solution. Catalytic activity was regained for example in the vesicular system in Section 2.4.9.^[6] The Sun group reported that photocatalytic systems, comparable to the ones used in

Chapter 2, were reactivated after the adjustment of the pH and the addition of new photosensitizer and electron acceptor (Figure 3.1).^[5] Hence the replacement of the commonly used ruthenium-based photosensitizers by more stable alternatives is crucial for the development of highly efficient photocatalytic water oxidizing systems.

Colloidal quantum dots are semiconductor nano-particles, which are dispersed in a solvent. The quantum dots are either “naked” or surrounded by a shell of stabilizing ligands. The quantum dot’s electronic and physical properties are determined by its size, shape and ligand environment.^[7] The band gap energy particularly depends on the material and the size of the quantum dots, due to the confinement of the electron hole pair by the size of the nanocrystal. When the size decreases below a certain level, the band structure of the bulk semiconductors changes and slightly different energies in the bulk material are compressed into a single, intense transition in quantum dots. The oscillator strength is concentrated into a few possible transitions, which results in an absorption spectrum of the quantum dots comparable to molecular photosensitizers (Figure 3.2). These changes can be drastic, *e.g.* the band gap of CdS can be tuned from 2.5 eV up to 4.5 eV by going from bulk material to colloidal quantum dots.^[8]

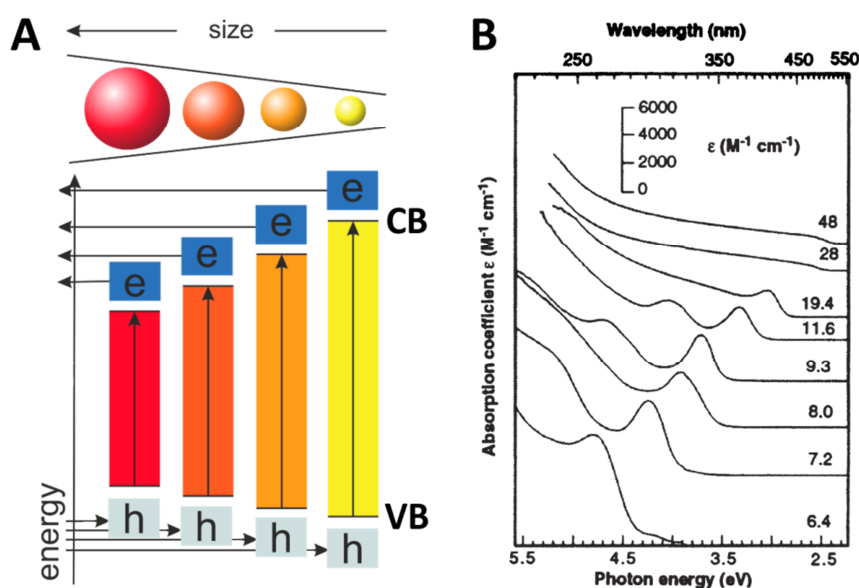


Figure 3.2 - A: Schematic representation of how the size of colloidal quantum dots affects the position of the band edges and the size of the bands gap. The band gap widens with decreasing size of the nanocrystals. Valence band (VB) potentials are shifted to positive and the conduction band (CB) edge shifts to negative potentials. **B:** Absorption spectra of CdS quantum dots with different sizes. With decreasing size the spectra shift to the blue and look more like those of molecular compounds, because the oscillator strength is concentrated to a few transitions (From [8]. Reprinted with permission from AAAS.)

The properties of quantum dots can be tuned to a variety of different demands by changing the following parameters: material, size, shape, stabilizing agent and nature of the quantum dot (core/shell or core). They found application in quantum-dot-sensitized solar cells, as photodetectors, in light emitting diodes or in photoelectrochemical cells for fuel generation.^[9, 10]

Colloidal quantum dots have been already successfully introduced in the reductive half-reaction of water splitting. Exceptional longevity and turnovers were achieved in systems composed of quantum dots and homogeneous catalysts. The combination of CdSe nanocrystals and a homogeneous nickel-based reduction catalyst showed high activity for at least 360 hours and a total of more than 600.000 TONs, whereas systems with small molecule photosensitizers typically cease activity after less than 50 hours due to bleaching of the dye.^[11] Several groups reported an increase in hydrogen generation in systems where the quantum dots were brought in close proximity to the hydrogen evolution catalyst by either co-immobilizing them on supports or by adsorbing the catalysts on the quantum dots.^[12-15]

The same effect could be achieved by using vesicles to immobilize quantum dots within the membrane and incorporate suitable catalysts into the outer and inner membrane layer. This system would ensure a close distance of quantum dots and catalysts, which is important for an efficient electron transfer (Figure 3.3).

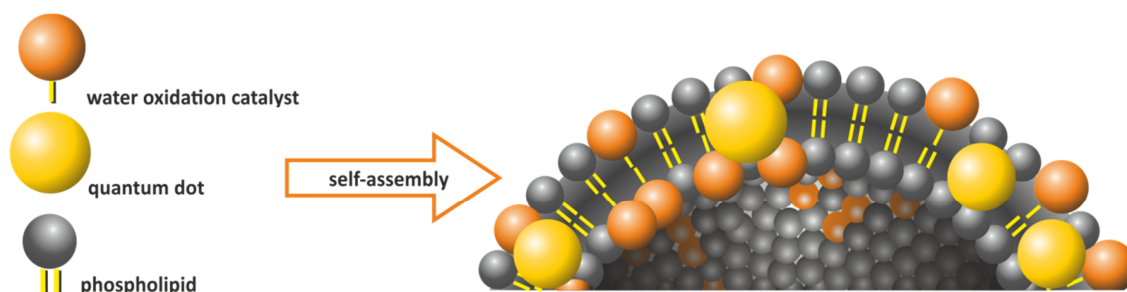


Figure 3.3 - Schematic representation of the self-assembly process of quantum-dot-functionalized vesicles.

Quantum dots incorporated into bilayer membranes found applications in various fields of biodiagnostics, such as sensing,^[16] imaging^[17] or targeting.^[18] The membrane of phospholipid vesicles is known to protect quantum dots against photodegradation, which was shown in a recently published report by Salaita *et al.*^[19] They functionalized **DOPC**, **DMPC** and **DSPC** phospholipid vesicles within the two leaflets with 3 nm CdSe quantum dots capped with oleic acid ligands. The physical properties of the membrane were not altered significantly by the incorporation. Quantum dots encapsulated in gel phase membranes proved to be extremely stable against photooxidation at ambient conditions. Molecular dynamics calcula-

tions confirmed that quantum dots in gel phase membranes distort the leaflet. Membranes in the fluid phase do not cover the complete quantum dot and thus protect them less against photooxidation with oxygen.

Although quantum dots are already established in proton reduction, they have found no application in water oxidation so far. However, there are some reports about charge transfer from a water oxidation catalyst to a quantum dot.

Sykora *et al.* adsorbed different Ru-polypyridine complexes on CdSe quantum dots with a diameter of 2.3 nm and observed ultra-fast hole transfer from the quantum dot to the Ru-complex in the range of 5 ps by transient absorption and time-resolved photoluminescence spectroscopy.^[20] The oxidation potential of the Ru-complexes was around 1.5 V and they stated the valence band edge for the CdSe quantum dots to be over 2.0 V. In a subsequent study, they investigated the interaction of CdSe quantum dots with a smaller diameter, and thus a larger band gap and similar Ru-complexes.^[21] In contrast to the previous study, this time energy transfer was the main reason for the observed photoluminescence quenching. They attributed this to the larger overlap of the quantum dot's and the Ru-complex's absorption spectrum. Nevertheless, they showed that a hole transfer to Ru-complexes is possible, even if the interplay of these two mechanisms seems to be intricate.

Another interesting example for photoinduced charge transfer from a semiconductor nanocrystal to a water oxidation catalyst was published by the group of Dukovic in 2013.^[22] They investigated the charge transfer dynamics between CdS nanorods and a mononuclear ruthenium water oxidation catalyst derived from the [Ru(bpy)(tpy)Cl] complexes, which were introduced by Thummel *et al.*^[23] This water oxidation catalyst showed an oxidation potential of 1.2 V, which is comparable to our system using catalyst **7** or **8** (Figure 3.4), and had shown a good performance in chemical water oxidation using Ce^{IV} as a sacrificial acceptor before. They introduced ethylester moieties on the bpy ligand for the immobilization of the catalyst on the surface of the nanorods. A very efficient hole transfer from the semiconductor to the catalyst was observed, which was confirmed by transient absorption spectrometry. An electron transfer to the newly generated Ru^{III} in the water oxidation catalyst followed the hole transfer. This charge transfers were confirmed by additional tests using a hole scavenger (ascorbate) or an electron scavenger (methylene blue). The initial hole transfer was 1-3 orders of magnitude faster than the electron transfer at low surface-coverage conditions.

3.2 Results and Discussion

3.2.1 Characterization of Quantum Dot Solutions

CdSe quantum dots were synthesized using different approaches and ligands. In general, a characterization is possible using TEM, or UV/Vis spectroscopy. In this work, the diameter of the synthesized quantum dots was estimated by UV/Vis spectroscopy. The position of the lowest energy absorption peak is characteristic for every diameter of CdSe quantum dots. Peng *et al.* reported an empirical equation, which describes the correlation of the position of this absorption peak and the particle diameter (Equation 3.1)

$$D = 1.6122 \cdot 10^{-9} \lambda^4 - 2.6575 \cdot 10^{-6} \lambda^3 + 1.6242 \cdot 10^{-3} \lambda^2 - 0.4277 \lambda + 41.57 \quad (3.1)$$

The concentration of a quantum dot solution can be estimated by UV/Vis spectroscopy as well. Peng *et al.* found that the extinction coefficient of a certain quantum dot is also correlated to the particle's diameter. From a series of experiments they calculated an equation for this correlation (Equation 3.2).

$$\varepsilon = 5857 D^{2.65} \quad (3.2)$$

The correlation of the extinction coefficient and the size was found to be completely independent of the solvent, ligand shell and the synthetic method of the investigated quantum dots. Equation 3.2 is just valid for quantum dots with a certain size distribution. The size distribution is indicated by the half-width-half-maximum (HWHM) of the lowest energy absorption band. The measured absorption of a random quantum dot solution has to be corrected using Equation 3.3, because the equation was generated based on quantum dots with a HWHM of 14 nm.

$$A = A_m \cdot \frac{hwhm_m}{14nm} \quad (3.3)$$

3.2.2 Incorporation of Quantum Dots into Vesicular Membranes

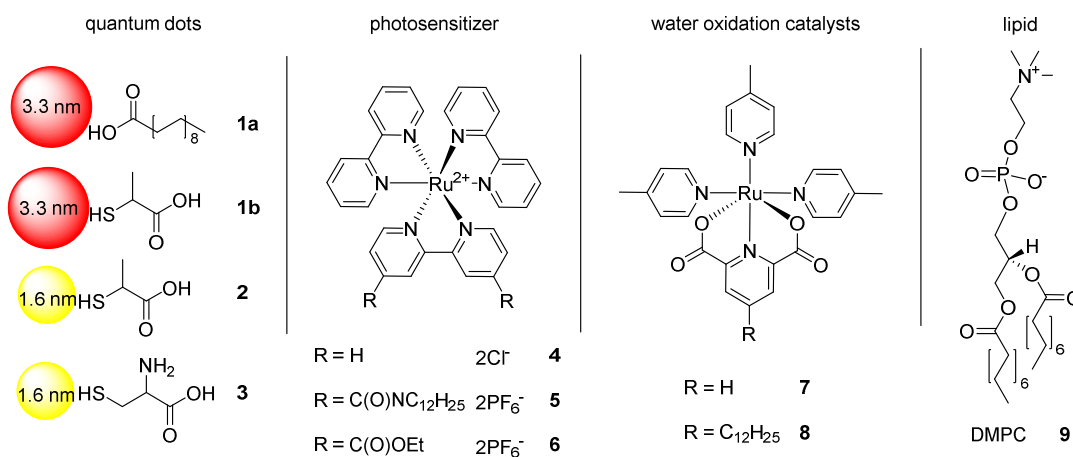


Figure 3.4 - Quantum dots, photosensitizers, water oxidation catalysts and the lipid used in photochemical water oxidation.

The quantum dots for the incorporation into vesicular membranes were synthesized by a hot injection method, following the report by Salaita *et al.*^[19] The oleic acid used as the stabilizing agent in the original report could be detrimental for a water oxidation system due to the double bond in the alkyl chains. From the experiments in Section 2.2 we know that lipids with double bonds shut down photochemical water oxidation. This effect could also occur due to the oxidation of the double bonds in the ligand environment of the quantum dots. Therefore stearic acid was used as the stabilizing ligand in quantum the dot synthesis. The quantum dots were synthesized by a hot injection method, in which the Se-precursor is injected into a hot Cd-precursor solution. The precursors were prepared in octadecene. Tributyl phosphine was employed for the preparation of the Se-precursor (Figure 3.5).

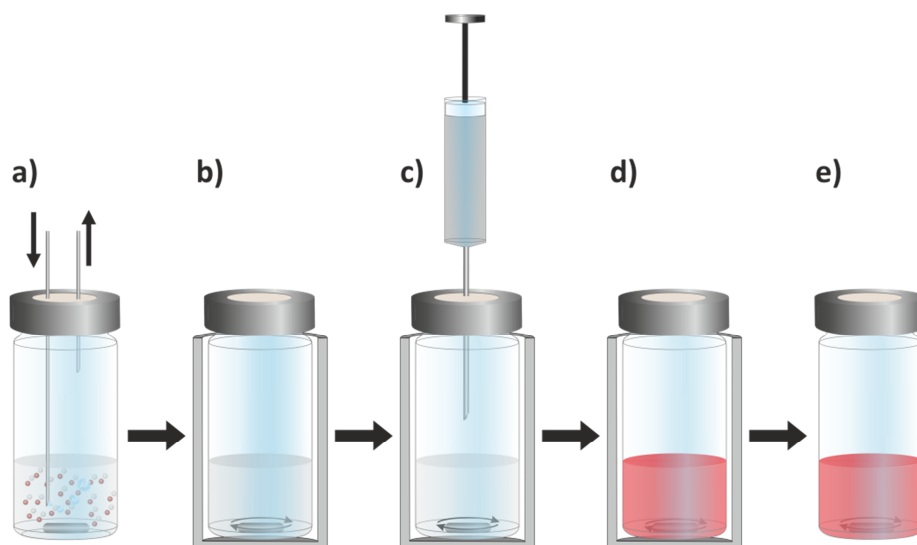


Figure 3.5 - Schematic representation of the hot injection method for the quantum dot synthesis. a) Degassing of the CdO and stearic acid in octadecene, b) dissolution at 280 °C, c) injection of the Se-precursor at 250 °C, d) stirring at 250 °C for 20 s, e) cooling to r.t.

This method produced quantum dots with a moderate size distribution with a HWHM of 22 nm around a diameter of 3.3 nm (Figure 3.6). The quantum dots were soluble in CHCl_3 , THF and THF:water mixtures with up to 5 vol% of water.

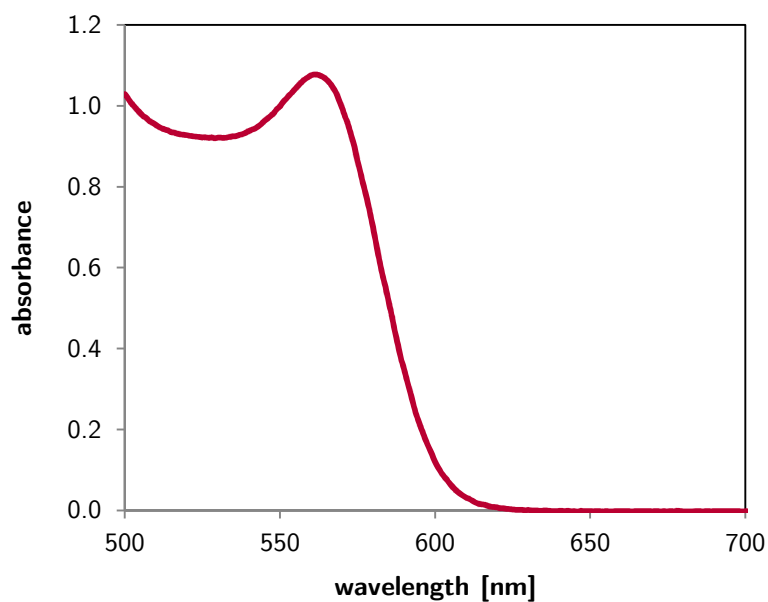


Figure 3.6 - Absorption spectrum of a typical sample of quantum dots **1a** in THF.

The preparation method for the encapsulation of quantum dots within phospholipid bilayers is equal to the preparation of functionalized vesicles from Chapter 2 and follows the reported procedure from Salaita *et al.* Stock solutions of all compounds in CHCl_3 were mixed together and the solvent was removed. After the addition of buffer, the solution was homogenized in an ultrasonic bath to yield small unilamellar vesicular solutions. The concentration of quantum dots in the membranes used by Salaita was very low. They used only 0.02 mol% of quantum dots in their assemblies. This concentration is too low for a conventional water oxidation system utilizing small molecule photosensitizers. DMPC (**9**, Figure 3.4) vesicles containing the ruthenium biscarboxylate water oxidation catalyst **8** and the quantum dots **1a** were prepared together with persulfate as the sacrificial electron acceptor to investigate the concentration dependency of quantum dots in photochemical water oxidation (Table 3.1). The samples differed by increasing amounts of quantum dots incorporated into the vesicular membrane.

Table 3.1 - Composition of the DMPC vesicular samples containing quantum dots **1a** and catalyst **8** in 50 mM phosphate buffer pH = 7.0.

Entry	c_{DMPC} [μM]	c_{8} [μM]	c_{1a} [μM]	$c_{\text{Na}_2\text{S}_2\text{O}_8}$ [μM]
1	987	12.5	0.2	2500
2	983	12.5	5.0	2500
3	975	12.5	12.5	2500
4	938	12.5	50.0	2500
5	863	12.5	125	2500

Applying the conditions of Salaita *et al.* (Table 3.1, Entry 1) resulted in a homogenous clear vesicular dispersion. This dispersion was irradiated with blue light LEDs and the amount of oxygen was detected with the oxygen sensor. No change in the oxygen content was detected during the irradiation. Sonication of the sample containing 5.0 μM of quantum dots **1a** resulted in a bleared, reddish solution (Table 3.1, Entry 2). The irradiation of this sample also resulted in no detectable oxygen formation. The preparation of higher concentrated solutions of quantum dot **1a** in vesicular membranes (Table 3.1, Entry 3-5) was not possible. Sonication of these samples did not yield homogeneous solutions. Hence, these samples were not subjected to irradiation.

3.2.3 Quantum Dots in Homogeneous Solution

Quantum Dots 1a

The prior experiments showed that the incorporation of quantum dots into membranes of phospholipid vesicles allows only very low concentrations of quantum dots. Therefore, the following experiments were conducted in homogeneous solution to simplify the system and to increase the quantum dots concentration. The originally reported water oxidation system by the Sun group utilizing the photosensitizer **6** and the catalyst **7** worked in water/acetonitrile mixtures.^[24] These mixtures are not suitable for quantum dots **1a** because their solubility in water-miscible solvents is limited to THF with a maximal water content of 5 vol%. Both the water oxidation catalyst **7** and the quantum dots **1a** were well soluble in this mixture. Besides two samples containing the quantum dots **1a** and catalyst **7**, a third sample was prepared containing the photosensitizer **5**. This sample was irradiated to control whether a photochemical water oxidation is possible under these conditions (Table 3.2).

Table 3.2 - Composition of samples containing catalyst **7** and either quantum dot **1a** or photosensitizer **5** in a mixture of THF:H₂O (95:5).

Entry	c_7 [μ M]	c_{1a} [μ M]	c_5 [μ M]	$c_{Na_2S_2O_8}$ [μ M]
1	10	180	-	2500
2	50	180	-	2500
3	50	-	500	2500

Neither the samples containing quantum dots **1a**, nor the sample with photosensitizer **5** evolved a measurable amount of oxygen after a continuous irradiation with blue LEDs (455 nm) for 1 h. This implies that a photocatalytical water oxidation is not possible under these solvent conditions.

A possible explanation is that the low water content could change the equilibrium of water binding to the oxidation catalyst and therefore inhibit the water oxidation. The water content cannot be increased in this system using quantum dots **1a** with stearic acid ligands. However, the solubility of quantum dots can be changed by an exchange of the stabilizing ligand shell. An exchange of the stearic acid by, for example 2-mercaptopropionic acid turns the quantum dots **1b** hydrophilic. The exchange was performed in a biphasic system of toluene and phosphate buffer (Figure 3.7).

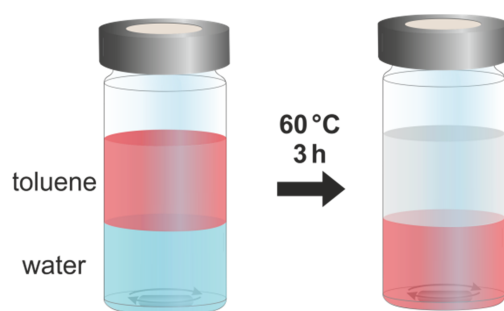


Figure 3.7 - Schematic representation of the ligand exchange from stearic acid to 2-mercaptopropionic acid.

The resulting quantum dots **1b** were soluble in phosphate buffer at slightly basic conditions of pH 8.5. An acetonitrile content of 10 vol% was necessary to ensure a sufficient solubility of the water oxidation catalyst **7** and **8**. Photosensitizer **6** was employed for the control in these experiments due to the insufficient solubility of photosensitizer **5** under these conditions.

Table 3.3 - Composition of homogeneous samples containing quantum dots **1b** and catalyst **7** or **8** in phosphate buffer (pH 8.5) and 10 % acetonitrile.

Entry	c_7 [μM]	c_8 [μM]	c_{1b} [μM]	c_6 [μM]	$c_{\text{Na}_2\text{S}_2\text{O}_8}$ [μM]
1	50	-	180	-	2500
2	-	50	180	-	2500
3	50	-	-	500	2500

Again, none of the samples containing quantum dots **1b** as the photosensitizer produced any detectable amount of oxygen during the irradiation (Table 3.3, Entry 1 and 2). However, a significant amount of oxygen was evolved by the control experiment with photosensitizer **6**. Hence, photocatalytic oxygen evolution employing catalyst **7** is possible under these conditions.

Quantum Dots 2

The position of the valence band edge shifts to the positive when the size of the quantum dots is reduced due to the higher quantum confinement.^[9] Therefore, a reduction of the size leads to higher driving forces for the hole transfer from the quantum dot to the catalyst. The hydrophilic quantum dots **2** were synthesized following a procedure reported by Wu *et al.*^[13]

In contrast to the method used for the synthesis of quantum dots **1a**, this procedure takes place in water at 100 °C. Na_2SeSO_3 is used as the selenium precursor and CdCl_2 can be

employed directly as the cadmium source. This synthetic method is slower and therefore can be followed by UV/Vis spectroscopy (Figure 3.8). The formation of 1.6 nm quantum dots **2** with 2-mercaptopropionic acid ligands needed around 60 min. This synthetic route produced quantum dots with a modest size distribution and a HWHM of 35–40 nm.

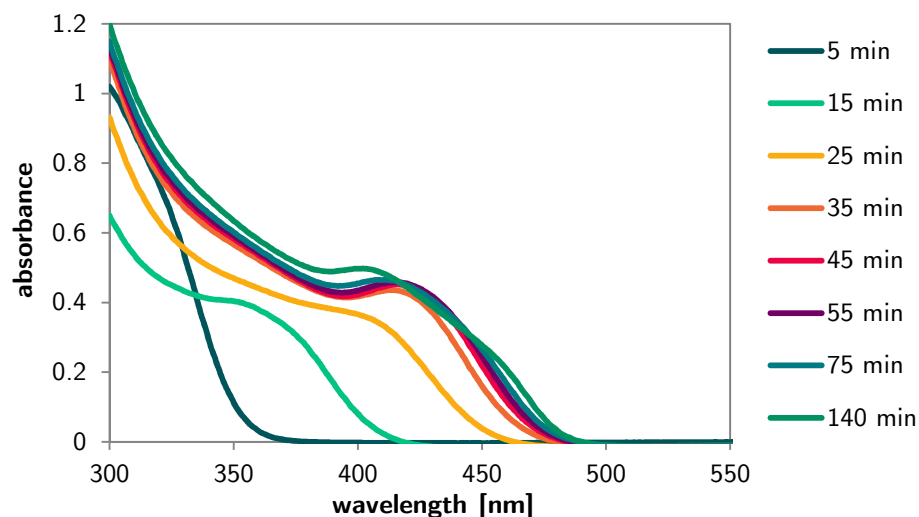


Figure 3.8 - Absorption spectra of the reaction solution of quantum dots **2** at different reaction times.

Three samples with increasing concentrations of water oxidation catalyst **7** and the maximal concentration of quantum dots **2** were irradiated in phosphate buffer solution at pH 8.5 (Table 3.4). Catalyst **7** was chosen due to its better water solubility compared to catalyst **8**.

Table 3.4 - Composition of homogeneous samples with quantum dots **2** and catalyst **7** in 50 mM phosphate buffer (pH 8.5).

Entry	c_7 [μM]	c_2 [μM]	$c_{\text{Na}_2\text{S}_2\text{O}_8}$ [μM]
1	12.5	125	2500
2	125	125	2500
3	375	125	2500

The samples were irradiated with blue light LEDs and the oxygen concentration was determined with the on-line sensor. There was no oxygen evolution detected in the three samples. The residual oxygen, which remains in every sample after degassing, decreased after the irradiation started. This could indicate that the oxygen oxidizes the quantum dots under irradiation.

Quantum Dots 3

A fluorescence quenching study was performed to get a deeper insight into the mechanism and to investigate, if an electron transfer from the quantum dots to the electron acceptor and a hole transfer from the quantum dot to the catalyst is possible. The quantum dots **2** showed only a very weak fluorescence. In contrast, quantum dots **3** are known for their excellent fluorescence properties.^[25] They are stabilized by cysteine ligands instead of 2-mercaptopropionic acid. The preparation is comparable to the procedure for quantum dots **2** and was published by Park *et al.* The reaction proceeds at room temperature and takes days instead of minutes. In return, the quantum dots **3** exhibit an exceptional narrow size distribution and a HWHM of only 8 nm (Figure 3.9).

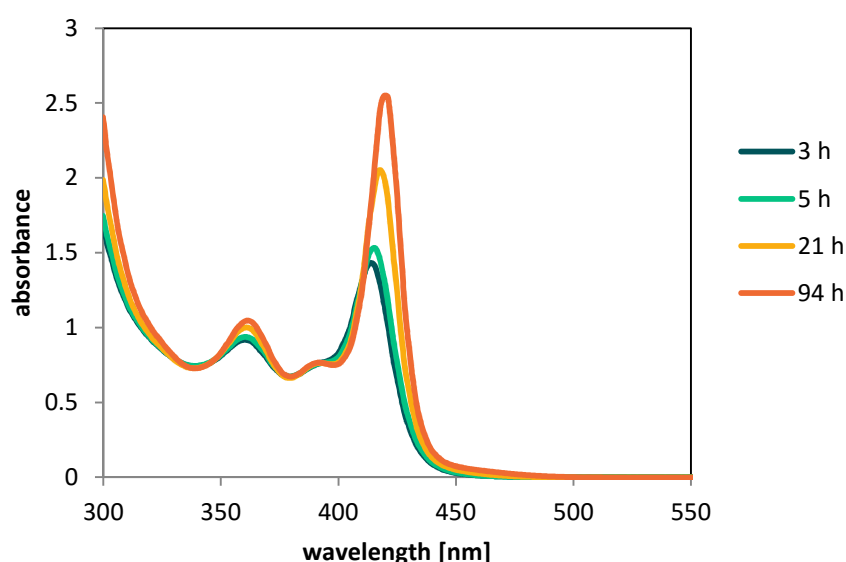


Figure 3.9 - Absorption spectra of the reaction solution of quantum dots **3** at increasing reaction times.

3.2.4 Fluorescence Quenching of Quantum Dots 3

First, the quenching of the fluorescence of quantum dots **3** by persulfate was investigated. A 1 M persulfate solution was added to a degassed 11 μ M solution of quantum dots **3** in Millipore water and the fluorescence ($\lambda_{\text{ex}} = 448$ nm) was recorded. As shown in Figure 3.10, the fluorescence of the sample was not quenched significantly after the addition of persulfate. This indicates that an electron transfer between persulfate and the quantum dots **3** is unlikely. One possible explanation could be the coulombic repulsion of the negatively charged quantum dots **3** and the persulfate anion. To prove this assumption, a solution of positively

charged methyl viologen was added to a similar sample of quantum dots **3** and the fluorescence was monitored (Figure 3.11).

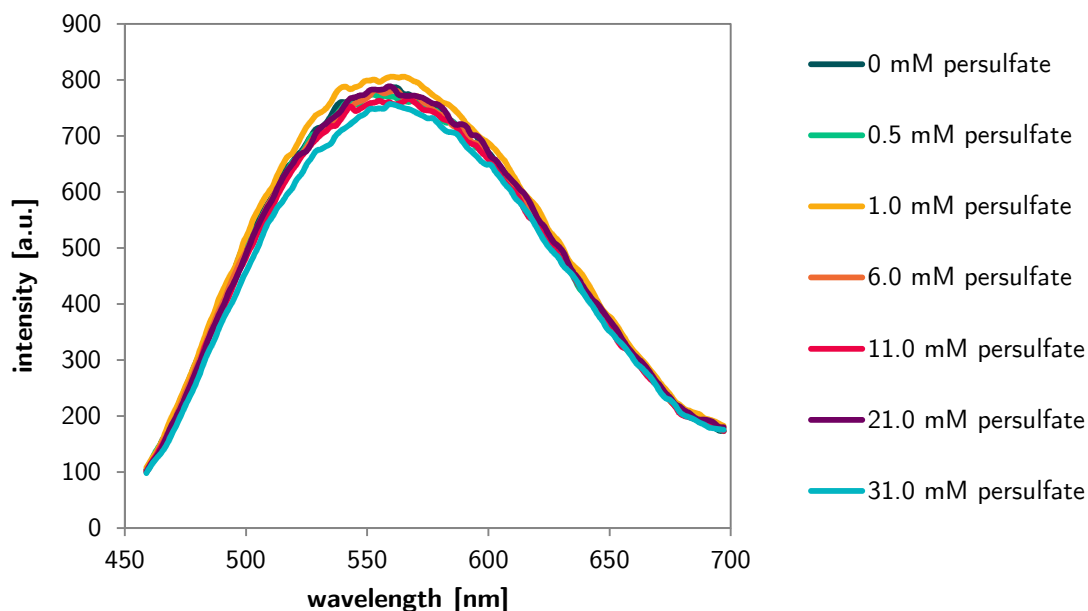


Figure 3.10 - Fluorescence spectra of a sample of quantum dots **3** (11 μM) in Millipore water with increasing amounts of $\text{Na}_2\text{S}_2\text{O}_8$.

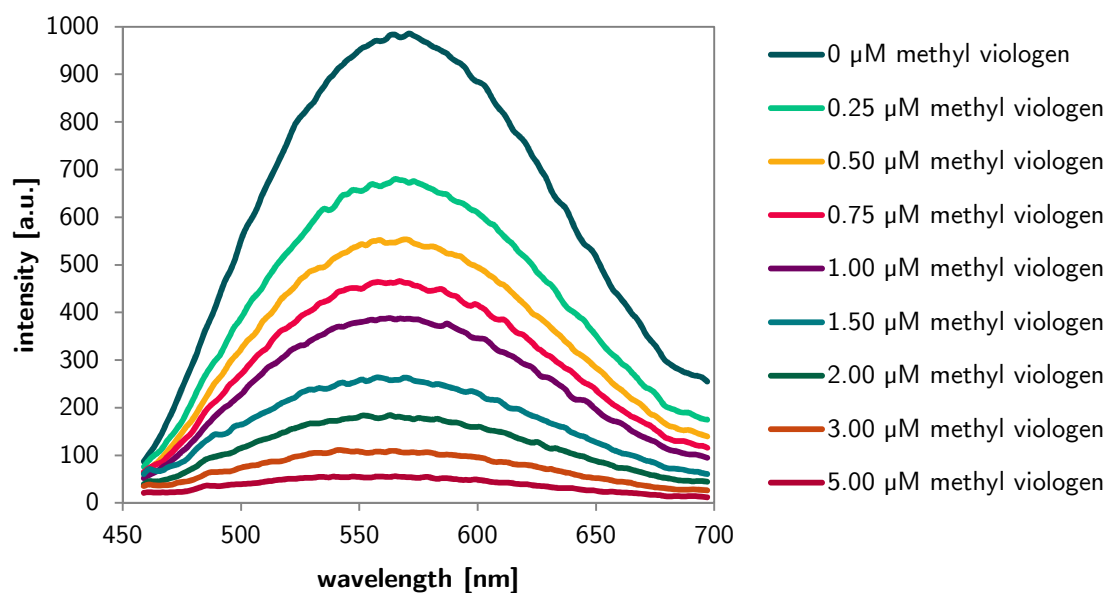


Figure 3.11 - Fluorescence spectra of a sample of quantum dots **3** (11 μM) in Millipore water with increasing amounts of methyl viologen.

The fluorescence intensity was decreasing drastically after the addition of methyl viologen to quantum dots **3** (Figure 3.11). Already a concentration of 0.5 μM methyl viologen caused a reduction in fluorescence of about 50 %. For the quenching of the quantum dots fluorescence, two different model systems have to be taken into account: First, the Stern-Volmer model for dynamic quenching and second, the Langmuir model for static quenching due to adsorbed quenchers. In this case, the results for both models are inconclusive (Figure 3.12). Hence, it is not possible to conclude if the quenching process is collision or adsorption controlled, but the quenching itself is very efficient.

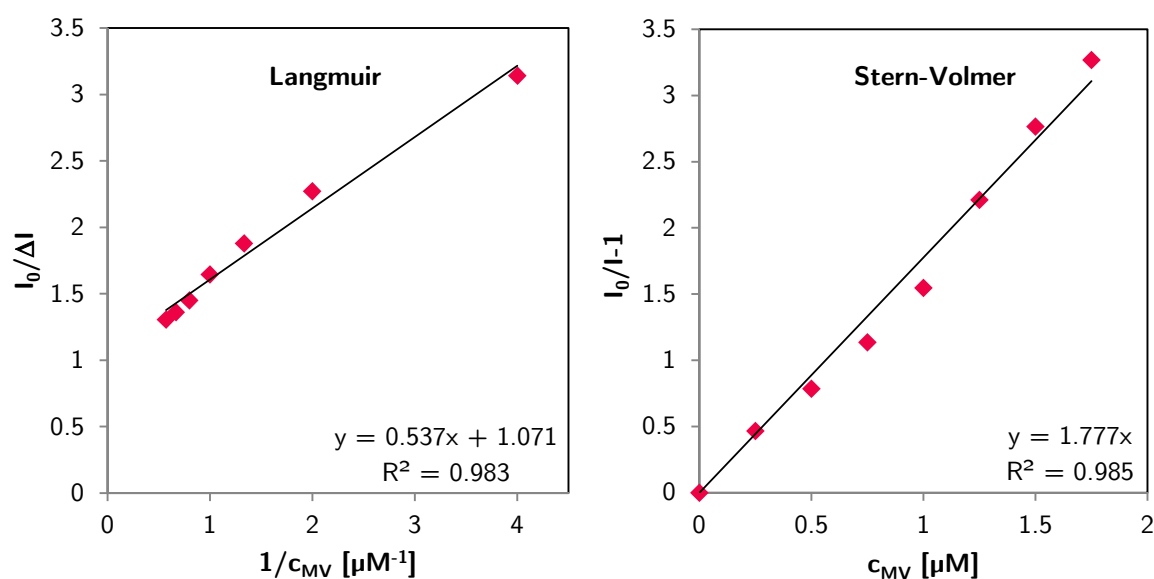


Figure 3.12 - Left: Langmuir quenching study with quantum dots **3** (11 μM) and methyl viologen. Right: Stern-Volmer quenching model for the quenching of quantum dot **3** with methyl viologen.

Beside the electron transfer from the quantum dots to the acceptor, the hole transfer from the quantum dots to the water oxidation catalyst is of great importance for a working water oxidation system. Therefore, the fluorescence quenching of quantum dots **3** with the water oxidation catalyst **7** was investigated in a further experiment (Figure 3.13).

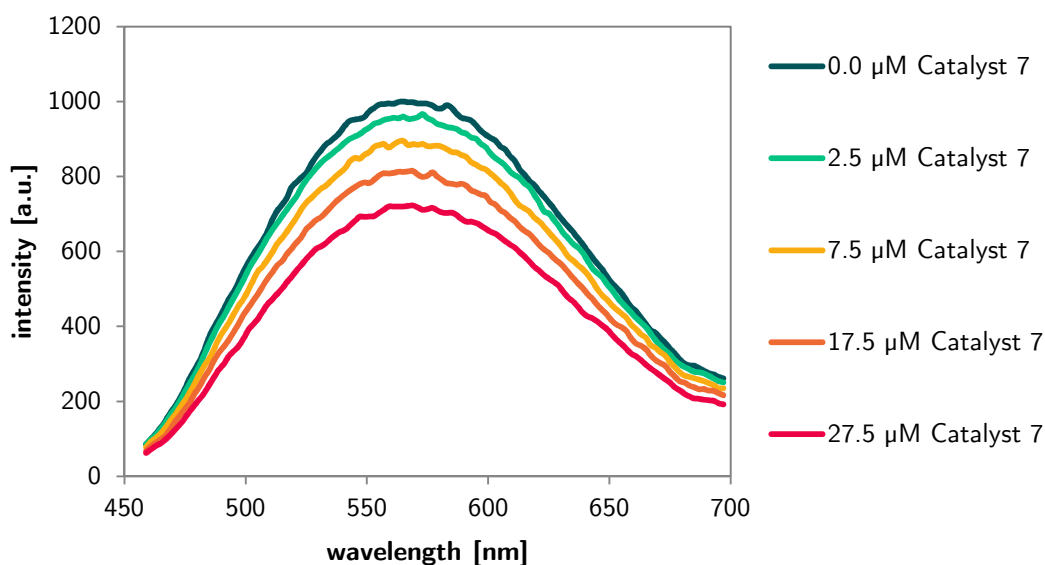


Figure 3.13 - Fluorescence spectra of a sample of quantum dots **3** in Millipore water with increasing amounts of water oxidation catalyst **7**.

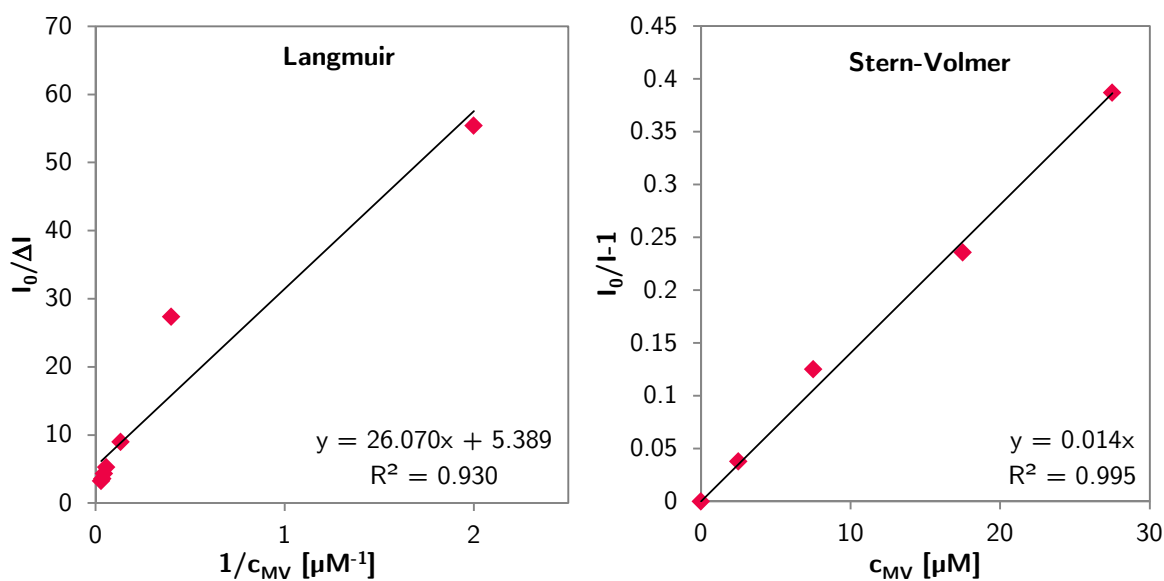


Figure 3.14 - Left: Langmuir quenching study with quantum dots **3** (11 μM) and water oxidation catalyst **7**. Right: Stern-Volmer quenching model for the quenching of quantum dot **3** with catalyst **7**.

The fluorescence quenching is less efficient compared with the quenching with methyl viologen. In this case, the Stern Volmer quenching model fits the measurement series for the interaction of catalyst and quantum dots **3** better, compared with the Langmuir model. Thus, the main quenching pathway is collision-controlled. However, the fact that the quenching of

quantum dots **3** with methyl viologen was not exclusively collision-dependent supports the assumption that the coulombic attraction of methyl viologen and the quantum dots **3** plays a major role for the very efficient quenching.

3.2.5 Water Oxidation with Quantum Dots **3** and Methyl Viologen

The difference in the quenching constants for methyl viologen and the water oxidation catalyst **7** by two orders of magnitude could cause problems in the water oxidation, such as electron back transfer. Another problem in water oxidation using methyl viologen is the rapid reaction of reduced viologen with oxygen, which complicates analysis. Therefore, the use of persulfate to terminally oxidize the methyl viologen radical cation could be beneficial. An experiment showed that reduced methyl viologen can be oxidized with persulfate (Figure 3.15).

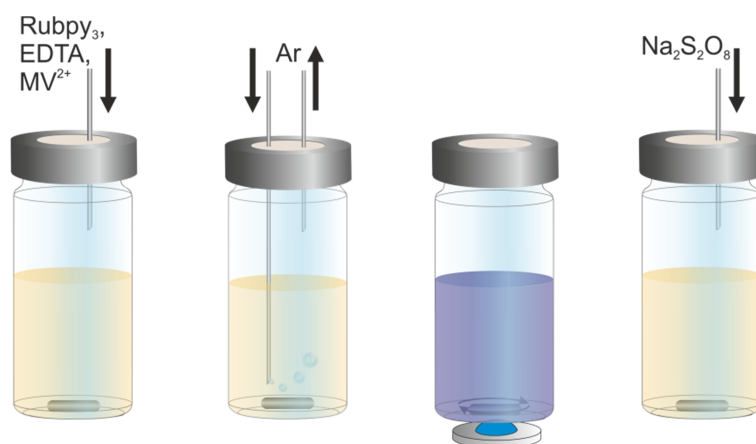


Figure 3.15 - Schematic representation of the experiment for the oxidation of reduced methyl viologen with persulfate.

A solution containing tris-(2,2'-bipyridine)ruthenium (**4**), ethylenediaminetetraacetate (EDTA) and methyl viologen was degassed with argon and irradiated with blue LEDs ($\lambda = 455$ nm). Immediately, a blue color developed, which indicated the reduction of methyl viologen to its radical cation.^[26] The color remained unchanged until the addition of a $\text{Na}_2\text{S}_2\text{O}_8$ solution, after which the blue color disappeared immediately. In contrast, an addition of degassed water did not change the blue color. This implies that a quenching of reduced methyl viologen with persulfate is possible.

In an attempt to use methyl viologen as a mediator in a homogeneous water oxidation system with quantum dots **3** as the photosensitizer, three samples were prepared. The reaction

mixtures contained quantum dots **3**, methyl viologen, and water oxidation catalyst **7** in Millipore water (Table 3.5). Persulfate was added to these solutions.

Table 3.5 - Composition of samples containing the mediator methyl viologen, the water oxidation catalyst **7**, the quantum dots **3** and persulfate in Millipore water.

Entry	c_7 [mM]	c_3 [mM]	$c_{\text{methyl viologen}}$ [mM]	$c_{\text{Na}_2\text{S}_2\text{O}_8}$ [mM]
1	0.10	1.00	5.00	20.0
2	0.10	0.10	5.00	20.0
3	0.10	0.01	5.00	20.0

Unfortunately, the quantum dots **3** precipitated after the addition of persulfate. A lower concentration of quantum dots **3** did not prevent the precipitation. Therefore, it was not possible to prepare a sample which was not precipitating.

3.3 Conclusion

Different sized quantum dots bearing stearic acid, 2-mercaptopropionic acid and cysteine ligands, respectively, were successfully synthesized and characterized by UV/Vis spectroscopy. They were incorporated into vesicles or used in homogeneous solution and were tested towards photochemical water oxidation. No oxygen evolution was detected with functionalized vesicles, as well as in homogeneous solution.

The coulombic repulsion of water soluble quantum dots and persulfate might be one reason for the failing reaction. Fluorescence quenching studies proved that persulfate cannot quench the quantum dots' fluorescence, when the stabilizing ligands were negatively charged. In contrast, the fluorescence was quenched very efficiently by the oxidant methyl viologen. However, the quenching constant for the quenching of quantum dots **3** with the water oxidation catalyst **7** is two orders of magnitude lower. A working photocatalytic water oxidation system using methyl viologen as a mediator was not achieved due to precipitation of the quantum dots **3** after the addition of persulfate.

3.4 Experimental Part

3.4.1 General Methods and Material

Absorption spectra were recorded on a Varian Cary BIO 50 UV/VIS/NIR spectrometer. A 10 mm Hellma quartz cuvette was used.

Fluorescence spectroscopy has been carried out on a Varian Cary Eclipse fluorimeter with 10 mm Hellma quartz cuvettes at 25 °C.

A Fibox 3 fibre optic oxygen sensor purchased from PreSens Precision Sensing GmbH was used for monitoring the amount of oxygen.

Gas chromatography was performed on an Inficon Micro GC 3000 with a 3 Å mol sieve column, a thermal conductivity detector and Ar as a carrier gas.

A Bandelin Sonorex RK 102 H was used for the sonication of vesicular samples.

3.4.2 Synthesis of Photosensitizers and Catalysts

The photosensitizers **5** and **6** and the water oxidation catalysts **7** and **8** were synthesized according to literature.^[6]

3.4.3 Quantum Dot Synthesis

The quantum dots **1a**,^[19] **2**^[13] and **3**^[25] were synthesized following adapted literature procedures.

Synthesis of 3 nm CdSe Quantum Dots **1a**

In a typical procedure, stearic acid (450 mg, 1.6 mmol), and CdO (51.2 mg, 0.4 mmol) were added to a 20 mL crimp cap vial containing octadecene (8 mL). The vial was sealed and purged with nitrogen before the temperature was raised to 280 °C in an aluminum heating block. After the solution turned clear, the vial was transferred into a 250 °C heating block and a selenium stock solution (181 mg, 2.29 mmol) in tributyl phosphine (575 µL, 2.3 mmol) and octadecene (1.75 mL) was quickly injected into the reaction to commence nucleation and growth of the nanocrystals. After ca. 20 s at 250 °C, the vial was cooled to r.t. Hexane (10 mL) and MeOH (20 mL) were added. The hexane phase was extracted twice with MeOH (20 mL each). The quantum dots were precipitated by the addition of acetone to the hexane/octadecene phase to achieve a 1:1 mixture. They were separated by centrifugation and

decantation. The precipitate was washed with acetone and the resulting suspension was centrifuged and decanted.

Synthesis of Quantum Dots **1b**

Water (4.5 mL) was added to a sample of quantum dots **1a** in toluene (4.5 mL). 2-Mercaptopropionic acid (65 μ L, 0.7 mmol) was added to this two-phase system and the resultant solution was stirred at 60 °C for 3 h. After this time, the quantum dots were partly dissolved in the water phase and partly precipitated. The pH was adjusted to ca. 8 by an addition of NaOH (1 M). The now completely dissolved quantum dots **1b** were separated from the toluene.

Synthesis of 1.6 nm CdSe Quantum Dots **2**

Selenium powder (40 mg, 0.5 mmol) was added to an aqueous 15 mM sodium sulfite solution (100 mL, 1.50 mmol). The suspension was stirred at 130 °C over night until the solid selenium powder was dissolved and a colorless transparent Na₂SeSO₃ solution was obtained. The Na₂SeSO₃ solution (10 mL) was injected into an argon saturated solution of CdCl₂ (46 mg, CdCl₂ · xH₂O) in Millipore water (190 mL) at pH = 9 in the presence of 2-mercaptopropionic acid (26 μ L, 0.29 mmol). The resulting mixture was refluxed to control the growth of CdSe quantum dots **2**. The size of the quantum dots was monitored by UV/Vis spectroscopy during the reaction. After refluxing, the solution was concentrated to ca. 6 mL at the rotary evaporator and the quantum dots were precipitated by the addition of isopropanol (10 mL). The quantum dots were separated by centrifugation and decantation.

Synthesis of 1.6 nm CdSe Quantum Dots **3**

Selenium powder (100 mg, 1.27 mmol) was dissolved in water (100 mL) containing sodium sulfite (478 mg, 1.5 mmol) over night at 90 °C to create a Na₂SeSO₃ stock solution. Aqueous stock solutions of cysteine (1 M, 1.32 mL, 1.32 mmol), NaOH (1 M, 3.75 mL, 3.75 mmol), CdCl₂ (0.5 M, 0.3 mL, 0.15 mmol), and Na₂SeSO₃ (50 mM, 0.75 mL, 37.5 μ mol) were added sequentially in 10 min intervals to water (94 mL). The resultant yellowish solution was stirred at room temperature for several days. The quantum dot growth was monitored by UV/Vis spectroscopy. The solution was concentrated to ca. 6 mL at the rotary evaporator and the quantum dots were precipitated by an addition of isopropanol (10 mL). The quantum dots were separated by centrifugation and decantation.

3.4.4 Water Oxidation Experiments

Vesicular Water Oxidation Systems

Appropriate volumes (Table 3.6) of stock solutions of DMPC (**9**), quantum dots **1a** and water oxidation catalyst **8** in chloroform were mixed in a 10 mL crimp top vial to obtain a total amphiphile concentration of 1 mM and the solvent was removed at 85 °C and under reduced pressure. 2.5 mL of aqueous phosphate buffer (50 mM, pH = 7.0) containing 2.5 mM sodium persulfate were added and the vial was closed with a septum-cap. Sonication in an ultrasonic bath at 45 °C, 20 °C above the main phase transition temperature, for 20 min should yield a vesicular solution.

Table 3.6 - Composition of vesicles for photochemical water oxidation with quantum dots **1a**.

V_{1a}^a [μ L]	V_8^b [μ L]	V_9^c [μ L]	c_{1a} [μ M]	c_8 [μ M]	c_9 [μ M]	$c_{S_2O_8^{2-}}$ [mM]	V_{buffer} [mL]
7.4	31.3	247	0.2	12.5	987	2.5	2.5
184	31.3	246	5.0	12.5	983	2.5	2.5
460	31.3	244	12.5	12.5	975	2.5	2.5
1838	31.3	235	50.0	12.5	938	2.5	2.5
4596	31.3	216	125	12.5	863	2.5	2.5
^a c (stock solution) = 68 μ M			^b c (stock solution) = 1 mM		^c c (stock solution) = 10 mM		

These solutions were transferred into a 2 mL screw cap vial under a nitrogen atmosphere which was equipped with a Fibox 3 optical oxygen sensor spot. They were irradiated with a blue LED ($\lambda = 455$ nm).

Water Oxidation in Homogenous Systems Containing THF

Appropriate amounts of stock solutions (Table 3.7) of water oxidation catalyst **8** or photosensitizer **5** in acetonitrile were evaporated in a 10 mL crimp cap vial. The residue was dissolved in either a THF:water (95:5) mixture containing quantum dots **1a** or in pure THF:water (95:5). Then an aqueous stock solution of persulfate (1 M) was added. The resulting solutions were deoxygenated with argon, irradiated with blue LEDs ($\lambda = 455$ nm) and the oxygen content was determined with GC.

Table 3.7 - Composition of homogeneous solutions of THF:water (95:5) for photochemical water oxidation with quantum dots **1a**.

V_{1a}^a [mL]	V_7^b [μ L]	V_5^c [μ L]	c_{1a} [μ M]	c_7 [μ M]	c_5 [μ M]	$c_{S_2O_8^{2-}}$ [mM]	$V_{sol.}$ [mL]
4.5	45	-	180	10	-	2.5	4.5
4.5	225	-	180	50	-	2.5	4.5
-	225	1125	-	50	500	2.5	4.5
^a c (stock solution) = 180 μ M			^b c (stock solution) = 1 mM			^c c (stock solution) = 2 mM	

Water Oxidation in Homogeneous Solution with Acetonitrile

Appropriate amounts (Table 3.8) of stock solutions of water oxidation catalysts **7** or **8** and photosensitizer **6** were evaporated in a 10 mL crimp cap vial. The residue was dissolved in acetonitrile (450 μ L). A solution of quantum dots **1b** in phosphate buffer (4.05 mL, pH 8.5, 50 mM) was added. Pure phosphate buffer was employed for the sample containing photosensitizer **6**. An aqueous stock solution of persulfate (1 M) was added, the mixtures were deoxygenated with argon and irradiated with blue LEDs ($\lambda = 455$ nm). The amount of evolved oxygen was determined with GC.

Table 3.8 - Composition of homogeneous solutions of quantum dots **1b** for photochemical water oxidation in phosphate buffer (pH 8.5, 50 mM) with 10 % acetonitrile.

V_{1b}^a [mL]	V_7^b [μ L]	V_8^b [μ L]	V_6^b [μ L]	c_{1b} [μ M]	c_7 [μ M]	c_8 [μ M]	c_6 [μ M]	$c_{S_2O_8^{2-}}$ [mM]
4.05	225	-	-	180	50	-	-	2.5
4.05	-	225	-	180	-	50	-	2.5
-	225	-	1125	-	50	-	500	2.5
^a c (stock solution) = 200 μ M			^b c (stock solution) = 1 mM			^c c (stock solution) = 2 mM		

Water Oxidation in Homogeneous Solution with Quantum Dots **2**

Appropriate volumes (Table 3.9) of a stock solution of water oxidation catalyst **7** were evaporated in a 10 mL crimp cap vial. A stock solution of quantum dots **2** in phosphate buffer (pH 8.5, 50 mM), phosphate buffer and an aqueous stock solution of persulfate (1 M) were added to the residue. The solution was deoxygenated with nitrogen, transferred in a 2 mL screw cap vial equipped with a Fibox3 optical oxygen sensor and irradiated with a blue light LED ($\lambda = 455$ nm).

Table 3.9 - Composition of homogeneous solutions of quantum dots **2** for photochemical water oxidation in phosphate buffer (pH 8.5, 50 mM) with 10 % acetonitrile.

V_2^a [mL]	V_7^b [μ L]	V_{buffer}^b [μ L]	c_2 [μ M]	c_7 [μ M]	$c_{\text{S}_2\text{O}_8^{2-}}$ [mM]	V_{tot}
1.49	31.3	1.01	125	12.5	2.5	2.5
1.49	313	1.01	125	125	2.5	2.5
1.49	938	1.01	125	375	2.5	2.5
^a c (stock solution) = 210 μ M			^b c (stock solution) = 1 mM			

Water Oxidation with Quantum Dots 3 and Methyl Viologen

Appropriate volumes of a stock solution of water oxidation catalyst **7** were evaporated in a 10 mL crimp cap vial. A stock solution of quantum dots **3** in Millipore water (pH 8.3), Millipore water and an aqueous stock solution of persulfate (1 M) were added to the residue. All samples precipitated after the addition of persulfate.

3.5 References

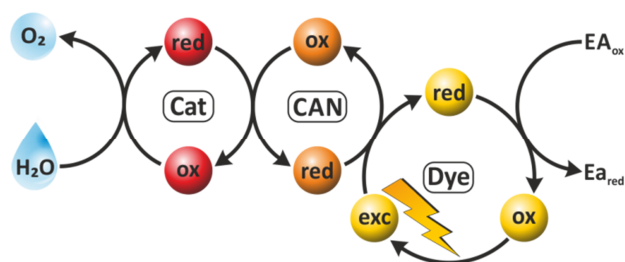
- [1] J. A. Gilbert, D. S. Eggleston, W. R. Murphy, D. A. Geselowitz, S. W. Gersten, D. J. Hodgson, T. J. Meyer, "Structure and redox properties of the water-oxidation catalyst $[(bpy)_2(OH_2)RuORu(OH_2)(bpy)_2]^{4+}$ ", *J. Am. Chem. Soc.* **1985**, 107, 3855-3864.
- [2] S. W. Gersten, G. J. Samuels, T. J. Meyer, "Catalytic oxidation of water by an oxo-bridged ruthenium dimer", *J. Am. Chem. Soc.* **1982**, 104, 4029-4030.
- [3] M. D. Kärkäs, O. Verho, E. V. Johnston, B. Åkermark, "Artificial Photosynthesis: Molecular Systems for Catalytic Water Oxidation", *Chem. Rev.* **2014**.
- [4] L. Wang, L. Duan, Y. Wang, M. S. G. Ahlquist, L. Sun, "Highly efficient and robust molecular water oxidation catalysts based on ruthenium complexes", *Chem. Commun.* **2014**, 50, 12947-12950.
- [5] L. Wang, L. Duan, L. Tong, L. Sun, "Visible light-driven water oxidation catalyzed by mononuclear ruthenium complexes", *J. Catal.* **2013**, 306, 129-132.
- [6] M. Hansen, F. Li, L. Sun, B. König, "Photocatalytic water oxidation at soft interfaces", *Chem. Sci.* **2014**, 5, 2683-2687.
- [7] I. J. Kramer, E. H. Sargent, "The Architecture of Colloidal Quantum Dot Solar Cells: Materials to Devices", *Chem. Rev.* **2013**, 114, 863-882.
- [8] A. P. Alivisatos, "Semiconductor Clusters, Nanocrystals, and Quantum Dots", *Science* **1996**, 271, 933-937.
- [9] J. Jasieniak, M. Califano, S. E. Watkins, "Size-Dependent Valence and Conduction Band-Edge Energies of Semiconductor Nanocrystals", *ACS Nano* **2011**, 5, 5888-5902.
- [10] M. B. Wilker, K. J. Schnitzenbaumer, G. Dukovic, "Recent Progress in Photocatalysis Mediated by Colloidal II-VI Nanocrystals", *Isr. J. Chem.* **2012**, 52, 1002-1015.
- [11] Z. Han, F. Qiu, R. Eisenberg, P. L. Holland, T. D. Krauss, "Robust Photogeneration of H_2 in Water Using Semiconductor Nanocrystals and a Nickel Catalyst", *Science* **2012**, 338, 1321-1324.
- [12] W.-J. Liang, F. Wang, M. Wen, J.-X. Jian, X.-Z. Wang, B. Chen, C.-H. Tung, L.-Z. Wu, "Branched Polyethylenimine Improves Hydrogen Photoproduction from a CdSe Quantum Dot/[FeFe]-Hydrogenase Mimic System in Neutral Aqueous Solutions", *Chem. Eur. J.* **2015**, 21, 3187-3192.
- [13] F. Wang, W.-J. Liang, J.-X. Jian, C.-B. Li, B. Chen, C.-H. Tung, L.-Z. Wu, "Exceptional Poly(acrylic acid)-Based Artificial [FeFe]-Hydrogenases for Photocatalytic H_2 Production in Water", *Angew. Chem. Int. Ed.* **2013**, 52, 8134-8138.

- [14] C.-B. Li, Z.-J. Li, S. Yu, G.-X. Wang, F. Wang, Q.-Y. Meng, B. Chen, K. Feng, C.-H. Tung, L.-Z. Wu, "Interface-directed assembly of a simple precursor of [FeFe]-H₂ase mimics on CdSe QDs for photosynthetic hydrogen evolution in water", *Energy Environ. Sci.* **2013**, 6, 2597-2602.
- [15] J.-X. Jian, Q. Liu, Z.-J. Li, F. Wang, X.-B. Li, C.-B. Li, B. Liu, Q.-Y. Meng, B. Chen, K. Feng, C.-H. Tung, L.-Z. Wu, "Chitosan confinement enhances hydrogen photogeneration from a mimic of the diiron subsite of [FeFe]-hydrogenase", *Nat. Commun.* **2013**, 4.
- [16] J. D. Marshall, M. J. Schnitzer, "Optical Strategies for Sensing Neuronal Voltage Using Quantum Dots and Other Semiconductor Nanocrystals", *ACS Nano* **2013**, 7, 4601-4609.
- [17] W. T. Al-Jamal, K. T. Al-Jamal, B. Tian, L. Lacerda, P. H. Bomans, P. M. Frederik, K. Kostarelos, "Lipid-Quantum Dot Bilayer Vesicles Enhance Tumor Cell Uptake and Retention in Vitro and in Vivo", *ACS Nano* **2008**, 2, 408-418.
- [18] G. Gopalakrishnan, C. Danelon, P. Izewska, M. Prummer, P.-Y. Bolinger, I. Geissbühler, D. Demurtas, J. Dubochet, H. Vogel, "Multifunctional Lipid/Quantum Dot Hybrid Nanocontainers for Controlled Targeting of Live Cells", *Angew. Chem. Int. Ed.* **2006**, 45, 5478-5483.
- [19] W. Zheng, Y. Liu, A. West, E. E. Schuler, K. Yehl, R. B. Dyer, J. T. Kindt, K. Salaita, "Quantum Dots Encapsulated within Phospholipid Membranes: Phase-Dependent Structure, Photostability, and Site-Selective Functionalization", *J. Am. Chem. Soc.* **2014**, 136, 1992-1999.
- [20] M. Sykora, M. A. Petruska, J. Alstrum-Acevedo, I. Bezel, T. J. Meyer, V. I. Klimov, "Photoinduced Charge Transfer between CdSe Nanocrystal Quantum Dots and Ru-Polypyridine Complexes", *J. Am. Chem. Soc.* **2006**, 128, 9984-9985.
- [21] A. Y. Kuposov, P. Szymanski, T. Cardolaccia, T. J. Meyer, V. I. Klimov, M. Sykora, "Electronic Properties and Structure of Assemblies of CdSe Nanocrystal Quantum Dots and Ru-Polypyridine Complexes Probed by Steady State and Time-Resolved Photoluminescence", *Adv. Funct. Mater.* **2011**, 21, 3159-3168.
- [22] H.-W. Tseng, M. B. Wilker, N. H. Damrauer, G. Dukovic, "Charge Transfer Dynamics between Photoexcited CdS Nanorods and Mononuclear Ru Water-Oxidation Catalysts", *J. Am. Chem. Soc.* **2013**, 135, 3383-3386.
- [23] H.-W. Tseng, R. Zong, J. T. Muckerman, R. Thummel, "Mononuclear Ruthenium(II) Complexes That Catalyze Water Oxidation", *Inorg. Chem.* **2008**, 47, 11763-11773.
- [24] L. Duan, Y. Xu, M. Gorlov, L. Tong, S. Andersson, L. Sun, "Chemical and Photochemical Water Oxidation Catalyzed by Mononuclear Ruthenium Complexes with a Negatively Charged Tridentate Ligand", *Chem. Eur. J.* **2010**, 16, 4659-4668.

- [25] Y.-S. Park, A. Dmytruk, I. Dmitruk, A. Kasuya, Y. Okamoto, N. Kaji, M. Tokeshi, Y. Baba, "Aqueous Phase Synthesized CdSe Nanoparticles with Well-Defined Numbers of Constituent Atoms", *J. Phys. Chem. C* **2010**, 114, 18834-18840.
- [26] P. M. Hare, E. A. Price, D. M. Bartels, "Hydrated Electron Extinction Coefficient Revisited", *J. Phys. Chem. A* **2008**, 112, 6800-6802.

4 Photocatalytic Recycling of Ce^{IV} for Water Oxidation

4.1	Introduction	92
4.2	Results and Discussion	94
4.3	Conclusion	104
4.4	Experimental Part	105
4.5	References	110



Typical water oxidation catalysts can reach thousands of turnovers under the reaction conditions of chemical water oxidation utilizing the strong oxidant ceric ammonium nitrate (CAN). However, the same catalysts reach only several hundred TONs under photochemical reaction conditions with ruthenium-based photosensitizers. This chapter deals with the photochemical regeneration of Ce^{IV} to combine the advantages of chemical and visible light-driven water oxidation. Different approaches to detect Ce^{IV} by UV/Vis spectroscopy were examined and the photo-

chemical regeneration of CAN with the photocatalysts triphenyl pyrylium tetrafluoroborate and 9-mesityl-10-methylacridinium perchlorate was investigated.

4.1 Introduction

Visible light-driven water splitting is still the most promising technology to challenge the increasing energy demands of the future world's population.^[1]

Photochemical water splitting can be divided into two half reactions. First, the fuel producing proton reduction and second, the water oxidation, which is considered particularly difficult due to the multiple proton and electron transfers needed to evolve one molecule of dioxygen.^[2] The knowledge about water oxidation systems increased drastically over the last decades. Highly efficient molecular water oxidation catalysts based on different metal centers have been developed and improved.^[3] Various chemical oxidants have been used to assess the catalytic activity of these water oxidation catalysts.^[4]

Most commonly used is ceric ammonium nitrate (CAN, $\text{Ce}(\text{NH}_4)_2(\text{NO}_3)_6$). Beside the use in chemical water oxidation reactions, it has been employed for a variety of organic oxidation reactions.^[5] The Ce^{4+} ion in the complex center possesses a very strong oxidation potential of approximately 1.70 V vs NHE.^[6] Its weak absorption in the visible light region and its commercial availability rendered CAN the most widely used chemical oxidant in water oxidation reactions.

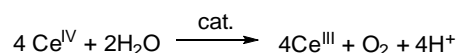


Figure 4.1 - Chemical water oxidation reaction utilizing Ce^{IV} as the terminal oxidant.

Other oxidants used in chemical water oxidation such as potassium peroxymonosulfate,^[7] sodium periodate^[8] or sodium hypochlorite^[9] are two-electron oxidants, which allows them to act as an oxygen-atom-transfer reagent. This questions the origin of the evolved oxygen and the usefulness of these reagents in water oxidation reactions.

The activity of homogeneous water oxidation catalysts increased tremendously over the past decades. For example, the performance of catalysts with ruthenium metal centers and carboxylate-containing backbones, which were developed by the Sun group, raised from several hundred to more than 100.000 TONs.^[10] However, the utilization of light as the driving force is the most important challenge to solve the world's energy issues and the activity of these catalysts decreases drastically under photochemical reaction conditions, when tris-(2,2'-bipyridine)ruthenium derivatives are used as the photosensitizers (Figure 4.2). The stability of these photosensitizers is the crucial issue of the commonly used three-component systems for photocatalytic water splitting.

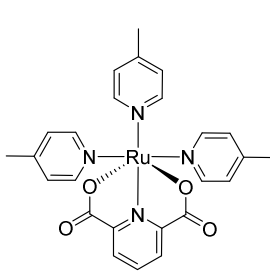
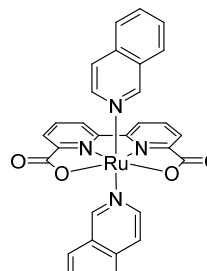
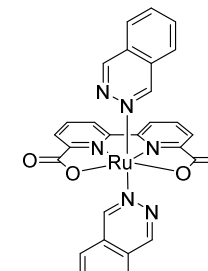
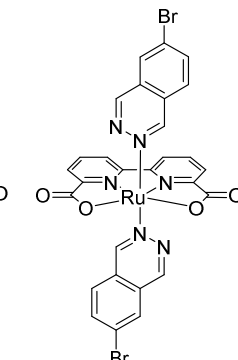
				
	1	2	3	4
photochem. TON	62	218	232	-
chemical TON	550	11300	61300	101000

Figure 4.2 - Structures and catalytic turnover under chemical and photochemical reaction conditions of the water oxidation catalysts **1**,^[11] **2**, **3** and **4**^[12] developed by the Sun group.

The use of Ce^{IV} as a mediator in photochemical water oxidation by the generation of Ce^{IV} from Ce^{III} could combine the photochemistry with the advantages of CAN-driven water oxidation. The oxidation potential of Ce^{III} is within the excited state oxidation potentials of some highly oxidizing dyes, for example the triphenyl pyrylium ion (TPP) or the 9-mesityl-10-methylacridinium ion ($\text{Acr}^{\text{+}}\text{-Mes}$), which makes an electron transfer from Ce^{III} to the excited dye feasible. The direct oxidation of the water oxidation catalyst by the excited state of a dye is very unlikely, because the oxidation of water to one molecule of dioxygen involves four electron and proton transfers. The use of Ce^{IV} as a stable mediator could avoid the necessity of a collision of the oxidized catalyst and the excited dye, which are two instable species. Therefore, the combination of photochemical and cerium-driven water oxidation was attempted in this chapter.

4.2 Results and Discussion

4.2.1 Chemical Ce^{IV} Generation

The absorption of the Ce^{IV} ion in the visible region could be utilized to examine a generation of Ce^{IV} from Ce^{III} with UV/Vis spectroscopy. An UV/Vis-based method would represent a quick and easy test method for a photooxidation of Ce^{III} to Ce^{IV}.

The chemical recycling of CAN by sodium bromate is literature-known and was used for example for the oxidation of arylmethanols^[13] and other secondary alcohols to reduce the amount of CAN required.^[14] A chemical oxidation of CeCl₃ with NaBrO₃ was carried out to examine, if a change in the absorbance spectrum can be used to prove the generation of Ce^{IV} by photochemical methods.

A solution of CeCl₃ (10 mM, 1 mL) in water was added to an aqueous NaBrO₃ (100 mM, 1 mL) solution. No change in the absorption spectrum, indicating the generation of Ce^{IV}, was observed. Ce^{IV} ions are potentially unstable at neutral pH conditions. Therefore, a chemical water oxidation is typically performed at acidic conditions. A widely used reaction medium for the ruthenium-based water oxidation complexes from the Sun group is a triflic acid solution at pH 1.^[12, 15] A test at pH 1 in triflic acid resulted in no formation of a absorption band in the region of Ce^{IV}.

The use of a stronger chemical oxidant than bromate, whose reduction is irreversible, could drive an oxidation of Ce^{III} to Ce^{IV}. The persulfate anion, a very strong oxidant with 2.0 V vs NHE,^[16] is commonly used for the oxidation of tris-(2,2'-bipyridine)ruthenium. The attempt to oxidize CeCl₃ with Na₂S₂O₈ in pH-1 triflic acid also led to no formation of a yellow color of the Ce^{IV} ion. This indicates that either a UV/Vis spectrum is not suitable or that the chemical oxidation of CeCl₃ is not working under these conditions.

4.2.2 Generation of Ce^{IV} with TPP

Although there was no way of proving the generation of Ce^{IV} in the chemical oxidation in section 4.2.1, a fluorescence quenching of a dye, which is supposed to be used for the photochemical oxidation, indicates that an electron transfer from Ce^{III} to the dye is feasible.

Triphenyl pyrylium tetrafluoroborate (TPP), an organic dye, possesses a high oxidation potential in the excited state of over 2.0 V vs. NHE.^[17] This is sufficient to oxidize Ce^{III} to Ce^{IV}. The absorbance of the dye used in the photochemical Ce^{IV}-regeneration should be sufficiently high and constant under the reaction conditions. The absorbance of a 100 μM TPP solution in

Millipore water at 400 nm is ca. 2.3, but decreases significantly with time. A steady absorption was observed in acetonitrile solutions. Mixtures of water and acetonitrile also led to a time dependent decrease in the absorbance (see section 4.4.3). This is due to a pseudo-acidic behavior of pyrylium dyes. Through the uptake of hydroxide ions, the pyrylium ring opens to form a diketone **5** (Figure 4.3). The pK_a value for this process is reported to be around 5.^[18]

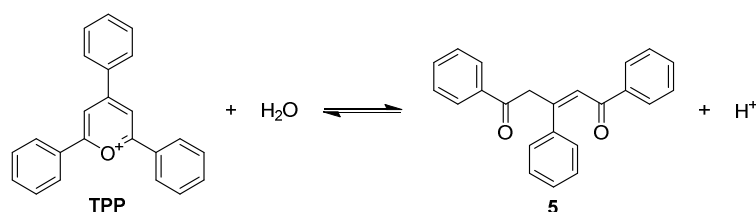


Figure 4.3 - Pseudo-acidic behavior of TPP salts in aqueous solutions.

This hydrolysis should be shut down in acidic solutions and indeed, the absorbance of TPP is constant, but lower in triflic acid solutions. The absorbance is only 0.2 at pH 1. A pH 3 solution of triflic acid seems to be a compromise between long-term stability and absorbance with $A_{\text{max}} = 0.9$ at 400 nm (see section 4.4.3).

For a fluorescence quenching study, TPP was dissolved in pH 3 triflic acid and the solution was degassed with argon. CeCl_3 solution in pH 3 triflic acid was titrated to the TPP solution and the fluorescence was recorded (Figure 4.4). The fluorescence of TPP was quenched by the Ce^{III} cations following a Stern-Volmer type quenching (Figure 4.5). This indicates the electron transfer from the Ce^{III} ion to the excited state of TPP.

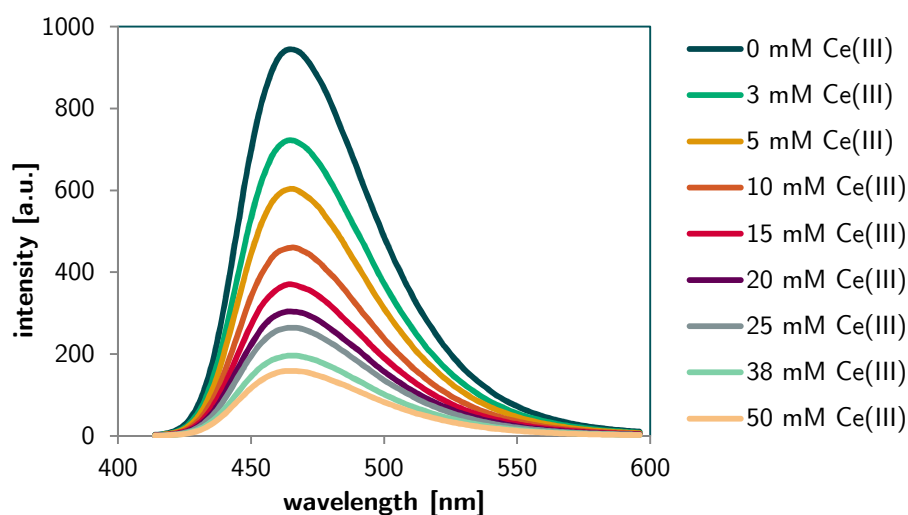


Figure 4.4 - Quenching of the fluorescence of TPP (0.1 mM, $\lambda_{\text{exc}} = 400$ nm) by CeCl_3 (1 M) in pH 3 triflic acid.

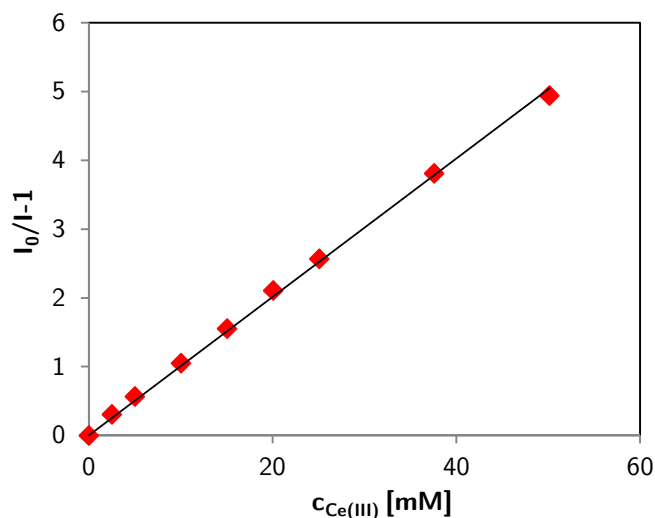


Figure 4.5 - Stern-Volmer quenching study of the fluorescence of TPP ($\lambda_{\text{em}} = 462 \text{ nm}$, 0.1 mM) by CeCl_3 .

4.2.3 Colorimetric Detection of Ce^{IV}

Detection of a Reaction by Methyl Viologen

Because a direct detection of Ce^{IV} generation by UV/Vis spectroscopy was not achieved, an indirect detection via a colored intermediate was investigated. Methyl viologen (**6**, Figure 4.6) is a known electron acceptor for photochemical systems based on tris-(2,2'-bipyridine)-ruthenium.^[19] The formation of the methyl viologen radical cation (**7**) by a reduction of methyl viologen can be followed by its blue color ($\lambda_{\text{max}} = 605 \text{ nm}$).^[20]

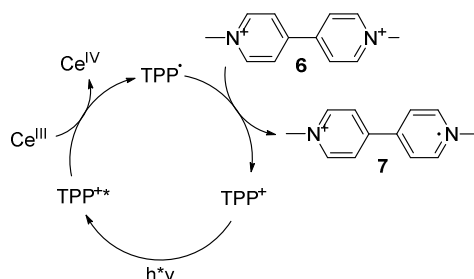


Figure 4.6: Schematic representation of the reduction of methyl viologen (**6**).

In an experiment, TPP, CeCl_3 and methyl viologen were added to pH 3 triflic acid and the degassed solution was irradiated with 400 nm in the spectrometer. A brown precipitate formed when methyl viologen with iodide as counter ions was used. This is most probably due to an oxidation of the iodine counter ions. A change to chloride counter ions prevented

the precipitation. However, no blue color, originating from the methyl viologen radical cation (7), was detected (see Section 4.4.4).

There are mainly two possible reasons, why this system did not yield an evolution of blue color. First, the reduction potential of the TPP radical (ca. -0.14 V vs. NHE) could be insufficient to reduce methyl viologen (ca. -0.48 V vs. NHE). However, those values have to be taken with care.^[17, 21] Second, a working cycle is generating the strong oxidant Ce^{IV} and the methyl viologen radical cation (7), a strong reductant, at the same time. These two highly reactive species could react in a fast redox back reaction to form Ce^{III} and methyl viologen (6).

Detection of Ce^{IV} with *p*-Aminoacetphenon

The colorimetric detection of Ce^{IV} with *p*-aminoacetphenon (AAP) was first shown by Sarma *et al.* in 1967.^[22] They claimed that Ce^{IV} is detectable in the presence of persulfate with this method. This is of importance, because persulfate is supposed to be the sacrificial electron acceptor in the desired photocatalytic water oxidation system. They proposed that the detected purple color originates from a oxidation product of AAP.

Four samples containing increasing amounts of cerium ammonium nitrate (CAN) were prepared and AAP was added to these solutions to obtain a calibration curve and to determine the limit of detection. Immediately after the addition of CAN, a purple color appeared and after 90 s the absorbance was not changing anymore. The absorbance follows the Lambert-Beer law and even a 5 μ M concentration of Ce^{IV} was detectable (see Section 4.4.5).

The photometrical detection of Ce^{IV} with AAP in a photocatalytic system was tested by an irradiation of a degassed sample that contained TPP (50 μ M), sodium persulfate (10 mM), CeCl₃ (10 mM) and AAP (3 mM) in triflic acid at pH 3. The cuvette was irradiated with LEDs (λ = 400 nm) in the spectrometer and a spectrum was recorded every 30 s (Figure 4.7).

Before irradiation, the UV/Vis spectrum was not changing which indicates that AAP is not oxidized by persulfate. After turning on the LED, a shoulder appeared at 500 nm. This could be due to the colored product of AAP oxidation. After about 90 s the shoulder became less distinct and the absorption of the whole spectrum increased. The samples turned brownish in color and in some cases a brown precipitate formed. A sample without Ce^{III}, but otherwise identical conditions, was prepared and irradiated to investigate if the color of the sample originated from the reaction of Ce^{IV} with AAP (see Figure 4.8).

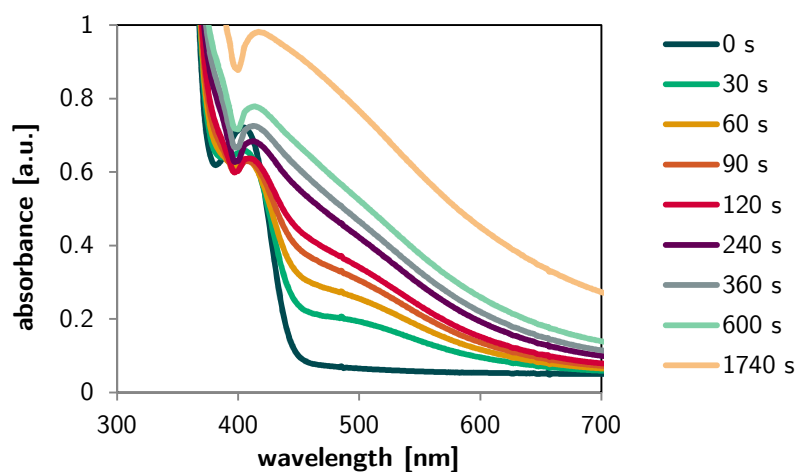


Figure 4.7 - Absorption spectra of a mixture of TPP (50 μ M), persulfate (10 mM), CeCl_3 (10 mM) and AAP (3 mM) in triflic acid at pH 3 after different irradiation times.

The two samples, with and without CeCl_3 , showed identical behavior when irradiated with 400 nm light. Thus, the color of the sample is not changing due to a reaction of Ce^{IV} with AAP. Although AAP is not reacting with persulfate in the dark, it forms a brown compound when irradiated with 400 nm. This could be due to an oxidation of AAP in the excited state by persulfate. The photoreduction of acetophenones from their triplet state in the presence of electron donors is well known in literature.^[23] For example, an oxidation of the amino group of AAP in the excited state by the strong oxidant persulfate could lead to the brown precipitate. Thus, the detection of Ce^{IV} with AAP is not suitable for the photochemical Ce^{IV} generation.

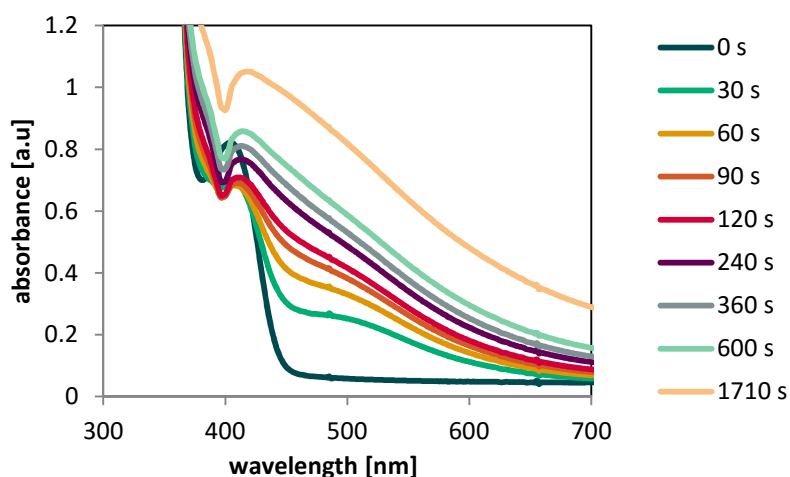


Figure 4.8 - Absorption spectra of a mixture of TPP (50 μ M), persulfate (10 mM) and AAP (3 mM) in triflic acid at pH 3 after increasing irradiation times.

Detection of Ce^{IV} with Tiron

This detection method was introduced by Hagop in 1982 and utilizes an oxidation of Fe^{II} to Fe^{III} by Ce^{IV} which is rapid and quantitative.^[24] The Fe^{III} produced is then complexed by the ligand Tiron (**8**, 4,5-dihydroxybenzene-1,3-disulfonate, Figure 4.9) to yield the strongly blue-colored complex **9**, whose concentration can be determined by UV/Vis spectroscopy (Figure 4.9).

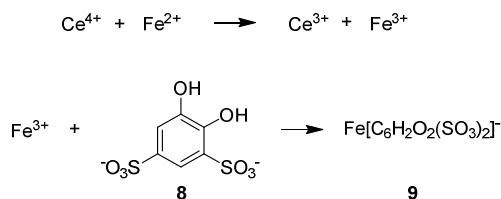


Figure 4.9 - Suggested reaction mechanism for the formation of the blue chromophore **9** formed from Fe^{III} and the ligand Tiron (**8**).^[24]

The persulfate concentrations used in water splitting experiments led to an immediate oxidation of Fe^{II} to Fe^{III}, even without Ce^{IV}, and therefore to the formation of the blue complex **9** in solution, although Hagop *et al.* claimed a high tolerance towards persulfate. This makes this detection method useless for the detection of Ce^{IV} in a photocatalytic water oxidation.

4.2.4 Water Oxidation as a Detection Method for Ce^{IV} Generation

Due to the lack of an appropriate detection method for Ce^{IV}, oxygen evolution was applied as the detection method of a successful generation of Ce^{IV}. Although the system becomes more complex by the introduction of the water oxidation catalyst **1**, the analysis becomes easier. A successful photochemical generation of Ce^{IV} can drive the water oxidation with catalyst **1** (Figure 4.10). The produced oxygen is then easy to detect, either by GC or with an online oxygen sensor.

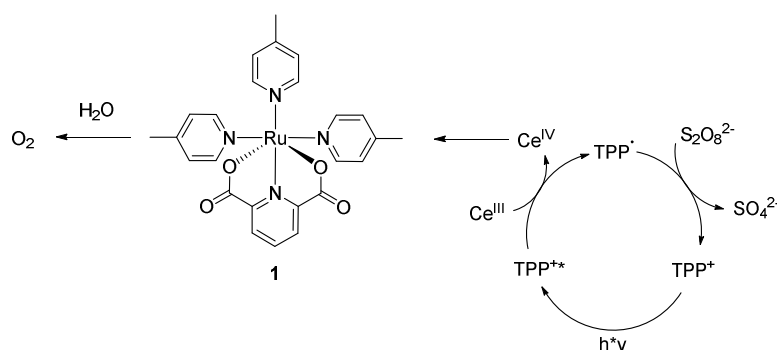


Figure 4.10 - Proposed mechanism for the photochemical generation of Ce^{IV} and detection of oxygen.

Two samples containing CeCl_3 as the Ce^{III} source, the electron acceptor persulfate, the photocatalyst TPP, and the water oxidation catalyst **1** were prepared in a triflic acid solution at pH 1 (Table 4.1) and the oxygen evolution in the liquid phase was determined with the Fibox optical sensor.

Table 4.1 - Composition of the samples for the generation of Ce^{IV} from CeCl_3 .

Entry	c_{CeCl_3} [mM]	$c_{\text{Na}_2\text{S}_2\text{O}_8}$ [mM]	c_1 [mM]	c_{TPP} [mM]	TON
1	10	10	0.05	0.05	-
2	5	5	0.1	0.1	-

The samples did not evolve a detectable amount of oxygen during the irradiation with a 400 nm LEDs. This could be due to the ligand environment of a potentially generated Ce^{IV} ion. These ligands and the acidity of the solution have a strong influence on the oxidation potential of Ce^{IV} ions.^[25] The oxidation potential of Ce^{IV} can be varied over a wide range from highly positive to slightly negative values in aqueous solution.

4.2.5 Regeneration of CAN

A change from Ce^{IV} generation to Ce^{IV} regeneration could solve the ligand environment issues. In the original publication by the Sun group catalyst **1** achieved a TON of 550 in CAN-driven chemical water oxidation. They used an excess of CAN of 3340 equivalents in these experiments. When this amount is lowered to a certain level, the water oxidation should stop before the catalyst is destroyed. A catalytic regeneration of the CAN would then increase the water oxidation turnover by a provision of new oxidation equivalents. Therefore, a series of experiments with increasing amounts of CAN was performed to find a suitable CAN concentration, which produces a reliably detectable amount of oxygen and could show improvements if the Ce^{IV} -regeneration is working (Table 4.2).

Taking into account that four molecules of CAN are consumed for the generation of one molecule of dioxygen, a 10-fold excess of CAN compared to catalyst **1** is not sufficient to produce a measureable amount of oxygen as expected (Entries 1 and 2, Table 4.2). The water oxidation experiments with a 50- and 100-fold excess of CAN (Entries 3 and 4) generated detectable amounts of dioxygen, but did not consume the CAN quantitatively. The conditions of entry 5 have been chosen for the regeneration experiments, because the amount of oxygen was easy to detect and nearly all CAN was consumed. Catalyst **1**'s ability to produce more oxygen is indicated by the quantitative conversion of CAN at a 200-fold excess (Entry 6).

Table 4.2 - Series of increasing CAN concentrations. A solution of **1** in MeCN was added to a solution of CAN in triflic acid (pH 1). The reaction solution contained 5 vol% of MeCN. % CAN represents the fraction of consumed CAN.

Entry	c_{CAN} [mM]	c_1 [mM]	TON	% CAN
1	0.05	0.05	-	0
2	0.5	0.05	-	0
3	2.5	0.05	7	62
4	5.0	0.05	21	86
5	7.5	0.05	35	95
6	10	0.05	52	99

The regeneration of CAN was investigated by the addition of a solution containing the photocatalyst TPP and persulfate as the sacrificial electron acceptor to solutions of CAN and water oxidation catalyst **1** (Table 4.3). These solutions were irradiated with LEDs and the evolved oxygen was determined with the GC. With these compounds in solution, the regeneration of CAN should be possible following the proposed mechanism in Figure 4.11.

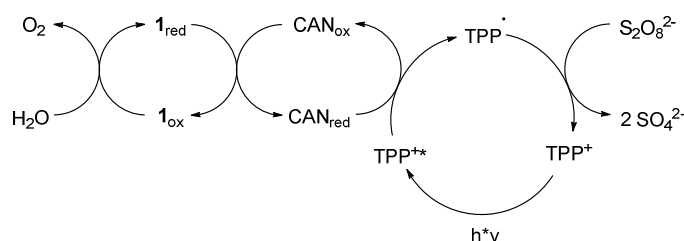


Figure 4.11 - Proposed mechanism for the photochemical regeneration of CAN.

When a sample containing **1**, CAN, TPP and persulfate was irradiated, the TON was lower than in an identical sample without TPP, persulfate and irradiation (Table 4.3, Entry 1 and Table 4.2, Entry 5). Only 15 TONs were observed with TPP, instead of 35 TONs without it. This could be due to two reasons. Either the TPP is interfering with the water oxidation system, or the irradiation has a detrimental effect on the TON. A sample without TPP was irradiated under identical conditions to figure out, if the irradiation causes the decrease in oxygen evolution (Table 4.3, Entry 2). The TPP had no influence on the amount of evolved oxygen. Both samples with and without TPP generated less oxygen than the control sample without TPP and irradiation. This implies that the irradiation causes the loss of activity and seems to be due to the absorption of CAN, which is an orange compound with strong absorption at 400 nm (Figure 4.12). It is known that CAN produces nitrate radicals when irradi-

ated with UV light.^[26] Thus, part of the CAN is degraded by the irradiation with 400 nm light. This assumption is supported by the fact that the TON increases with longer wavelength irradiation (Table 4.3, Entry 3 and 4). The catalytic activity is comparable to the control sample without irradiation when the sample is irradiated with a wavelength of 533 nm, where CAN is not absorbing (Table 4.3, Entry 4 and Table 4.2, Entry 5).

Table 4.3 - Compositions of the solutions containing CAN, persulfate, catalyst **1** and photocatalyst TPP or CAN and catalyst **1** in triflic acid pH 1 and the irradiation wavelength. The MeCN content was 5 vol%.

Entry	c_{CAN} [mM]	$c_{\text{Na}_2\text{S}_2\text{O}_8}$ [mM]	c_1 [mM]	c_{TPP} [mM]	TON	λ_{LED} [nm]
1	7.5	10	0.05	0.05	15	400
2	7.5	-	0.05	-	16	400
3	7.5	-	0.05	-	27	455
4	7.5	-	0.05	-	33	533

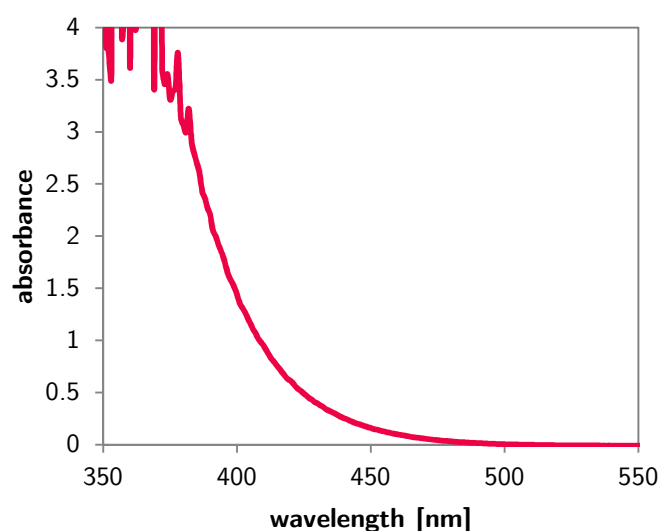


Figure 4.12 - Absorption spectrum of a 10 mM CAN solution in triflic acid (pH 1).

These results indicate that a system for the photochemical regeneration of CAN cannot be irradiated with light of a shorter wavelength than 450 nm. In conclusion, TPP is not a suitable dye for the photochemical regeneration of CAN.

4.2.6 Acr^+ -Mes for the Photochemical CAN Regeneration

The 9-mesityl-10-methylacridinium (Acr^+ -Mes, Figure 4.13) has been used for a variety of photochemical oxidations because of its high oxidation potential of the excited state.^[27] The

oxidation potential of over 2 V vs. NHE and the absorption at 455 nm make the $\text{Acr}^+\text{-Mes}$ a suitable candidate for the photochemical regeneration of CAN.

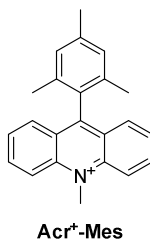


Figure 4.13 - Structure of $\text{Acr}^+\text{-Mes}$.

A series of experiments with increasing concentrations of $\text{Acr}^+\text{-Mes}$ was irradiated with 455 nm LEDs to investigate, if $\text{Acr}^+\text{-Mes}$ can catalyze the regeneration of CAN.

Table 4.4 - Samples containing CAN, persulfate, water oxidation catalyst **1** and photocatalyst $\text{Acr}^+\text{-Mes}$ in triflic acid (pH 1). The reaction solutions contained 5 vol% MeCN and were irradiated with 455 nm.

Entry	c_{CAN} [mM]	$c_{\text{Na}_2\text{S}_2\text{O}_8}$ [mM]	c_1 [mM]	$c_{\text{Acr}^+\text{-Mes}}$ [μM]	TON
1	7.5	10	0.05	25	19
2	7.5	10	0.05	50	19
3	7.5	10	0.05	100	18
4	7.5	10	0.05	250	16
5	7.5	10	0.05	500	14

The TONs of all samples showed that the addition of $\text{Acr}^+\text{-Mes}$ to the system does not improve the water oxidation. The irradiation of $\text{Acr}^+\text{-Mes}$ -containing solutions with 455 nm decreases the TON (Table 4.4) compared to irradiated solutions without $\text{Acr}^+\text{-Mes}$ (Table 4.3, Entry 3) and not irradiated solutions (Table 4.2, Entry 5). An increase of $\text{Acr}^+\text{-Mes}$ concentrations led to decreasing TONs. This can be explained by a possible degradation of the water oxidation catalyst by the excited state of $\text{Acr}^+\text{-Mes}$, which results in the lower TONs. Unfortunately, the photocatalyst $\text{Acr}^+\text{-Mes}$ is not suitable for the photochemical regeneration of CAN due to its detrimental effects on the water oxidation.

4.3 Conclusion

The chemical generation of Ce^{IV} with the aid of bromate was attempted under neutral, as well as under acidic conditions. No oxidation of CeCl_3 was observed by UV/Vis spectroscopy.

The conditions for a photochemical generation of Ce^{IV} with the photocatalyst TPP were investigated. It was found that pH 3 triflic acid solutions provide the right compromise between a sufficient absorption of TPP and the pseudo-acidic reaction of TPP in neutral media. The quenching of TPP's luminescence with CeCl_3 followed the Stern-Volmer equation. It implies that an electron transfer from Ce^{III} to TPP is possible.

The use of methyl viologen as an electron acceptor for a photometrical detection of Ce^{IV} was investigated. The detection of a blue color was not possible, probably due to a fast back reaction of Ce^{IV} and the methyl viologen radical cation.

The colorimetric determination of Ce^{IV} with AAP under the conditions of the fluorescence quenching experiments followed the Lambert-Beer law and proved to be sensitive enough. Unfortunately, this system was not suitable for the detection of Ce^{IV} under photochemical reaction conditions. The irradiation of reaction solutions containing AAP led to a precipitation of a brownish solid, which could originate from an oxidation of excited AAP by the strong oxidant persulfate.

The photochemical recycling of CAN was investigated. Suitable reaction conditions for a detection of the recycling by gas chromatography were developed. A system employing TPP as the photocatalyst was decreasing the TON compared to the dark reaction. It was found that the irradiation of solutions that contained CAN with light of a wavelength below 450 nm was detrimental for the water oxidation. This fact is explained by the absorption of CAN and the following photochemical reactions, which deteriorate the water oxidation system.

The replacement of TPP by the strongly oxidizing photocatalyst Acr^+-Mes was examined by irradiating solutions with 455 nm. The use of Acr^+-Mes led to a decrease of the TON compared with systems without it. This could be due to a degradation of the water oxidation catalyst **1** by the excited Acr^+-Mes .

4.4 Experimental Part

4.4.1 General Methods and Material

For NMR spectroscopy, a Bruker Avance 400 (^1H : 400 MHz, ^{13}C : 101 MHz, $T = 300\text{ K}$) was utilized.

Absorption spectra were recorded on a Varian Cary BIO 50 UV/VIS/NIR spectrometer. A 10 mm Hellma quartz cuvette was used.

Fluorescence spectroscopy was carried out on a Varian Cary Eclipse fluorimeter with 10 mm Hellma quartz cuvettes at $25\text{ }^\circ\text{C}$.

A Fibox 3 fibre optic oxygen sensor purchased from PreSens Precision Sensing GmbH was used for monitoring the amount of oxygen.

Gas chromatography was performed on an Inficon Micro GC 3000 with a 3 \AA mol sieve column, a thermal conductivity detector and Ar as a carrier gas.

A Bandelin Sonorex RK 102 H was used for the sonication of vesicular samples.

Time dependent absorption spectra under irradiation were recorded on an Agilent 8453 UV/Vis spectrometer with LED irradiation perpendicular to the optical pathway. The system was magnetically stirred from above the cuvette (Figure 4.14).

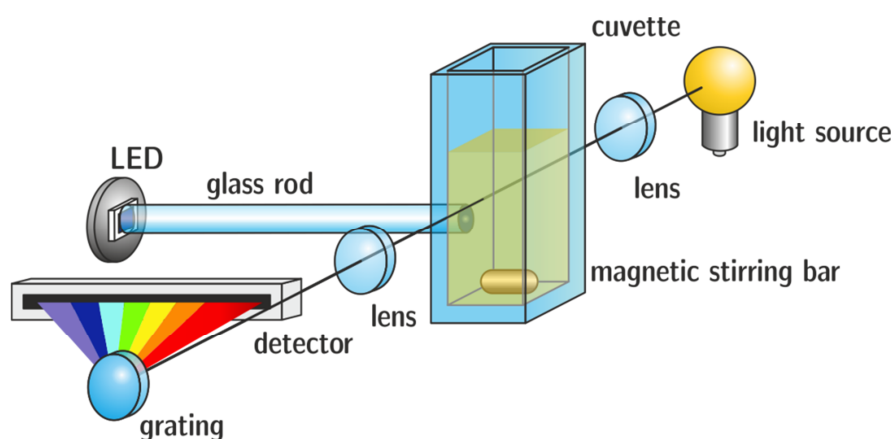


Figure 4.14 - Scheme of the setup for time-dependent UV/Vis measurements with online irradiation.

4.4.2 Synthesis of Catalyst 1

Water oxidation catalyst **1** was synthesized according to literature.^[11]

4.4.3 Stability of TPP

Three deoxygenated solutions of TPP (100 μM) in different solvents were prepared in a cuvette and were stirred in the photometer. UV/Vis spectra were recorded in constant intervals (Figure 4.15).

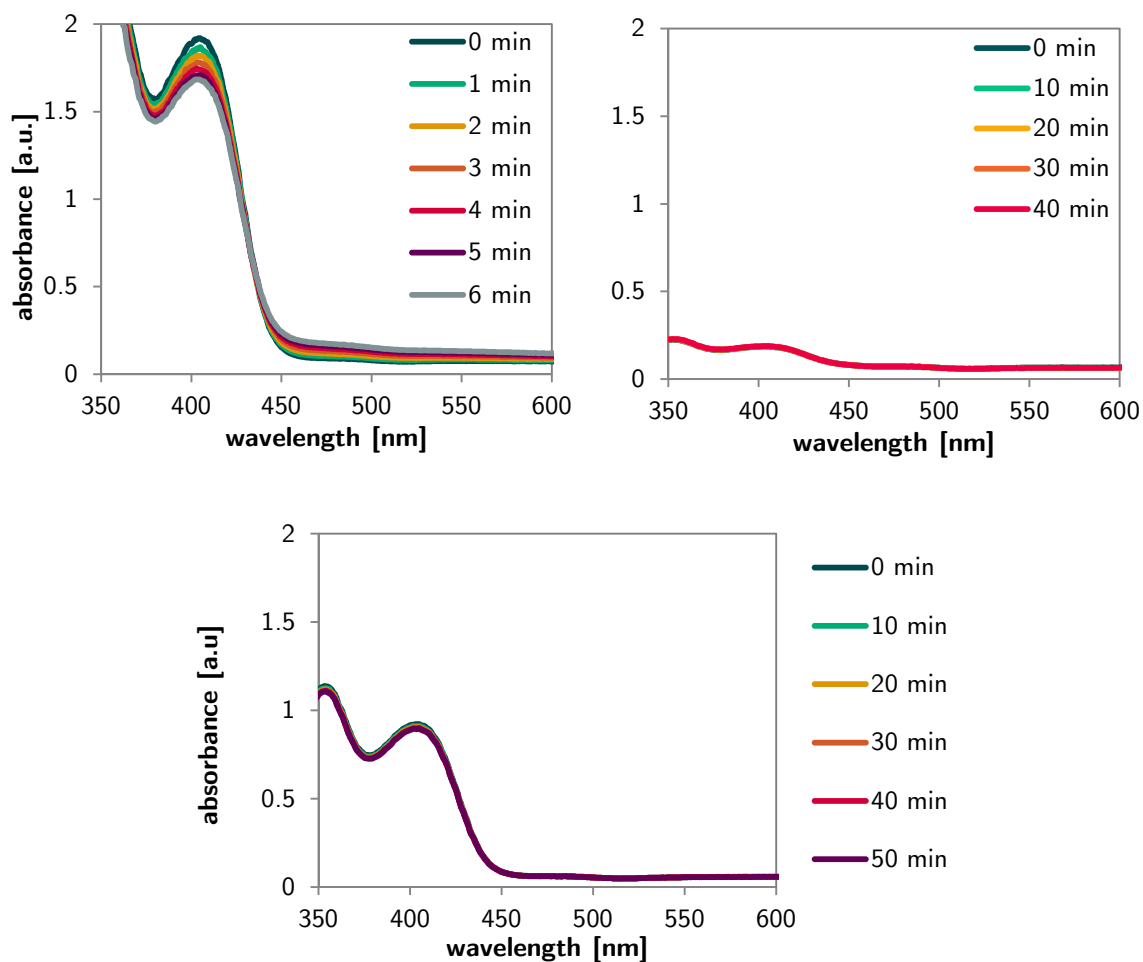


Figure 4.15 - Absorption spectra of a 100 μM solution of TPP; Top left: in Millipore water with 10 % MeCN. Top right: in pH 1 triflic acid. Bottom: in pH 3 triflic acid.

4.4.4 Detection of Ce^{IV} Generation by Methyl Viologen

A solution of TPP (50 μM), CeCl_3 (10 mM) and methyl viologen (6, 10 mM) in triflic acid at pH 3 was irradiated with a 400 nm LED in a cuvette in the UV/Vis spectrometer and the absorption spectra were recorded in constant intervals (Figure 4.16).

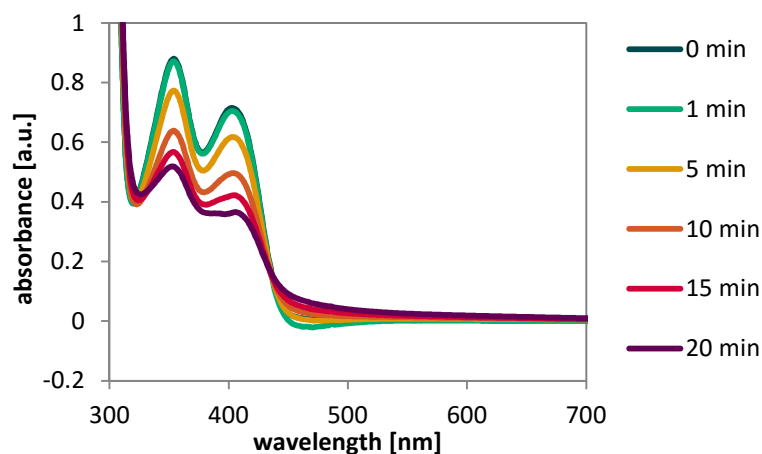


Figure 4.16 - Absorption spectra of a mixture of TPP (50 μM), CeCl_3 (10 mM) and methyl viologen (**6**, 10 mM) in triflic acid at pH 3 under 400 nm irradiation.

4.4.5 Calibration of the Ce^{IV} Detection Using AAP

Four samples with increasing amounts of CAN were prepared for the calibration of AAP-containing systems. Appropriate amounts of CAN (10 mM) solutions in triflic acid at pH 1 were added to solutions of AAP (3 mM) in triflic acid at pH 1 to achieve CAN concentrations of 5, 10, 50, 500 and 1000 μM . Immediately a violet color appeared and the absorbance spectra were recorded after 90 s.

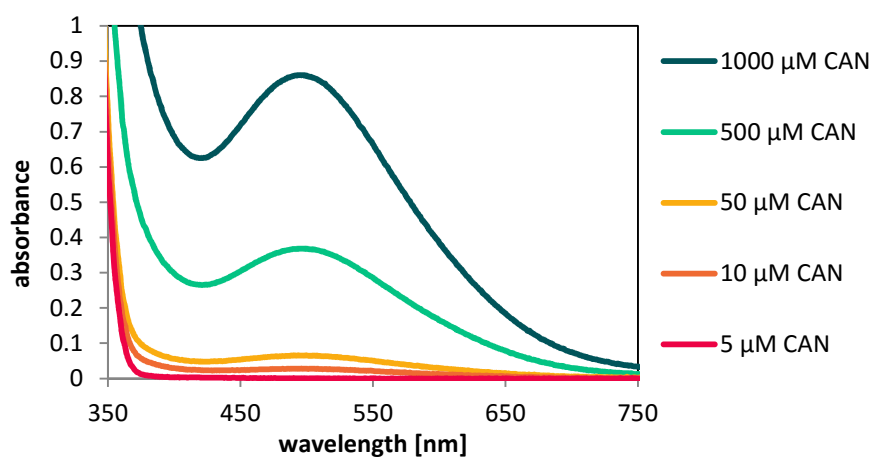


Figure 4.17 - Absorption spectra of a solution of AAP (3 mM) in triflic acid (pH 3) with increasing amounts of CAN.

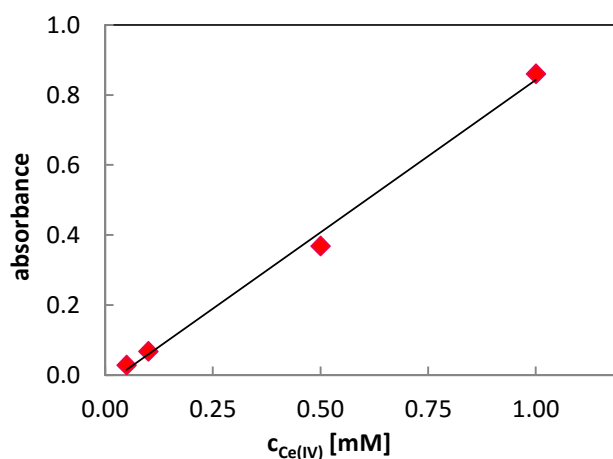


Figure 4.18 - Calibration curve for the detection of Ce^{IV} in triflic acid (pH 3) containing AAP (3 mM).

4.4.6 Water Oxidation Experiments

Ce^{IV} Generation

An appropriate amount of a stock solution of catalyst **1** in MeCN was evaporated and defined volumes of stock solutions of CeCl_3 , persulfate and TPP in triflic acid and triflic acid at pH 1 were added to the residue (Table 4.5). The solution was deoxygenated with argon.

Table 4.5 - Composition of samples for the generation of Ce^{IV} with TPP.

Entry	V_1^a [μL]	$V_{\text{CeCl}_3}^b$ [μL]	$V_{\text{S}_2\text{O}_8^{2-}}^c$ [μL]	V_{TPP}^d [μL]	c_1 [μM]	c_{CeCl_3} [μM]	$c_{\text{S}_2\text{O}_8^{2-}}$ [μM]	c_{TPP} [μM]	$V_{\text{triflic acid}}$ [mL]
1	100	200	200	100	50	10	10	50	1.5
2	200	100	100	200	100	5	5	100	1.6
^a c (stock sol.) = 1 mM ^b c (stock sol.) = 1 M ^c c (stock sol.) = 1 M ^d c (stock sol.) = 1 mM									

These solutions were transferred into a 2 mL screw cap vial under a nitrogen atmosphere which was equipped with a Fibox 3 optical oxygen sensor spot. The samples were irradiated with a LED ($\lambda = 400 \text{ nm}$).

CAN Regeneration

Appropriate volumes of stock solutions of CAN, persulfate and the photocatalysts TPP (Table 4.7) or $\text{Acr}^+\text{-Mes}$ (Table 4.8) in pH 1 triflic acid were mixed with pH 1 triflic acid in a 10 mL crimp cap vial. The solution was degassed with argon and a stock solution of cata-

lyst **1** in MeCN was added with a syringe. The irradiation with LEDs was started simultaneously to the addition of catalyst **1**. The final MeCN content was 5 vol%.

Table 4.6 - Composition of samples for the optimization of reaction conditions.

Entry	V_1^a [μL]	V_{CAN}^b [μL]	c_1 [μM]	c_{CAN} [mM]	$V_{\text{triflic acid}}$ [mL]
1	225	2.25	50	0.05	4.27
2	225	22.5	50	0.5	4.23
3	225	113	50	2.5	4.16
4	225	225	50	5.0	4.05
5	225	338	50	7.5	3.94
6	225	450	50	10	3.83

^a c (stock sol.) = 1 mM ^b c (stock sol.) = 0.1 M

Table 4.7 - Composition of samples for the regeneration of CAN with TPP.

Entry	V_1^a [μL]	V_{CAN}^b [μL]	$V_{\text{S}_2\text{O}_8^{2-}}^c$ [μL]	V_{TPP}^d [μL]	c_1 [μM]	c_{CAN} [mM]	$c_{\text{S}_2\text{O}_8^{2-}}$ [mM]	c_{TPP} [μM]	$V_{\text{triflic acid}}$ [mL]
1	225	338	45	225	50	7.5	10	50	3.67
2	225	338	-	-	50	7.5	-	-	3.94
3	225	338	-	-	50	7.5	-	-	3.94
4	225	338	-	-	50	7.5	-	-	3.94

^a c (stock sol.) = 1 mM ^b c (stock sol.) = 0.1 M ^c c (stock sol.) = 1 M ^d c (stock sol.) = 1 mM

Table 4.8 - Composition of samples for the regeneration of CAN with Acr^+-Mes .

Entry	V_1^a [μL]	V_{CAN}^b [μL]	$V_{\text{S}_2\text{O}_8^{2-}}^c$ [μL]	$V_{\text{Acr}^+-\text{Mes}}^d$ [μL]	c_1 [μM]	c_{CAN} [mM]	$c_{\text{S}_2\text{O}_8^{2-}}$ [mM]	$c_{\text{Acr}^+-\text{Mes}}$ [μM]	$V_{\text{triflic acid}}$ [mL]
1	225	338	45	113	50	7.5	10	25	3.78
2	225	338	45	225	50	7.5	10	50	3.67
3	225	338	45	450	50	7.5	10	100	3.44
4	225	338	45	1125	50	7.5	10	250	2.77
5	225	338	45	2250	50	7.5	10	500	1.64

^a c (stock sol.) = 1 mM ^b c (stock sol.) = 0.1 M ^c c (stock sol.) = 1 M ^d c (stock sol.) = 1 mM

4.5 References

- [1] N. S. Lewis, D. G. Nocera, "Powering the planet: Chemical challenges in solar energy utilization", *PNAS* **2006**, 103, 15729-15735.
- [2] M. Hambourger, G. F. Moore, D. M. Kramer, D. Gust, A. L. Moore, T. A. Moore, "Biology and technology for photochemical fuel production", *Chem. Soc. Rev.* **2008**, 38, 25-35.
- [3] M. D. Kärkäs, O. Verho, E. V. Johnston, B. Åkermark, "Artificial Photosynthesis: Molecular Systems for Catalytic Water Oxidation", *Chem. Rev.* **2014**.
- [4] A. R. Parent, R. H. Crabtree, G. W. Brudvig, "Comparison of primary oxidants for water-oxidation catalysis", *Chem. Soc. Rev.* **2013**, 42, 2247-2252.
- [5] V. Sridharan, J. C. Menéndez, "Cerium(IV) Ammonium Nitrate as a Catalyst in Organic Synthesis", *Chem. Rev.* **2010**, 110, 3805-3849.
- [6] E. Wadsworth, F. R. Duke, C. A. Goetz, "Present Status of Cerium(IV)-Cerium(III) Potentials", *Anal. Chem.* **1957**, 29, 1824-1825.
- [7] J. Limburg, R. H. Crabtree, G. W. Brudvig*, "Kinetic analysis of the O₂-forming reaction between [Mn(III)(dpa)₂]- (dpa=dipicolinate) and potassium peroxomonosulfate", *Inorg. Chim. Acta* **2000**, 297, 301-306.
- [8] D. G. H. Hetterscheid, J. N. H. Reek, "Periodate as an Oxidant for Catalytic Water Oxidation: Oxidation via Electron Transfer or O-Atom Transfer?", *Eur. J. Inorg. Chem.* **2014**, 2014, 742-749.
- [9] J. Limburg, J. S. Vrettos, L. M. Liable-Sands, A. L. Rheingold, R. H. Crabtree, G. W. Brudvig, "A Functional Model for O-O Bond Formation by the O₂-Evolving Complex in Photosystem II", *Science* **1999**, 283, 1524-1527.
- [10] L. Duan, L. Wang, F. Li, F. Li, L. Sun, "Highly Efficient Bioinspired Molecular Ru Water Oxidation Catalysts with Negatively Charged Backbone Ligands", *Accounts of Chemical Research* **2015**, 48, 2084-2096.
- [11] L. Duan, Y. Xu, M. Gorlov, L. Tong, S. Andersson, L. Sun, "Chemical and Photochemical Water Oxidation Catalyzed by Mononuclear Ruthenium Complexes with a Negatively Charged Tridentate Ligand", *Chem. Eur. J.* **2010**, 16, 4659-4668.
- [12] L. Wang, L. Duan, Y. Wang, M. S. G. Ahlquist, L. Sun, "Highly efficient and robust molecular water oxidation catalysts based on ruthenium complexes", *Chem. Commun.* **2014**, 50, 12947-12950.
- [13] T.-L. Ho, "Cerium(IV)-Oxidation with a Dual Oxidant System; Reaction of Some Arylmethanols", *Synthesis* **1978**, 1978, 936-936.

- [14] H. Tomioka, K. Oshima, H. Nozaki, "Cerium catalyzed selective oxidation of secondary alcohols in the presence of primary ones", *Tetrahedron Letters* **1982**, 23, 539-542.
- [15] L. Duan, F. Bozoglian, S. Mandal, B. Stewart, T. Privalov, A. Llobet, L. Sun, "A molecular ruthenium catalyst with water-oxidation activity comparable to that of photosystem II", *Nat. Chem.* **2012**, 4, 418-423.
- [16] K.-C. Huang, R. A. Couttenye, G. E. Hoag, "Kinetics of heat-assisted persulfate oxidation of methyl tert-butyl ether (MTBE)", *Chemosphere* **2002**, 49, 413-420.
- [17] P. Ramamurthy, S. Parret, F. Morlet-Savary, J. P. Fouassier, "Spin—orbit-coupling-induced triplet formation of triphenylpyrylium ion: a flash photolysis study", *J. Photochem. Photobiol. A* **1994**, 83, 205-209.
- [18] R. F. Khairutdinov, J. K. Hurst, "Cyclic Transmembrane Charge Transport Mediated by Pyrylium and Thiopyrylium Ions", *J. Am. Chem. Soc.* **2001**, 123, 7352-7359.
- [19] F. Teply, "Photoredox catalysis by [Ru(bpy)₃]²⁺ to trigger transformations of organic molecules. Organic synthesis using visible-light photocatalysis and its 20th century roots", *Collect. Czech. Chem. Commun.* **2011**, 76, 859-917.
- [20] P. M. Hare, E. A. Price, D. M. Bartels, "Hydrated Electron Extinction Coefficient Revisited", *J. Phys. Chem. A* **2008**, 112, 6800-6802.
- [21] R. Akaba, H. Sakuragi, K. Tokumaru, "Triphenylpyrylium-salt-sensitized electron transfer oxygenation of adamantylideneadamantane. Product, fluorescence quenching, and laser flash photolysis studies", *Journal of the Chemical Society, Perkin Transactions 2* **1991**, 291-297.
- [22] G. Somidevamma, M. S. Sarma, "p-Aminoacetophenone as a reagent for the colorimetric determination of cerium(IV)", *Talanta* **1967**, 14, 861-863.
- [23] S. Yabumoto, S. Shigeto, Y.-P. Lee, H.-o. Hamaguchi, "Ordering, Interaction, and Reactivity of the Low-Lying nπ* and ππ* Excited Triplet States of Acetophenone Derivatives", *Angew. Chem. Int. Ed.* **2010**, 49, 9201-9205.
- [24] W. A. Bashir, G. W. Hagop, S. Falamerz, "Indirect spectrophotometric determination of cerium(IV)", *Microchem. J.* **1982**, 27, 21-25.
- [25] N. A. Piro, J. R. Robinson, P. J. Walsh, E. J. Schelter, "The electrochemical behavior of cerium(III/IV) complexes: Thermodynamics, kinetics and applications in synthesis", *Coord. Chem. Rev.* **2014**, 260, 21-36.
- [26] U. Wille, "Inorganic Radicals in Organic Synthesis", *Chem. Eur. J.* **2002**, 8, 340-347.

- [27] K. Ohkubo, K. Mizushima, R. Iwata, K. Souma, N. Suzuki, S. Fukuzumi, "Simultaneous production of *p*-tolualdehyde and hydrogen peroxide in photocatalytic oxygenation of *p*-xylene and reduction of oxygen with 9-mesityl-10-methylacridinium ion derivatives", *Chem. Commun.* **2010**, 46, 601-603.

5 Summary

Within the scope of this thesis, different approaches towards photochemical and chemical water oxidations have been investigated. Metal-complex-functionalized vesicles catalyzed visible light-driven water oxidation. A replacement of the single molecule photosensitizers by quantum dots was investigated and an photochemical recycling of Ce^{IV} was studied.

Chapter 1 reviews the development of chemical and photochemical systems for artificial photosynthesis at dynamic self-assembled interfaces. The chapter highlights the most important reports on water oxidation, photocatalytic hydrogen production, overall water splitting systems and photocatalytic CO_2 reduction in vesicular and micellar systems, respectively. The role of the interface such as charge separation, back electron transfer suppression, solubilization or protection of sensitive intermediates is discussed for every mentioned system and a short outlook is provided.

Chapter 2 deals with the development of functionalized phospholipid bilayer vesicles for visible light-driven water oxidation. Molecular water oxidation catalysts and photosensitizers were modified with alkyl chains and co-embedded into phospholipid membranes to prepare functionalized small unilamellar vesicles. These aggregates photocatalytically produced molecular oxygen when irradiated with blue light from LEDs in phosphate buffer. The two dimensional assembly of photosensitizers and catalysts at the vesicle-water interface allowed photocatalytic water oxidation at very low overall catalyst concentrations of 500 nM, which are inoperable in homogeneous solutions. Functionalized, rigid gel phase membranes obtained the highest TONs. This indicates that phase separation enhances the photocatalytic activity of the assembly by clustering and limited dynamics of the embedded compounds. The concept of membrane co-embedding can be applied to various combinations, ratios and concentrations of photosensitizers and water oxidizing catalysts, providing a new approach to artificial photosynthesis.

Chapter 3 describes the attempt to use colloidal quantum dots as photosensitizers in photochemical water oxidation. Differently-sized CdSe quantum dots with several ligand environments were synthesized and characterized. Vesicular and homogeneous systems for photochemical water oxidation with quantum dots and homogeneous water oxidation catalysts have been prepared. Different combinations and ratios of quantum dots and catalysts were investigated towards oxygen evolution. A fluorescence quenching study revealed a charge transfer from quantum dots to methyl viologen and to a water oxidation catalyst, respectively. Regardless of the combinations and ratios of different quantum dots and water oxidation catalysts, no working photocatalytic water oxidation system was achieved.

Chapter 4 deals with the photocatalytic regeneration of the chemical oxidant Ce^{IV} , a commonly used agent for the chemical oxidation of water. Typical water oxidation catalysts reach higher catalytic activities under chemical water oxidation conditions. Therefore, the photochemical recycling of Ce^{IV} could enhance visible light-driven water oxidation reaction. Different approaches to detect the generation of Ce^{IV} by UV/Vis spectroscopy under photochemical water oxidation conditions were examined. Unfortunately, no system could fulfill the requirements due to unwanted side-reactions during the irradiation. The photochemical regeneration of ceric ammonium nitrate (CAN) with the photocatalysts triphenyl pyrylium (TPP) or 9-mesityl-10-methylacridinium ($\text{Acr}^{\text{+}}$ -Mes) was investigated. The system utilizing TPP proved to be not suitable due to the interaction of CAN and the light of 400 nm wavelength. The $\text{Acr}^{\text{+}}$ -Mes containing solutions also decreased the turnover of the water oxidation catalyst. In conclusion, the photochemical recycling of Ce^{IV} could not be realized.

6 Zusammenfassung

Im Rahmen der vorliegenden Doktorarbeit wurden verschiedene Ansätze zur photochemischen und chemischen Wasseroxidation untersucht. Mit Metallkomplexen funktionalisierte Vesikel wurden zur lichtgetriebenen Wasseroxidation eingesetzt. Untersucht wurden außerdem der Ersatz von molekularen Photosensibilisatoren durch Quantenpunkte, sowie die photochemische Regenerierung von Ce^{IV} .

Kapitel 1 zeigt die Entwicklung von photochemischen und chemischen Systemen zur künstlichen Photosynthese an dynamisch selbstorganisierten Grenzflächen auf. Das Kapitel nennt die wichtigsten Publikationen zu den Themen Wasseroxidation, photokatalytische Wasserstoffgenerierung, Wasserspaltung und lichtgetriebende CO_2 Reduktion in vesikulären bzw. Mizellen Systemen. Die Rolle der Grenzfläche, wie z.B. Ladungstrennung, Unterdrückung des Elektronenrücktransfers, Lösen von Komponenten oder Schützen von empfindlichen Zwischenstufen, wird für jedes System diskutiert. Zuletzt wird ein Ausblick auf die Entwicklung dieser Systeme gegeben.

Kapitel 2 handelt von der Entwicklung funktionalisierter Doppelschicht-Phospholipid Vesikel zur lichtgetriebenen Wasseroxidation. Molekulare Wasseroxidationskatalysatoren und Photosensibilisatoren wurden mit Alkylketten modifiziert und gemeinsam in Phospholipidmembranen eingebettet, um funktionalisierte unilamellare Vesikel herzustellen. Diese Liposomen oxidierten Wasser zu Sauerstoff, wenn sie in Phosphatpuffer mit blauem Licht aus LEDs bestrahlt wurden. Die zweidimensionale Anordnung der Photosensibilisatoren und Katalysatoren an der Lipid-Wasser Grenzschicht ermöglichte eine erfolgreiche photochemische Wasseroxidation bei äußerst niedrigen Katalysatorkonzentrationen von nur 500 nM, welche in homogenen Systemen nicht funktionsfähig sind. Funktionalisierte Membranen in der Gel-Phase, mit eingeschränkter lateraler Fluidität, zeigten die höchsten Ausbeuten an Sauerstoff. Das deutet darauf hin, dass die katalytische Aktivität aufgrund von eingeschränkter Beweglichkeit und Gruppierung der Komponenten durch die Phasentrennung in solchen Membranen erhöht wird. Das Konzept der Einbettung in Membranen kann auf ver-

schiedenste Kombinationen, Verhältnisse und Konzentrationen an Photosensibilisatoren und Katalysatoren angewendet werden und bietet somit einen neuen Ansatz zur Herstellung künstlicher Photosynthesysteme.

Kapitel 3 beschreibt den Versuch Photosensibilisatoren in der photochemischen Wasseroxidation durch kolloidale Quantenpunkte zu ersetzen. Quantenpunkte verschiedener Größen mit unterschiedlichen Ligandenhüllen wurden synthetisiert und charakterisiert. Vesikuläre und homogene Systeme zur photochemischen Wasseroxidation mit Quantenpunkten und homogenen Wasseroxidationskatalysatoren wurden hergestellt. Verschiedene Kombinationen und Verhältnisse von Quantenpunkten und Katalysatoren wurden auf die Entstehung von Sauerstoff hin untersucht. Eine Fluoreszenzlöschungsuntersuchung zeigte einen Ladungstransfer von den Quantenpunkten auf Methylviologen bzw. den Wasseroxidationskatalysator. Unabhängig von den gewählten Kombinationen und Verhältnissen der Quantenpunkte und der Katalysatoren konnte mit keinem System photochemisch Wasser oxidiert werden.

Kapitel 4 handelt von der photochemischen Regenerierung des chemischen Oxidationsmittels Ce^{IV} , einem häufig verwendetem Oxidans in der chemischen Wasseroxidation. Typische Wasseroxidationskatalysatoren erreichen höhere Umsätze unter den Bedingungen der chemischen Wasseroxidation. Deshalb könnte das photochemische Recycling von Ce^{IV} photochemische Wasseroxidationen deutlich verbessern. Verschiedene Ansätze zum photochemischen Nachweis von Ce^{IV} mit UV/Vis Spektroskopie wurden untersucht. Leider erfüllte keines der Systeme die Ansprüche aufgrund von unerwünschten Nebenreaktionen während der Beleuchtung. Die photochemische Regenerierung von Cerammoniumnitrat (CAN) mit Hilfe der Photokatalysatoren Triphenylpyrylium (TPP) und 9-Mesityl-10-Methylacridinium (Acr^+ -Mes) wurde untersucht. Das System mit TPP erwies sich als untauglich, aufgrund der Wechselwirkung von CAN mit dem Licht der Wellenlänge 400 nm. Die Acr^+ -Mes Lösungen verringerten ebenfalls den Umsatz des Wasseroxidationskatalysators. Schlussfolgernd konnte das photochemische Recycling von Ce^{IV} nicht realisiert werden.

7 Abbreviations

A	absorbance
AAP	1-(4-aminophenyl)ethan-1-one
Acr ⁺ -Mes	9-mesityl-10-methylacridinium
a.u.	arbitrary unit
Asc	ascorbic acid
bpy	2,2'-bipyridine
c	concentration
calc.	calculated
Cat	catalyst
CB	conduction band
chl- <i>a</i>	chlorophyll <i>a</i>
conc.	concentrated
CTAB	cetyl-trimethyl-ammonium bromide
Cyt <i>b6f</i>	cytochrom <i>b6-f</i> -complex
d/D	diameter
DCM	dichloro methane
decomp.	decomposition
DHP	dihexadecylphosphate
DMPC	1,2-dimyristoyl- <i>sn</i> -glycero-3-phosphocholine
DMSO	dimethyl sulfoxide
DODAB	dioctadecyldimethyl ammonium bromide
DODAC	dioctadecyldimethyl ammonium chloride
DPPC	1,2-dipalmitoyl- <i>sn</i> -glycero-3-phosphocholine
DSPA	1,2-distearoyl- <i>sn</i> -glycero-3-phosphoric acid
DSPC	1,2-distearoyl- <i>sn</i> -glycero-3-phosphocholine
DSPG	1,2-dioctadecanoyl- <i>sn</i> -glycero-3-phospho-(1'-rac-glycerol)
E	reduction potential
e ⁻	electron
E.A.	elemental analysis
em.	emission
Et	ethyl
exc.	excitation
Fd	ferredoxin

GC	gas chromatography
h+	hole
H ₂ ase	hydrogenase
HPLC	high performance liquid chromatography
HR-MS	High resolution mass spectrometry
HWHM	half width half maximum
IR	infra-red
K _q	fluorescence quenching rate constant
LED	light emitting diode
M	mol/L
m.p.	melting point
max	maximal
Me	methyl
MS	mass spectrometry
MV	methyl viologen
m/z	mass to charge
Na ₂ EDTA	sodium 2,2'-(ethane-1,2-diylbis((carboxymethyl)azanediyl))diacetate
NADH	Nicotinamide adenine dinucleotide
NADPH	Nicotinamide adenine dinucleotide phosphate
NHE	normal hydrogen electrode
NIR	near infra-red
NMR	nuclear magnetic resonance
OEC	oxygen evolution complex
PB-PEO	1,2-polybutadiene-polyethyleneoxide
PC	plastocyanin
Ph	phenyl
PhSH	thiophenol
Pic	4-methylpyridine
POPC	1-palmitoyl-2-oleoyl- <i>sn</i> -glycero-3-phosphocholine
ppm	parts per million
ppy	2-phenylpyridine
PQ	plastoquinon
PQH ₂	plastohydroquinon
PS	photosensitizer
PTT	phase transition temperature
PyCH ₂ OH	1-(hydroxymethyl)pyrene
Q _A	plastoquinon A
r.t.	room temperature
SDS	sodium lauryl sulfate
SMPC	1-stearoyl-2-myristoyl- <i>sn</i> -glycero-3-phosphocholine
SnTPP	tin tetraphenylporphyrin
sol.	solution
TEM	transmission electron microscopy

TEOA	trethanolamine
THF	tetrahydro furane
TON	turnover number
tot	total
TPP	triphenyl pyrylium tetrafluoroborate
tpy	2,6-bis(2-pyridyl)pyridine
UV	ultraviolet
v	volume
VB	valence band
Vis	visible
ZnTPPS4	zinc tetraphenylporphyrin tetrasulphonate
β	selectivity for oxygen generation

8 Curriculum Vitae

Personal Data

Name: Malte Hansen
Born: 16.10.1986 in Marburg/Lahn
Nationality: German

Education

12/2011 - 12/2015 **PhD Thesis** at the Institute of Organic Chemistry, University of Regensburg (Supervisor: Prof. Dr. B. König)
"Photochemical Water Oxidation at Dynamic Self-Assembled Interfaces"

10/2009 - 09/2011 **Master Studies** of Chemistry at the University of Regensburg
Master Thesis: *"Vesicular Ruthenium-Complexes for Visible Light Driven Water Oxidation"* (Supervisor: Prof. Dr. B. König)

10/2006 - 09/2009 **Bachelor Studies** of Chemistry at the University of Regensburg
Bachelor Thesis: *"Aufbau eines Imidazol-substituierten Schlüsselintermediats für die Synthese neuer potenzieller H4-Rezeptor Liganden"* (Supervisor: Prof. Dr. O. Reiser)

09/1997 - 06/2006 **Allgemeine Hochschulreife** (A-Levels) at the Martin-Luther-Gymnasium Marburg

Teaching experience

Since 12/2011 Teaching assistant in laboratory courses, supervisor for internship projects, teaching of chemists, biologists and medics in tutorial courses

Award, Scholar- and Memberships

03/2013	"ChemPlusChem" poster prize of the SupraChem 2013 conference in Münster
Since 2011	Membership of the Gesellschaft deutscher Chemiker (GDCh)
2011 - 2015	Travel grants from GDCh and Freunde der Universität Regensburg e.V.

Conference Contributions

- 1 *"Visible Light Driven Water Oxidation at Soft Interfaces"*
Poster, ORCHEM, **2014**, Weimar, Germany
- 2 *"Photocatalytic Water Oxidation at Soft Interfaces"*
Oral presentation, Symposium on Photochemical Water Splitting at Soft Interfaces **2014**, Regensburg, Germany
- 3 *"Visible Light Driven Water Oxidation with Functionalized Vesicles"*
Oral presentation, The 1st Workshop of China-Germany Joint Research Project on Photochemical Water Splitting at Soft Interfaces **2013**, Dalian, China
- 4 *"Photocatalytic Water Oxidation with Ruthenium-Complex Functionalized Vesicles"*
Poster, Supra Chem **2013**, Münster, Germany
- 5 *"Vesicular Ruthenium-Complexes for Visible Light Driven Water Oxidation"*
Oral presentation, Supra Chem **2012**, Strasbourg, France

Publications

M. Hansen, S. Troppmann and B. König, "Artificial Photosynthesis at Dynamic Self-Assembled Interfaces in Water", *Chem. Eur. J.* **2015**, DOI: 10.1002/chem.201503712

M. Hansen, F. Li, L. Sun and B. König, "Photocatalytic water oxidation at soft interfaces", *Chem. Sci.* **2014**, 5, 2683-2687

9 Danksagung

Ich möchte mich ganz herzlich bei all denen bedanken, die direkt oder indirekt an der erfolgreichen Fertigstellung meiner Dissertation mitgewirkt haben. Im speziellen danken möchte ich an dieser Stelle:

In erster Linie Prof König,
denn ohne ihn ging hier nur wönig.
Er hält das Arbeitsklima fit
und bezahlt auch mal nen China-Trip.
Danke für'n Doktor und den Master!
Ohne Dich wär's sicher nur'n Desaster.

Danke auch für das zweite Gutachten,
Prof. Pfitzner, dass Sie das mitmachten.

Danke auch dem dritten der Runde,
Herr Dr. Müller, in solch wichtiger Stunde.

Für den Prüfungsvorsitz danke ich hier,
Prof. Matysik, denn man braucht nun mal vier!

Danke auch an all die ander'n,
die schon lange durch die Uni wandern,
Petra, Regina, Viola und Britta
ihr macht die Bürokratie weniger bitter.
Ernst und natürlich auch Simone
wegen euch läuft's hier prima, zweifelsohne!

Lieber Rudi, an Dich ein besonderer Dank,
warst bei der GC immer ne helfende Hand.
Dein Lieblingsverein könnt a besserer sein,
aber Das kann ich natürlich auch verzeihen.

Christina und Simon, Thomas und Sonay,
eure Praktika waren leider zu schnell vorbei.
Spaß hat's mit euch immer gemacht,
gemeinsam geforscht und auch viel gelacht!

Nun kommen wir zum wichtigsten Part,
Troppi, mit mir war's manchmal auch hart!
Fast fünf Jahre hast Du mich ertragen,
hast mir geholfen bei all meinen Fragen.
Ich hab die Zeit immer sehr genossen,
schade das sie jetzt ist abgeschlossen!
Vergessen werd ich sie ganz sicher nie,
wie könnt ich das auch, bei so nem Genie ;)

Der gute, alte 11 Uhr-Mensa-Geh-Kern,
ach was hab ich euch alle doch gern.
Der Andi, der Mischko und die Anna,
der Manuel, die Nadja und der Tonda.
Ihr habt das Essen zum Highlight gemacht,
hab gerne mit euch meine Zeit dort verbracht.
Das Essen war dann auch nicht so wichtig,
die Gespräche, ja, die machten süchtig!

Die Truppe um Willi, Caro und Thea,
ohne euch, wäre mein Arbeitstag leer.
Dank für Kaffees, Bier und Gespräche,

ohne die die Motivation ganz sicher bräche.
Für meinen Erfolg ward ihr wirklich wichtig,
ich kann euch sagen, ihr macht es richtig!

Manuel, danke für all deine Sachen ;),
deinen Rat und Tat, die vieles möglich machen.

Anna, danke für die tolle Zeit,
schon im Studium ging es oft nur zu zweit.

Mischko, danke, nicht nur für deine Geschichten,
auch für 9gag, das Filmen und das Vernichten,
von großen Mengen Kaffee und Bier,
die Kaffeekasse dankte es Dir.

Man soll ja auch nicht die Alumni vergessen,
Respekt vor dem Alter hab ich immer besessen.
Also danke ich Benno, Andi, Balki und Sanne,
dank euch verlief der Anfang hier ohne Panne.

Vergessen? Nein, ganz sicher nicht!
Zu danken dem AK, mehr als nur Pflicht.

Eine Freude war's mir immer hier zu sein
bei solchen Kollegen fühlt man sich daheim.

Danke, für eine fantastische Zeit,
wieder zurückzukehren? Da bin ich allzeit bereit!

Ganz zum Schluss, aber doch unfassbar wichtig,
ist das es auch läuft im Privatleben richtig!

Anna, ohne Dich wär sowieso alles mies,
bist für mich da, wenn's auch wird mal fies.

Du und die Mäuse seid meine sichere Bank
Deswegen gilt euch mein größter Dank.

Klar, der Familie gilt auch mein Dank,
für euren Support, nicht nur auf der Bank.

Jemand vergessen? Ach nehmt's nicht so schwer,
diesen Teil liest ja eh kein Mensch mehr.

Ich denke an euch, wird auch immer so bleiben,
nur halt eben gerade nicht beim schreiben ;)